Control of fluidized bed spray granulation processes

Dissertation

zur Erlangung des akademischen Grades

**Doktoringenieur
(Dr.-Ing.)**

von Stefan Palis

geb. am 07.08.1981 in Magdeburg

Zusammenfassung

Die Wirbelschichtsprühgranulation ist ein industriell bedeutendes Verfahren zur Gewinnung von festen Granulaten aus einer Suspension oder Lösung. Hierbei wird zunächst eine Schüttung von Feststoffpartikeln durch einen aufwärtsgerichteten Gasstrom fluidisiert. Das sich ausbildende Wirbelbett wird anschließend mit der Suspension oder Lösung besprüht, die sich auf dem Einzelpartikel absetzt. Bei geeigneten Prozessbedingungen, d.h. Gasfeuchte und Gastemperatur, kommt es dann zur Verdunstung der flüssigen Phase und damit verbunden zur Bildung einer neuen Feststoffschicht auf den Einzelpartikeln. Diese unterscheiden sich untereinander durch ihre Größe, was auf eine entsprechende Partikelgrößenverteilung führt.

Im großtechnischen Maßstab wird die Wirbelschichtsprühgranulation kontinuierlich betrieben. Hierbei können jedoch je nach Prozessbedingungen neben den gewünschten stationären Zuständen auch Instabilitäten in Form von nichtlinearen Oszillationen auftreten. Es handelt sich hierbei um ein Phänomen, das auch von anderen partikelbildenen Prozessen, wie beispielsweise der kontinuierlichen Kristallisation, bekannt ist. In der Regel führen solche Oszillationen zu periodisch variierenden Produkteigentschaften und sind daher unerwünscht. Im Rahmen dieser Arbeit wird untersucht wie sich dieses unerwünschte Verhalten mittels regelungstechnischer Methoden beherrschen lässt. Es werden hierzu zwei typische Anlagenschemen, die kontinuierliche Wirbelschichtsprühgranulation mit interner und externer Produktklassierung, betrachtet.

In Kapitel 2 werden die entsprechenden Modelle vorgestellt und deren Stabilitätsverhalten analysiert. Die Modellierung der Partikelgrößenverteilung mit Hilfe von Populationsbilanzen führt auf nichtlineare partielle Integrodifferentialgleichungen. Zur Regelung können prinzipiell Verfahren der endlich (nach einer entsprechenden Diskretisierung) und unendlich dimensionalen Regelungstheorie verwendet werden.

In Kapitel 3 werden unter Verwendung von Verfahren der linearen endlich dimensionalen robusten Regelungstheorie Regler entworfen, die ein nominelles Streckenmodell, d.h. die lineare endlich dimensionale Approximation des Prozesses in der Umgebung um eine nominelle Ruhelage, stabilisieren. Die Robustheitseigenschaften der so entworfenen Regler werden benötigt, um die robuste Stabilität bezüglich zweier Fehler zu garantieren. Zum einen sind dies Fehler, die aus der Abweichung der linearen endlich dimensionalen Approximationen des Prozesses an Ruhelagen verschieden von der nominellen folgen. Zum anderen Fehler, die aus der Diskretisierung, d.h. der endlichen dimensionalen Approximation des verteilten Modells, resultieren. Beide Fehler werden in Kapitel 3 ausführlich analysiert. Es zeigt sich, dass die entworfenen Regler die Stabilität der Partikelgrößenverteilung in einer Umgebung um die stationäre Partikelgrößenverteilung garantieren. Wie Simulationen belegen, erlauben die entworfenen Regler in Kombination mit einer geeigneten Anfahrstrategie einen stabilen Anlagenbetrieb im interessierenden Parameterbereich.

In Kapitel 4 wird ein neues Regelungskonzept vorgestellt, das den Entwurf eines stabilisierenden Reglers direkt am nichtlinearen unendlich dimensionalen Modell ermöglicht. Die Grundidee ist hierbei, die üblichen Stabilitätsanforderung, d.h. Konvergenz des Fehlers in der Partikelgrößenverteilung in einer Norm (L_1, L_2 oder L_∞-Norm), abzuschwächen und lediglich die Konvergenz in einem verallgemeinerten Abstandsmaß, einer Diskrepanz, zu fordern. Durch die Verwendung der diskrepanzbasierten Stabilitätstheorie kann damit, eine geeignete Wahl der Diskrepanzen vorausgesetzt, ein analytischer Reglerentwurf durchgeführt werden. Für die berechneten Regelgesetze kann unter gewissen Bedingungen auch die punktweise Konvergenz des Fehlers in der Partikelgrößenverteilung, d.h. Konvergenz im Sinne der L_∞-Norm und damit auch in der L_1 und L_2-Norm, gezeigt werden. Neben dem einfachen und intuitiven Entwurf belegen Simulationsergebnisse auch ein deutlich verbessertes Übergangsverhalten im Vergleich zu den zuvor betrachteten endlich dimensionalen Ansätzen.

Abstract

Fluidized bed spray granulation is an important industrial process for solid granule pro-
duction from suspensions or solutions. First of all, a packed bed of solid particles is
fluidized by an upwards directed gas flow. Then the fluidized bed is sprayed with the
suspension or solution, which settles on the particles. Under appropriate conditions, i.e.
gas humidity and temperature, the liquid phase evaporates and a new solid layer forms
on the particles. As the particles differ in size this results in a particle size distribution.
For large-scale production fluidized bed spray granulations are operated continuously.
Here, beside the desired steady state operation instabilities as nonlinear oscillations may
occur depending on the specific process conditions. This phenomenon is also known from
other particulate processes like continuous crystallization. In general, these oscillations
result in periodical variations of product properties and are therefore undesired. In this
Thesis, control oriented approaches are investigated to overcome this problem. Therefore,
two typical production schemes, i.e. the fluidized bed spray granulation with internal and
external product classification, are studied.
In Chapter 2 the associated models are presented and their stability behavior is analyzed.
The modelling of the particle size distribution by population balances results in nonlinear
partial integro-differential equations. For control design methods of finite dimensional,
after an appropriate discretization step, and infinite dimensional control theory can be
applied.
In chapter 3 controllers are derived applying linear finite dimensional robust control the-
ory. They allow for stablization of a nominal plant model, i.e. a linear finite dimensional
approximation of the plant in the neighborhood of a nominal steady state. The robustness
margin of the designed controllers is used to guarantee robust stability with respect to
two errors. On the one hand, errors resulting from deviations of linear finite dimensional
approximations of the plant at steady states different from the nominal steady state. On
the other hand, errors resulting from the discretization, i.e. the finite dimensional ap-
proximation of the distributed parameter system. Both errors are investigated in detail
in chapter 3. It will be shown, that the proposed controllers guarantee stability of the
particle size distribution in a neighborhood of the steady state particle size distribution.
As will be demonstrated by means of simulations the designed controllers, in combination
with an appropriate start-up strategy, permit a stable plant operation in the parameter
range of interest.
In chapter 4 a new control concept is presented, which allows a direct stabilizing con-
trol design using the nonlinear infinite dimensional plant model. The basic idea is to
weaken the standard stability requirements, i.e. convergence of the error particle size
distribution in a norm (L_1, L_2 or L_∞-norm), and to require convergence in a generalized
distance measure, called discrepancy. Applying discrepancy based stability theory and se-

lecting appropriate discrepancies this approach allows an analytical control design. Under some additional conditions the proposed controller can be shown to guarantee pointwise convergence, i.e. convergence in the sense of the L_∞-norm and hence in the L_1 and L_2-norm. Besides the simple and intuitive design, in comparison to linear finite dimensional approaches the discrepancy based controllers show an improved transition behavior in simulations.

Notation

μ_i	i-th moment, i.e. $\int_0^\infty L^i n \, dL$
$\dot{n}_*$	particle flux
n	number density distribution
L	diameter
A	overall surface
V	overall volume
$\delta(L)$	Dirac delta function
$\sigma(L)$	Heaviside step function
$\dot{V}_e$	volume based suspension injection rate
$\dot{m}_e$	mass based suspension injection rate
G	growth rate
B	birth rate
b	nucleation parameter
h	bed height
K	drain
μ_M	mill grade
T_*	separation function
Subscripts	
out	removed particles
product	product particles
noz	nozzle
fines	fine particles
oversize	oversized particles
product	product particles
mill	milled particles

Table 1: Continuous fluidized bed spray granulation with internal and external product classification

$W_1(s)$	precompensator
$W_2(s)$	postcompensator
$G(s)$	transfer function
δ_g	gap metric
A, B, C, D	system matrices of a state space model
M, N	denominator and numerator of a transfer function
$\mathcal{L}$	Laplace transform
$L(\mathcal{X})$	bounded linear operator from $\mathcal{X}$ to $\mathcal{X}$
$L(\mathcal{X}, \mathcal{Y})$	bounded linear operator from $\mathcal{X}$ to $\mathcal{Y}$
$T(.)$	Semigroup
$D(A)$	domain of A
$\rho(A)$	resolvent set of A
$R(s; A)$	resolvent of A
P_n	projection operator
W_c	controllability gramian
W_o	observability gramian
σ_i	Hankel singular value
$V(x)$	Lyapunov function
$\rho(\varphi, t)$	discrepancy of φ
$L_f h(x)$	Lie derivative of $h(x)$ along $f(x)$
Subscripts	
s	steady state
r	reduced model
n	n-dimensional approximation
o	observable state
uo	unobservable state
c	controllable state
uc	uncontrollable state
Δ	uncertain model set

Table 2: Linear and nonlinear control design

Contents

Chapter 1

Introduction

1.1 Process description

Granulation is an important class of production processes in food, chemical and pharmaceutical industries. It is used to produce granules from liquid products, e.g. solutions or suspensions. More and more frequently, granulation is combined with fluidized bed technology. Here, a fluidized bed is formed from solid particles under appropriate conditions, e.g. by passing a gas or liquid through the solid material. Important properties of the fluidized bed are the fluid like behavior, an enlarged active surface caused by increased bed porosity and good particle mixing. In addition, fluidization technology allows a combination of different processes like drying, coating, mixing, granulation, agglomeration, heating or pneumatic transport [4, 8, 7].
For research purposes a pilot plant shown in Fig. 1.1 has been installed at the chemical engineering department of the Otto-von-Guericke University, which allows for different process configurations. One typical fluidized bed spray granulation scheme is depicted in Fig. 1.2.
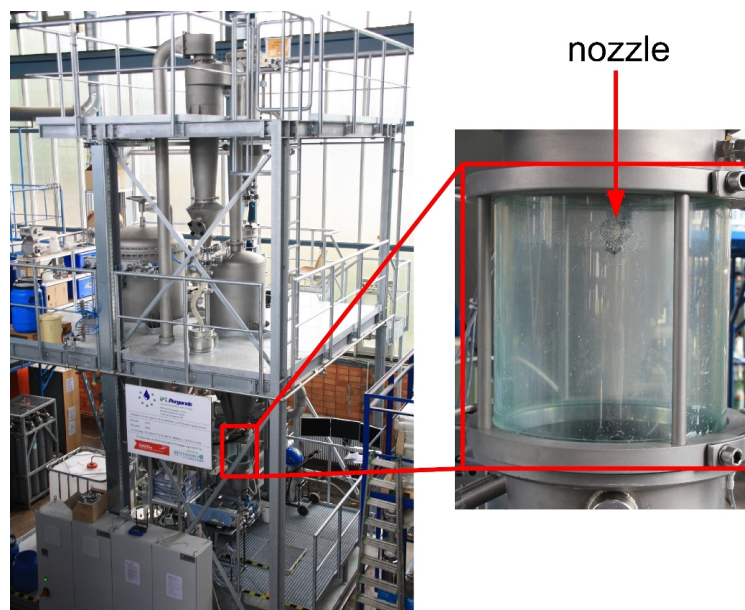
Figure 1.1: NaWiTec fluidized bed spray granulator (left) and process chamber (right)
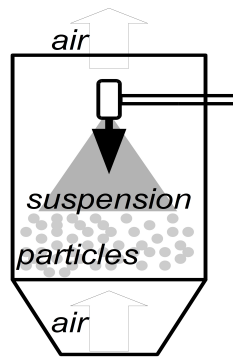
Figure 1.2: Typical granulation process

Here, the solid particles are fluidized by an air stream with predefined pressure, temperature and humidity. Then a liquid, e.g. solution or suspension, is injected, which settles on the particles. Due to the low humidity and increased temperature the liquid fraction, i.e. the solvent or the external phase, is evaporated. The remaining solid forms a new layer on the particle surface as shown in Fig. 1.3.
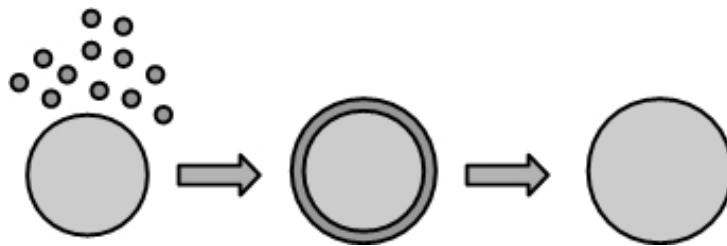
Figure 1.3: Particle growth

Besides the described layered growth in fluidized bed spray granulation operation additional mechanisms may occur:

1. Nucleation, i.e. particle formation based on liquid evaporation. Meaning the creation of new particles from droplets sprayed into the process chamber due to the evaporation of the liquid in the droplet as depicted in Fig. 1.4.
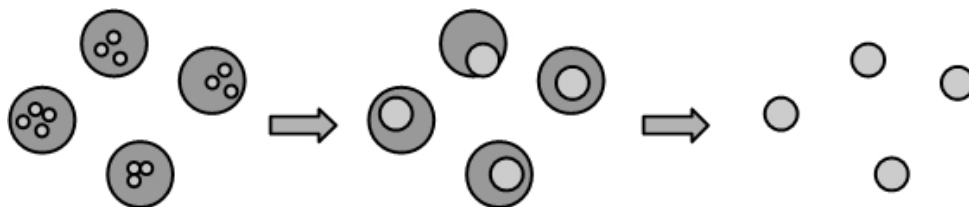
Figure 1.4: Nucleation

2. Particle breakage or attrition due to particle-particle contact or particle wall contact as shown in Fig. 1.5.

3. Particle agglomeration due to the formation of liquid particle-particle bonds as depicted in Fig. 1.6.
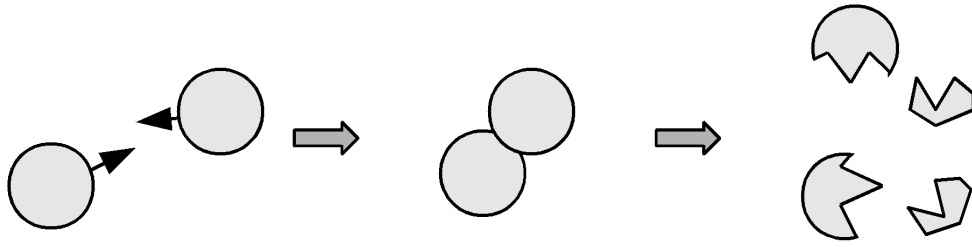
Figure 1.5: Particle breakage
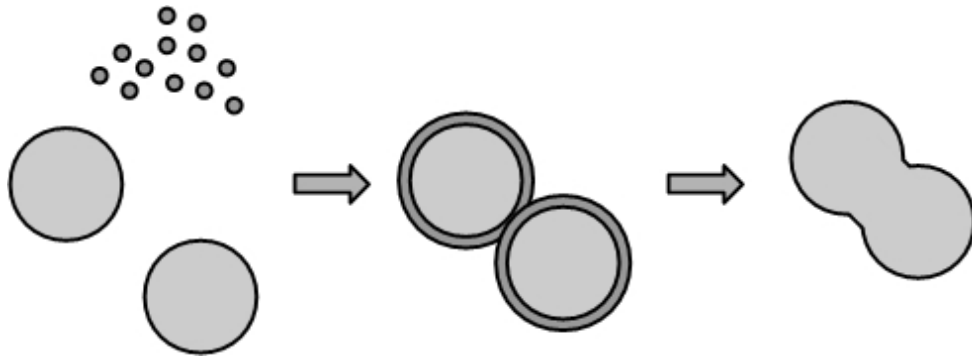
Figure 1.6: Agglomeration

From a modeling point of view, fluidized bed spray granulation processes and particulate processes in general can be described by population balances. Here, an individual particle property as for example characteristic size is introduced as an internal coordinate. This property may change from particle to particle, giving rise to a property distribution, like the particle size distribution. The distribution dynamics of the particle ensemble can be described by a population balance equation [10]

$$\frac{\partial n}{\partial t} = \frac{\partial G(\xi)n}{\partial \xi} + F(n, \xi),\qquad(1.1)$$

where ξ is an internal coordinate like for example particle size, $n(t, \xi)$ is the number density of the particle size distribution, $G(\xi)$ is the associated growth and $F(n, \xi)$ accounts for sinks and sources in the domain of ξ.

1.2 Motivation

It is well known that continuous fluidized bed spray granulation depending on the process configuration exhibit nonlinear limit cycles as depicted in Fig. 1.7 and reported in [1, 4, 12]. These are connected to a loss of stability of the steady state for a certain range of parameters.

In most cases these instabilities do have a negative effect on product quality and plant productivity and are therefore undesired. This is no specific behavior for fluidized bed spray granulation as similar patterns of behavior have been observed for other particulate processes like crystallization processes [40, 26]. Fig. 1.8 shows an example with nonlinear oscillations occurring in an industrial KCl crystallizer.
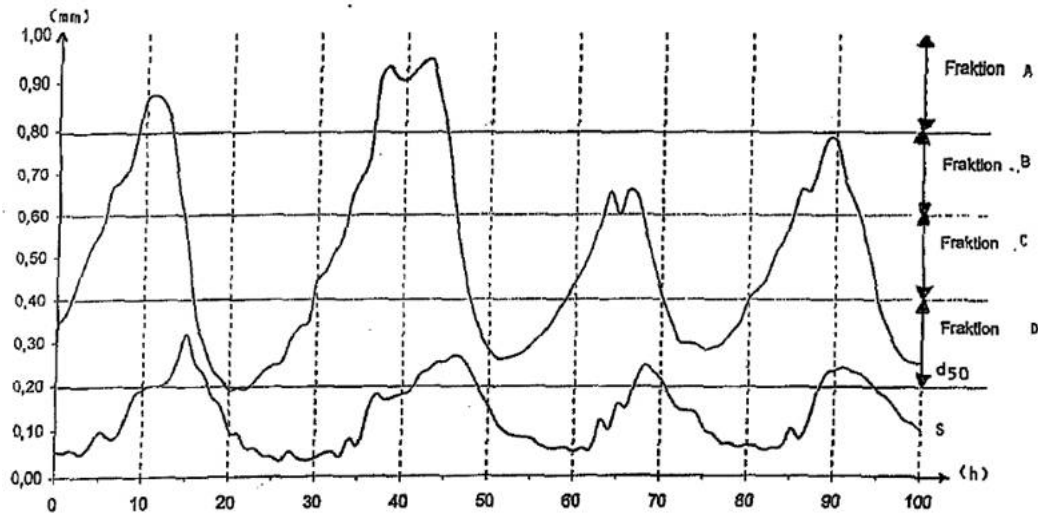
Figure 1.7: Limit cycles occurring in fluidized bed spray granulation operation according to Schütte et. al. [11]
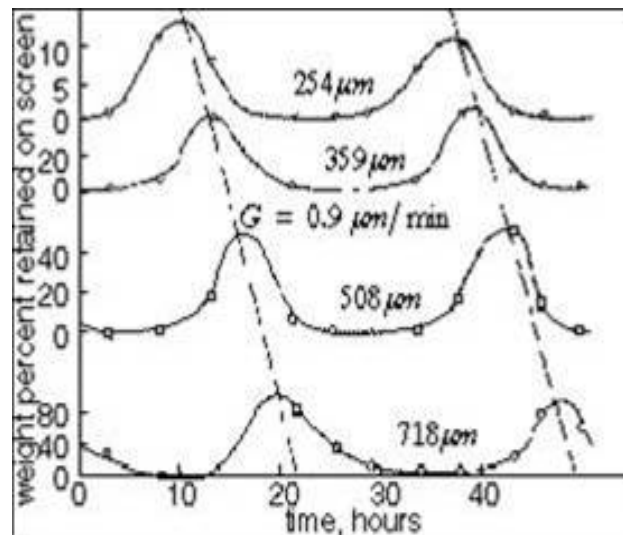
Figure 1.8: Limit cycles occurring in industrial KCl crystallizer operation according to Randolph [39]

Typically, these instabilities give undesired time behavior of the particle size distribution in the granulator and the associated product quality. Possible solutions are redesign, e.g. avoiding parameter combinations in the region of instability, or constructive measures like for example buffer tanks augmentation, or stabilization via feedback control. The latter approach should be preferred as it gives the possibility to operate the process over the full range of parameters and needs no reconstruction. In addition, feedback control improves process dynamics even in the stable region. It allows a direct adjustment of the desired product properties and permits the rejection of unforeseen disturbances.

However, from a control theory point of view, stabilizing control design is a very challenging task as population balance models for continuously operated particle processes

represent nonlinear distributed parameter systems. So far, main emphasis in this field
was on crystallization processes. Here, several approaches for stabilizing control design
have been proposed, using linear (e.g. [31]) and nonlinear (e.g. [27, 28, 29, 30]) lumped
models or linear (e.g. [36, 37, 38]) and nonlinear infinite dimensional models, i.e. applying
the control approach presented in chapter 4 [35]. The lumping can be achieved by

1. Numerical discretization of the process model [31]. Here, the model can be dis-
   cretized in time and the internal coordinate or only in the internal coordinate lead-
   ing to finite dimensional discrete time or continuous time control problems. As will
   be shown in Appendix A applying an appropriate discretization scheme convergence
   to the original process model can be proven. Using this result one can show that
   the finite dimensional controller derived guarantees stability for the original system
   under additional conditions.

2. The method of moments can be used to derive a lumped model with the moments
   of the particle size distribution being the system states [27, 28, 29, 30]. In special
   cases the moments are closing and this approach gives a finite dimensional system of
   small order describing the dynamics of the moments of the original system. If this is
   not the case, several methods have been proposed in order to force a closing model,
   e.g. quadrature method of moments [5], direct quadrature method of moments [2].
   However, convergence of the approximate moment models to the moments of the
   original model is still an issue. In addition, a controller stabilizing the moment
   model generally does not imply stabilization of the particle size distribution of the
   original model [3].

When dealing with the infinite dimensional model a controller can be derived by

1. Linearization leading to an infinite dimensional state space model or transfer func-
   tion [54, 57]. Using infinite dimensional extensions of

   - H_∞-control theory [58],

   - optimal control theory [82, 93, 60, 55],

   - pole placement [86, 85],

   - root locus theory [95, 81]

   - internal model control [89],

   a controller can be derived being again infinite dimensional. Therefore, for a practi-
   cal implementation, an additional reduction step has to be taken, which may result
   in a loss of stability and performance.

2. Applying generalized Lyapunov stability theory, i.e. stability with respect to two
   discrepancies. This new approach proposed in this Thesis admits direct control
   design without any additional model reduction or simplification step. In addition,
   stability in the traditional sense, i.e. convergence in a L_p or L_∞-norm can be
   guaranteed under some conditions. Beyond, the scope of the present Thesis it was
   also successfully applied to crystallization processes in [35].

Compared to crystallization processes, only little work has been reported on the control of granulation processes. Main emphasis was on drum granulation (e.g. [13, 14]), for which no open loop instabilities have been reported in the open literature. Therefore, the results presented in this Thesis are the first in the field of control design for fluidized bed spray granulation processes. Parts of them have been published in advance [32, 33, 34].

1.3   Thesis overview

In chapter 2 the investigated continuous fluidized bed spray granulation processes are described introducing the associated population balances models. Chapter 3 is devoted to linear finite dimensional control design using discrete approximations of the underlying population balance models. In order to derive a linear controller with guaranteed stability for the distributed parameter system at different steady states of interest several aspects have to be carefully investigated:

1. The set of steady state solutions and linear finite dimensional approximations have to be calculated.

2. The set of linear finite dimensional models for different set points has to be embedded into the set of a nominal model and an appropriate uncertainty model.

3. Convergence of the applied numerical discretization scheme has to be guaranteed in order to derive an estimate for the discretization error.

4. Applying linear robust control theory, a controller has to be derived such that its robustness margin covers the family of all infinite dimensional linear approximations of the original plant in order to guarantee stability in a certain neighborhood of the path of set points.

5. In order to allow for changes in the set point and automatic process start-up an appropriate feedforward control has to be designed.

In chapter 4 a new nonlinear control approach for particulate processes, called discrepancy based control, is developed and applied to continuous fluidized bed spray granulation. After calculating the steady state solutions analytically and briefly reviewing stability and control theory for distributed parameter systems, the concept of a generalized distance measure, called discrepancy, and the associated stability theory are introduced. On the basis of the stability with respect to two discrepancies nonlinear control laws for continuous fluidized bed spray granulation are derived and tested by means of numerical simulations.

Chapter 2

Continuous fluidized bed spray granulation

Two typical continuous fluidized bed spray granulation processes applied in industry are continuous fluidized bed spray granulation with internal [12] and external [4] product classification. Interestingly, both are reported to exhibit the aforementioned qualitative change in stability. Thus both will be studied in this Thesis.

In this chapter the associated population balance models of both configurations are presented. Afterwards the qualitative process behavior is studied by numerical bifurcation analysis. Here, the numerical parameter continuation results in a set of steady state solutions and the associated set of linear models. The steady state solutions will be used to derive a start-up strategy for the linear control design. Whereas, the set of linear models will serve in chapter 3 to derive a nominal model and an associated uncertainty model for robust control design.

2.1 Continuous fluidized bed spray granulation with internal product classification

The process scheme of continuous fluidized bed spray granulation with internal product classification is depicted in Fig. 2.1. The granulator consists of a granulation chamber, where the particle population is fluidized through an air stream and coated by injecting a suspension $\dot{V}_e$.

The associated particle growth has been described in [6] under the assumption that the suspension evenly distributes on the particle surfaces A. Hence, the growth rate G is inverse proportional to the second moment μ_2. In Vreman et. al. [12] the growth rate has been slightly modified to account for internal nucleation. In this extended approach only a certain part of the injected suspension $((1-b)\dot{V}_e)$ contributes to the particle growth

$$G = \frac{2(1-b)\dot{V}_e}{\pi \int_0^\infty L^2 n dL} = \frac{2(1-b)\dot{V}_e}{\pi \mu_2}, \qquad (2.1)$$

with $b \in [0, 1]$. The rest of the suspension $(b\dot{V}_e)$ results in new nuclei due to drying spray droplets, which completely dry before hitting existing particles in the bed. Here, it is assumed that the size distribution of the formed nuclei is a normal distribution with a mean diameter L_0 as depicted in Fig. 2.2.
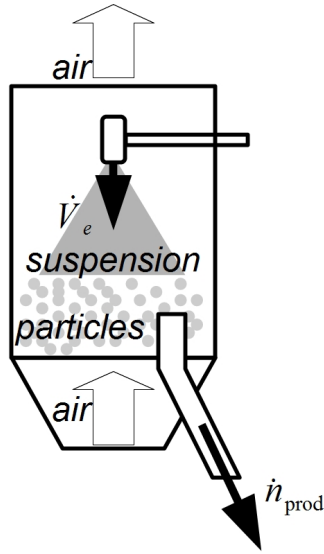
Figure 2.1: Process scheme
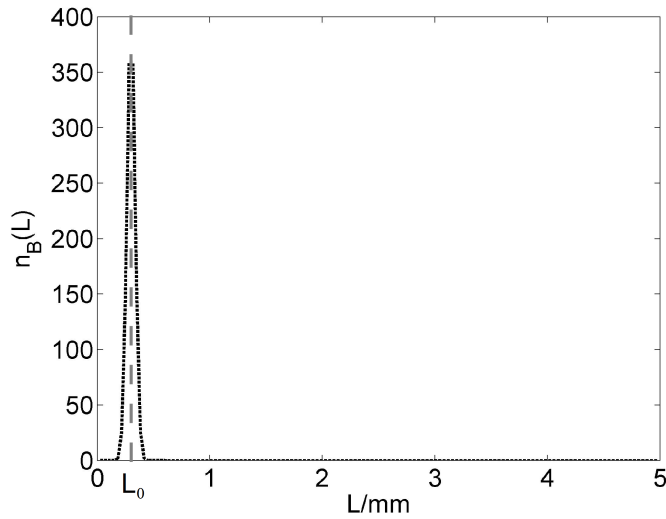
Figure 2.2: Normal distribution of formed nuclei $n_B(L)$

$$B = \frac{b\dot{V}_e}{\frac{1}{6}\varrho\pi} \frac{e^{-\frac{(L-L_0)^2}{a^2}}}{\int_0^\infty L^3 e^{-\frac{(L-L_0)^2}{a^2}} dL} = \frac{b\dot{V}_e}{\frac{1}{6}\varrho\pi} n_B(L) \tag{2.2}$$

The nucleation parameter b, which determines how much of the injected suspension results in new particles, is assumed to depend only on the bed height h, which can be obtained from

$$h = \frac{V}{(1-\varepsilon)A}, \tag{2.3}$$

where ε is the bed porosity. In the following the bed porosity ε is assumed to be constant. With increasing bed height h the free distance for the spray droplets decreases resulting in a decreasing nuclei formation. The minimum of the nucleation parameter b_∞ is reached, when the bed reaches the height of the nozzle. For further increasing bed height the
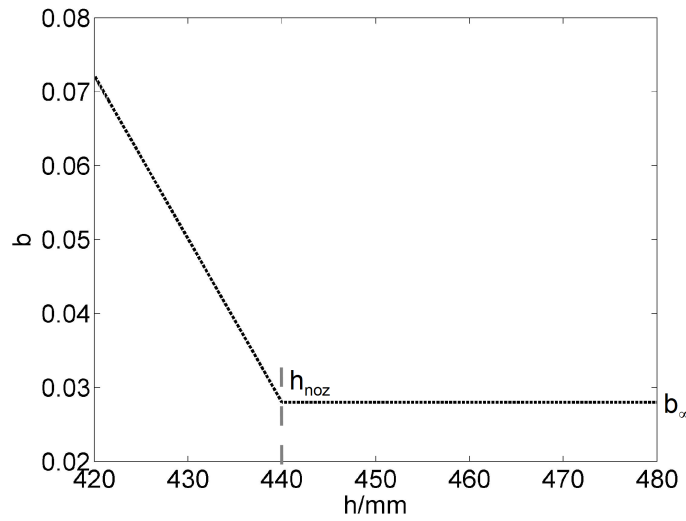
Figure 2.3: Dependence of the nucleation parameter b on the bed height h according to Vreman et al. [12] with $h_{noz} = 440mm$

nucleation parameter b is assumed to remain constant at b_∞. For a minimum bed height of 0 it is assumed that 100 % of the injected suspension forms new particles giving a nucleation parameter of $b = 1$. As can be seen in Fig. 2.3 the nucleation parameter b is interpolated linearly between the two limiting situations $h = 0$ and $h = h_{noz}$ resulting in the following expression

$$b = b_\infty + max\left(0, (1 - b_\infty)\frac{h_{noz} - h}{h_{noz}}\right).\tag{2.4}$$

Product particles are continuously removed through an air sifter with counter current flow, which separates small from large particles. The large particles pass the air sifter while the small particles are reblown into the granulation chamber. The associated non-ideal separation function T shown in Fig. 2.4

$$T(L) = \frac{\int_0^L e^{-\frac{(L'-L_1)^2}{a^2}}dL'}{\int_0^\infty L^3 e^{-\frac{(L-L_1)^2}{a^2}}dL}\tag{2.5}$$

results with the drain K in the following outlet flow

$$\dot{n}_{prod} = KT(L)n.\tag{2.6}$$

To describe the process, a population balance model for the particle size distribution has been proposed recently in [12] consisting of the following particle fluxes

- $\dot{n}_{prod}$ particle flux due to product removal,

- B particle flux due nuclei formation,

and particle growth associated with the size independent growth rate G

$$\frac{\partial n}{\partial t} = -G\frac{\partial n}{\partial L} - \dot{n}_{prod} + B.\tag{2.7}$$
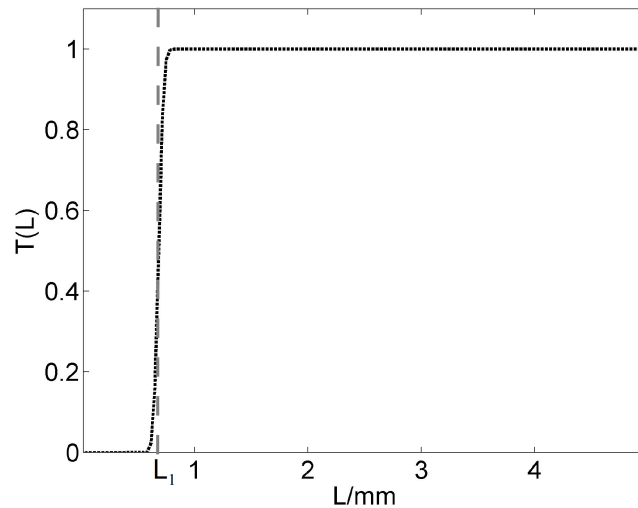
Figure 2.4: Non-ideal separation function T due to classifying product removal

For numerical simulation the model equations are semi-discretized with the finite volume method (1st order upwind flux discretization) with 150 grid points. Time integration is performed using *ode15s* from the Matlab ODE suite and the third order strong stability preserving Runge-Kutta [51] given in Appendix A. Details regarding the numerical method are presented in Appendix A. The model parameters used are given in table 2.1.

A	$5 \cdot 10^6 mm^2$
h_{noz}	$440mm$
ε	0.5
$\dot{V}_e$	$1.67 \cdot 10^5 \frac{mm^3}{s}$
b_∞	0.028
L_0	$0.3mm$
L_1	$0.7mm$
K	$1.92 \cdot 10^{-4}\frac{1}{s}$

Table 2.1: Plant parameters

Starting with an initial particle size distribution as depicted in Fig. 2.5, which is the steady state particle size distribution for $\dot{V}_{e,0} = 16800\frac{mm^3}{s}$, the model shows interesting dynamic behavior. For sufficiently high suspension injection rates and an associated bed height higher than the nozzle height, transition processes decay and the particle size distribution and its moments $\mu_0, \ldots, \mu_3$ reach a stable steady state (Fig. 2.6). Decreasing the suspension injection rate below a critical value gives rise to nonlinear oscillations in the particle size distribution and its moments $\mu_0, \ldots, \mu_3$ (Fig. 2.7).
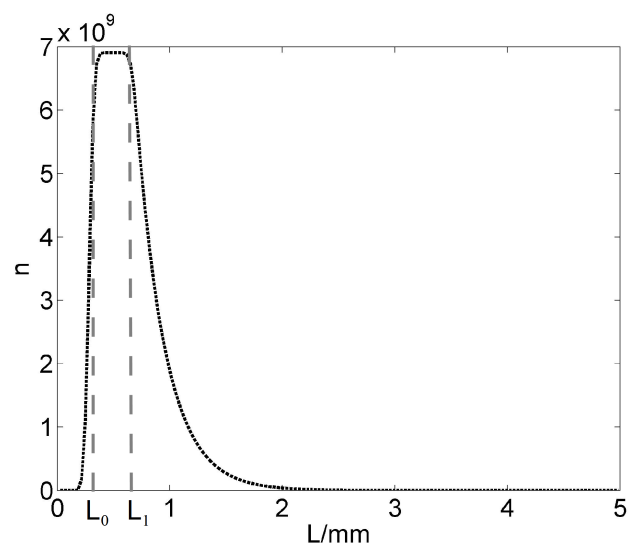
Figure 2.5: Initial condition
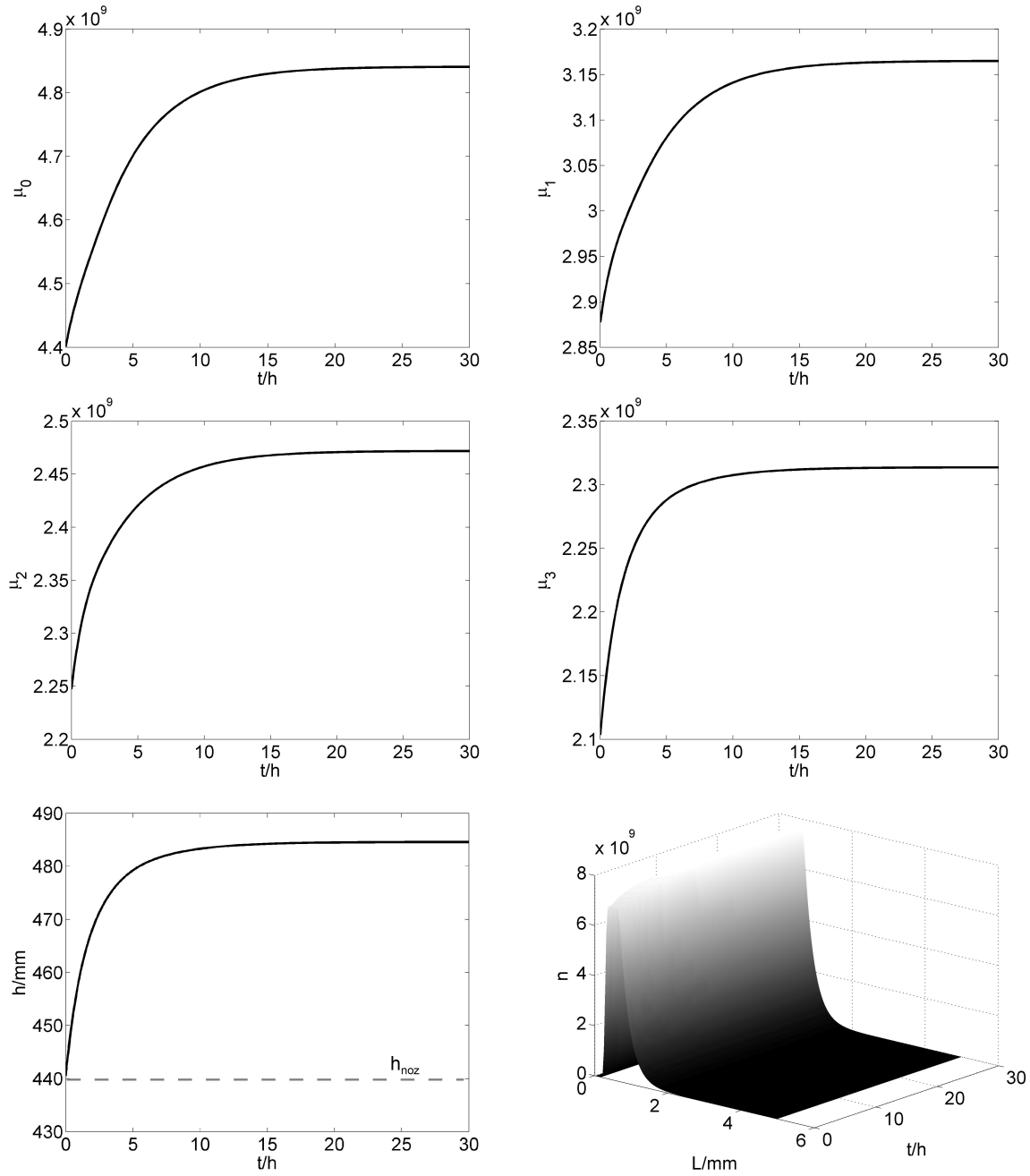
Figure 2.6: Open-loop simulation in the stable region $\dot{V}_e = 1.1 \cdot \dot{V}_{e,0}$
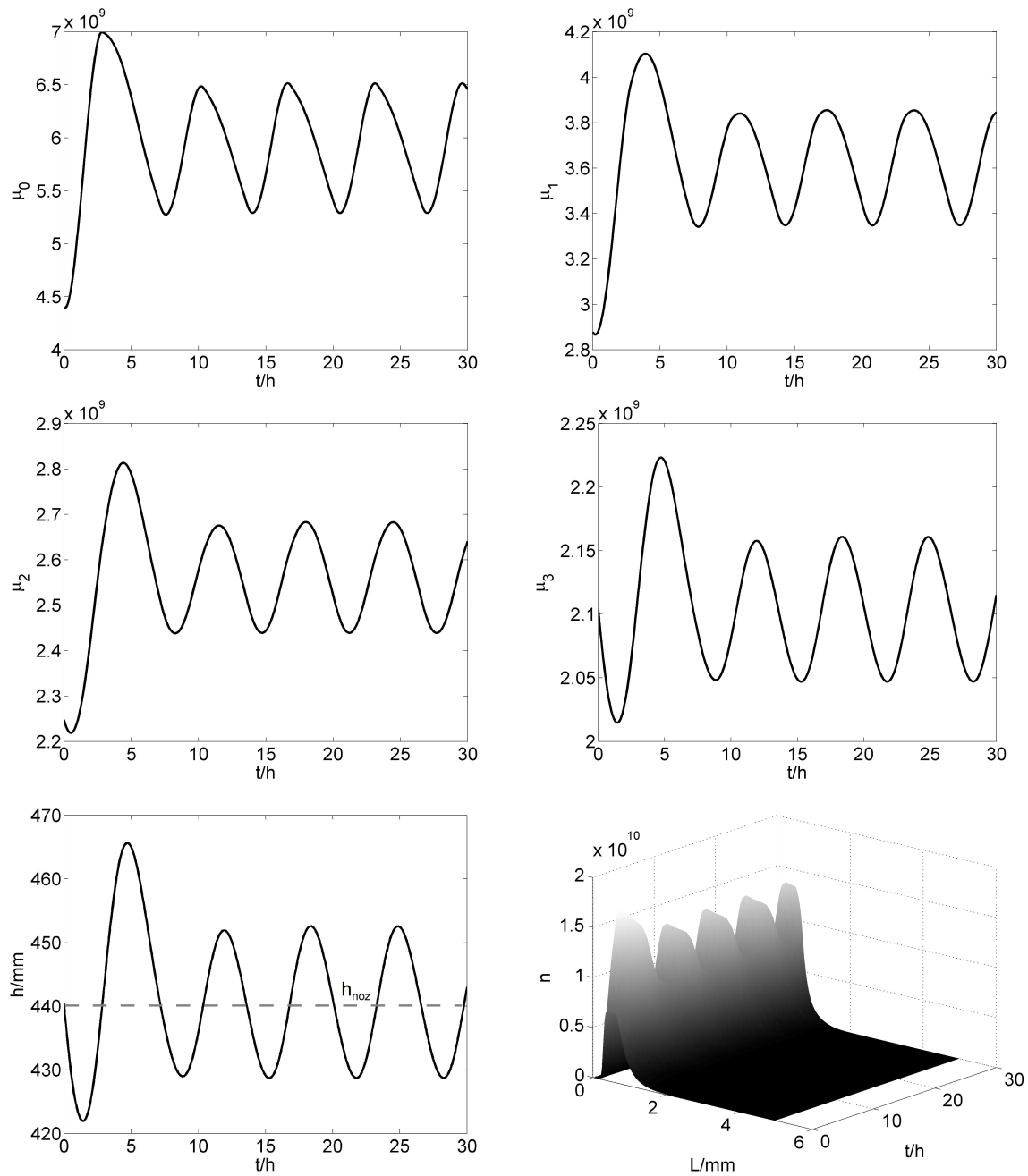
Figure 2.7: Open-loop simulation in the unstable region $\dot{V}_e = 0.9 \cdot \dot{V}_{e,0}$

Here, the associated mechanism is as follows:

- For a bed height smaller than the nozzle height an increased production of nuclei with mean diameter L_0 takes place due to spray drying (Fig. 2.8 a).

- This results in a high number of small particles and a reduced growth rate.

- After a certain time the bed height reaches the nozzle height, resulting in a small and constant production of nuclei and a higher growth rate (Fig. 2.8 b and c).

- When the peak of the particle size distribution reaches the critical particle radius L_1 the associated particles are removed from the granulator (Fig. 2.8 d). This is connected with a decrease of the bed height below the nozzle height and hence the process repeats.

In contrast, a high suspension rate results in a permanent high production of nuclei, a higher growth rate and therefore a bed height being bigger than the nozzle height. Hence, after a transition time the steady state particle size distribution is reached and no oscillations occur.
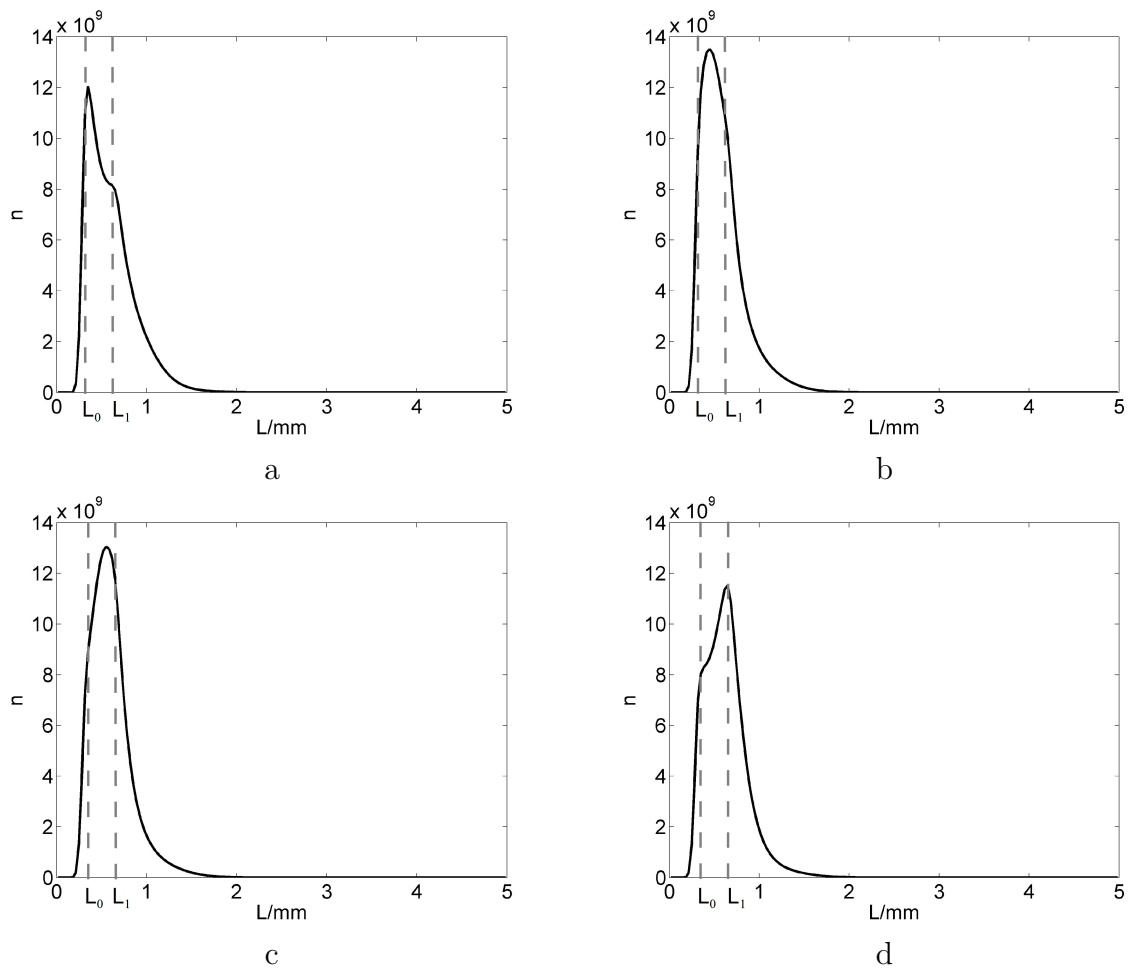
Figure 2.8: Mechanism of oszillations

2.2 Continuous fluidized bed spray granulation with external product classification

In contrast to the continuous fluidized bed spray granulation with internal product classification in the continuous fluidized bed spray granulation with external production new nuclei are generated from a oversize fraction by a mill. Typically, nucleation due to spray drying is negligible in this configuration. The process scheme is depicted in Fig. 2.9. The granulator consists of a granulation chamber, where the particle population is fluidized through an air stream and coated by injecting a suspension $\dot{m}_e$. The associated particle growth has been described in [6]

$$G = \frac{2\dot{m}_e}{\varrho A} = \frac{2\dot{m}_e}{\varrho \pi \mu_2}. \tag{2.8}$$
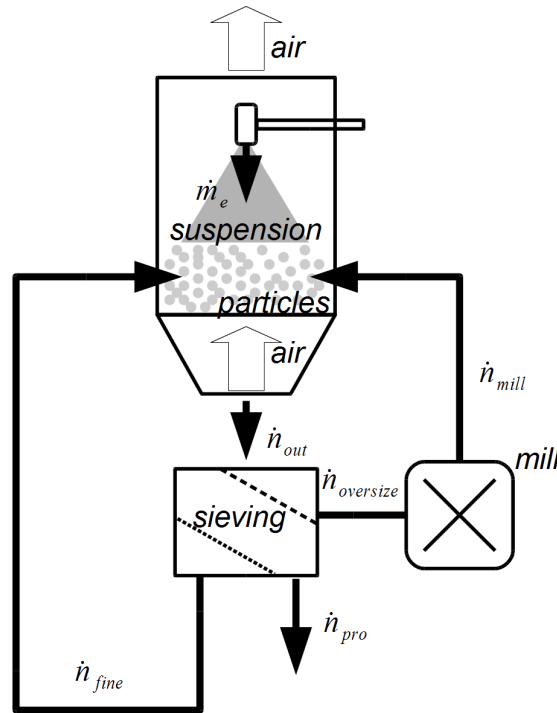
Figure 2.9: Process scheme

In the continuous configuration of the fluidized bed spray granulation particles are continuously removed in order to achieve a constant bed mass, which correlates to a constant third moment of the particle number distribution $\mu_3 = \int_0^\infty L^3 n dL$.
The particle flux being removed from the granulator is

$$\dot{n}_{out} = Kn. \tag{2.9}$$

where K is the drain which follows from the assumption of a constant bed mass and which is derived later. The removed particles are then sieved in two sieves and separated into three classes:
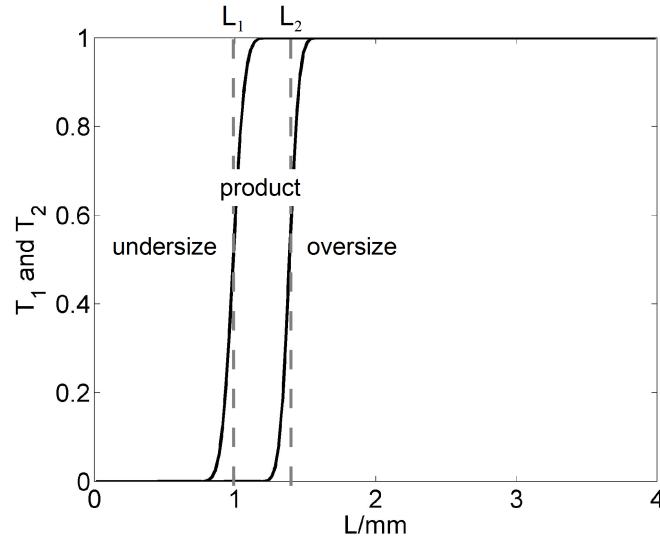
Figure 2.10: Non-ideal separation functions T_1 and T_2 due to sieving

1. Fine particles, which are fed directly back to the granulator

$$\dot{n}_{fines} = (1 - T_2)(1 - T_1)\dot{n}_{out},$$ (2.10)

2. Product particles, which are removed from the whole process

$$\dot{n}_{prod} = T_2(1 - T_1)\dot{n}_{out},$$ (2.11)

3. Oversized particles, which are grinded in a mill and fed back to the ganulator

$$\dot{n}_{oversize} = T_1\dot{n}_{out}.$$ (2.12)

The separation functions T_1 and T_2 for the two screens are depicted in Fig. 2.10.

$$T_{1/2} = \frac{\int_0^L e^{-\frac{\left(L' - \mu_{1/2}\right)^2}{2\sigma_{1/2}^2}} dL'}{\int_0^\infty e^{-\frac{\left(L' - \mu_{1/2}\right)^2}{2\sigma_{1/2}^2}} dL'}.$$ (2.13)

To describe the process, a population balance model for the particle size distribution has been derived in [4]. In this Thesis a simplified model is used neglecting external seeding, attrition and overspray. Nevertheless, open-loop simulations give comparable results.
In the model fine particles are fed directly back to the granulator, which results in a cancellation of the associated sink and source. Hence the simplified population balance equation consists of the following particle fluxes:

- $\dot{n}_{prod}$ particle flux due to product removal,

- $\dot{n}_{oversize}$ particle flux due to oversize removal,

- $\dot{n}_{mill}$ particle flux due to particles fed back from the mill,
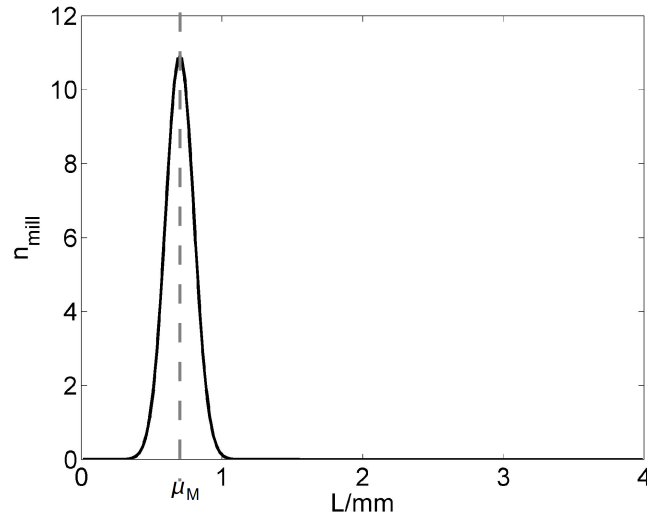
Figure 2.11: Particle size distribution of milled particles n_{mill}

and particle growth associated with the size independent growth rate G

$$\frac{\partial n}{\partial t} = -G\frac{\partial n}{\partial L} - \dot{n}_{prod} - \dot{n}_{oversize} + \dot{n}_{mill}. \tag{2.14}$$

The particle distribution fed back from the mill is assumed to be a normal distribution as shown in Fig. 2.11, where the mean diameter μ_M represents the mill grade. The particle flux from the mill is given by

$$\dot{n}_{mill} = 6\frac{e^{-\frac{\left(L-\mu_M\right)^2}{2\sigma_M^2}}}{\sqrt{2\pi}\pi\varrho\sigma_M}\int_0^\infty L^3\dot{n}_{oversize}dL. \tag{2.15}$$

Assuming ideal mass control the drain K is calculated such that the time derivative of μ_3 becomes zero implying a constant bed mass

$$\dot{\mu}_3 = \int_0^\infty L^3\frac{\partial n}{\partial t}dL = 0 \tag{2.16}$$

$$= \int_0^\infty L^3\left[-G\frac{\partial n}{\partial L} - \dot{n}_{oversize} - \dot{n}_{prod} + \dot{n}_{mill}\right]dL. \tag{2.17}$$

Because the mill is assumed to be mass conserving the third moments of the oversize flux and mill flux are equal resulting in

$$0 = \int_0^\infty L^3\left[-G\frac{\partial n}{\partial L} - \dot{n}_{prod}\right]dL \tag{2.18}$$

$$= 3G\int_0^\infty L^2ndL - K\int_0^\infty L^3T_2(1-T_1)ndL. \tag{2.19}$$

Here the fact that the particle size distribution vanishes at the boundary $(n(0,t) = \lim_{L\to\infty} n(L,t) = 0)$ has been used for integration by parts. Solving equation (2.19) for the drain K yields

$$K = \frac{3G \int_0^\infty L^2 n dL}{\int_0^\infty L^3 T_2 (1 - T_1) n dL}. \tag{2.20}$$

For numerical simulation the model equations are semi-discretized with the finite volume method (1st order upwind flux discretization) with 160 grid points. Time integration is performed using *ode15s* from the Matlab ODE suite and the third order strong stability preserving Runge-Kutta [51] given in Appendix A. Details regarding the numerical method are presented in Appendix A. The model parameters used are given in table 2.2.

Hold-up	
ϱ	$1.6 \cdot 10^{-3} \frac{g}{mm^3}$
m_{init}	$100 kg$
$\dot{m}_e$	$\frac{100}{3.6} \frac{g}{s}$
Screens	
μ_1	$1.4 mm$
σ_1	$0.055 mm$
μ_2	$1 mm$
σ_2	$0.065 mm$
Mill	
μ_M	$0.9 mm$
σ_M	$0.1 mm$

Table 2.2: Simulation parameters

The qualitative dynamical behavior of the fluidized bed spray granulation with external product classification strongly depends on the process parameters [4, 9]. For sufficiently high mill grade, transition processes decay and the particle size distribution reaches a stable steady state (Fig. 2.12). Decreasing the mill grade below a critical value gives rise to nonlinear oscillations (Fig. 2.13).
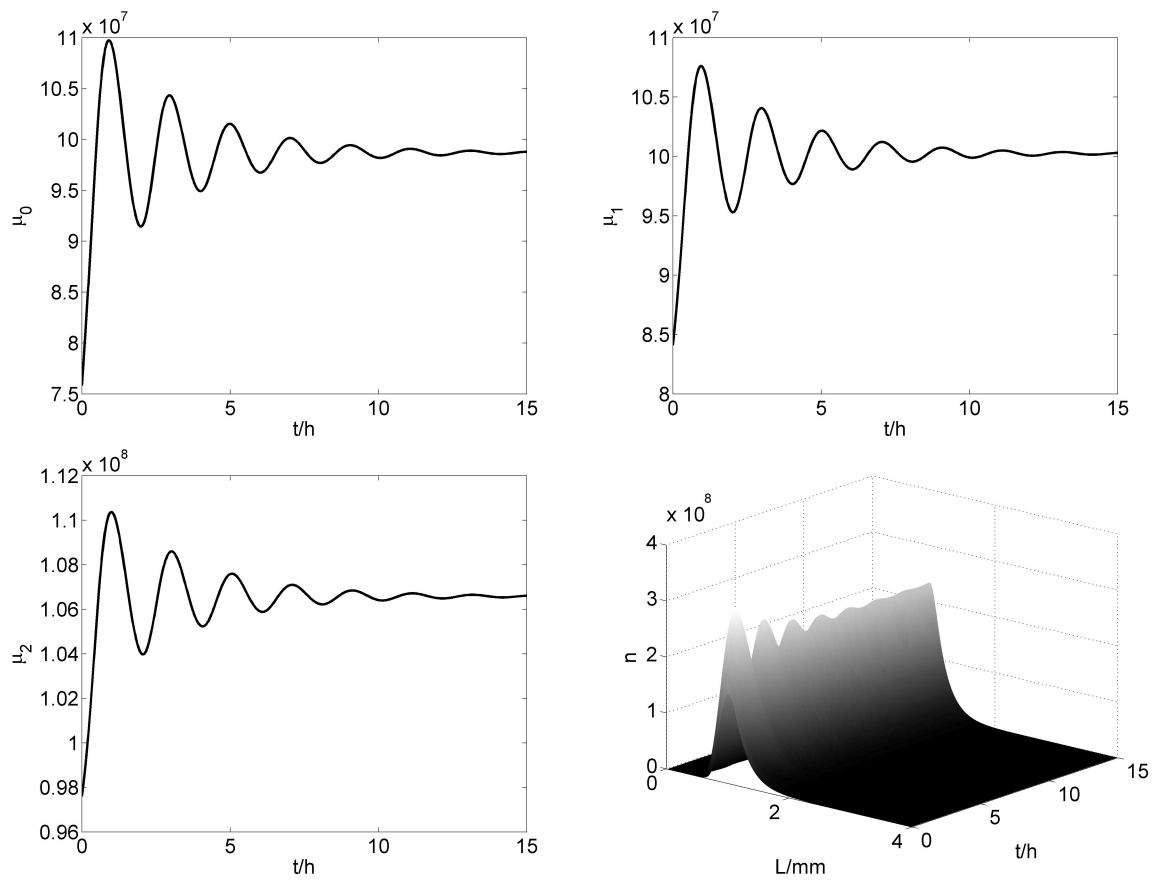
Figure 2.12: Open-loop simulation in the stable region $\mu_M = 0.8mm$
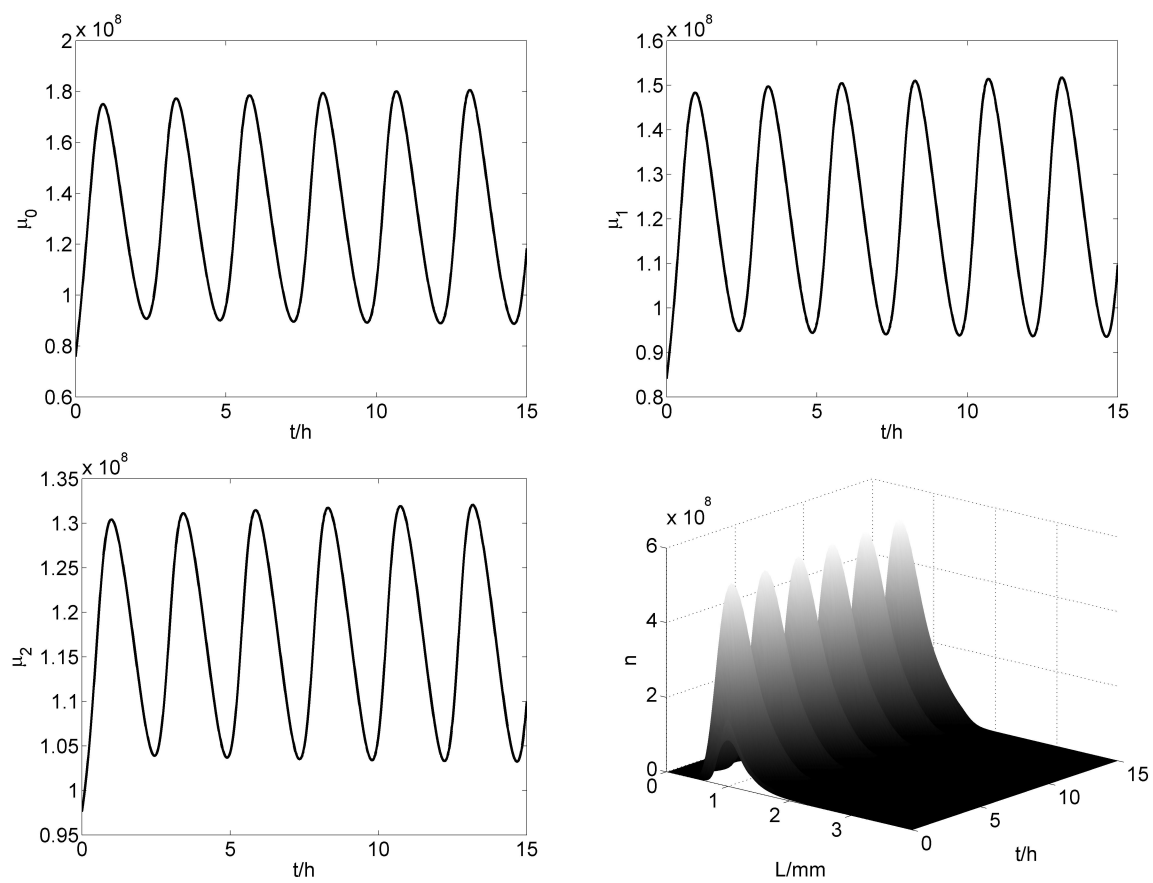
Figure 2.13: Open-loop simulation in the unstable region $\mu_M = 0.7mm$
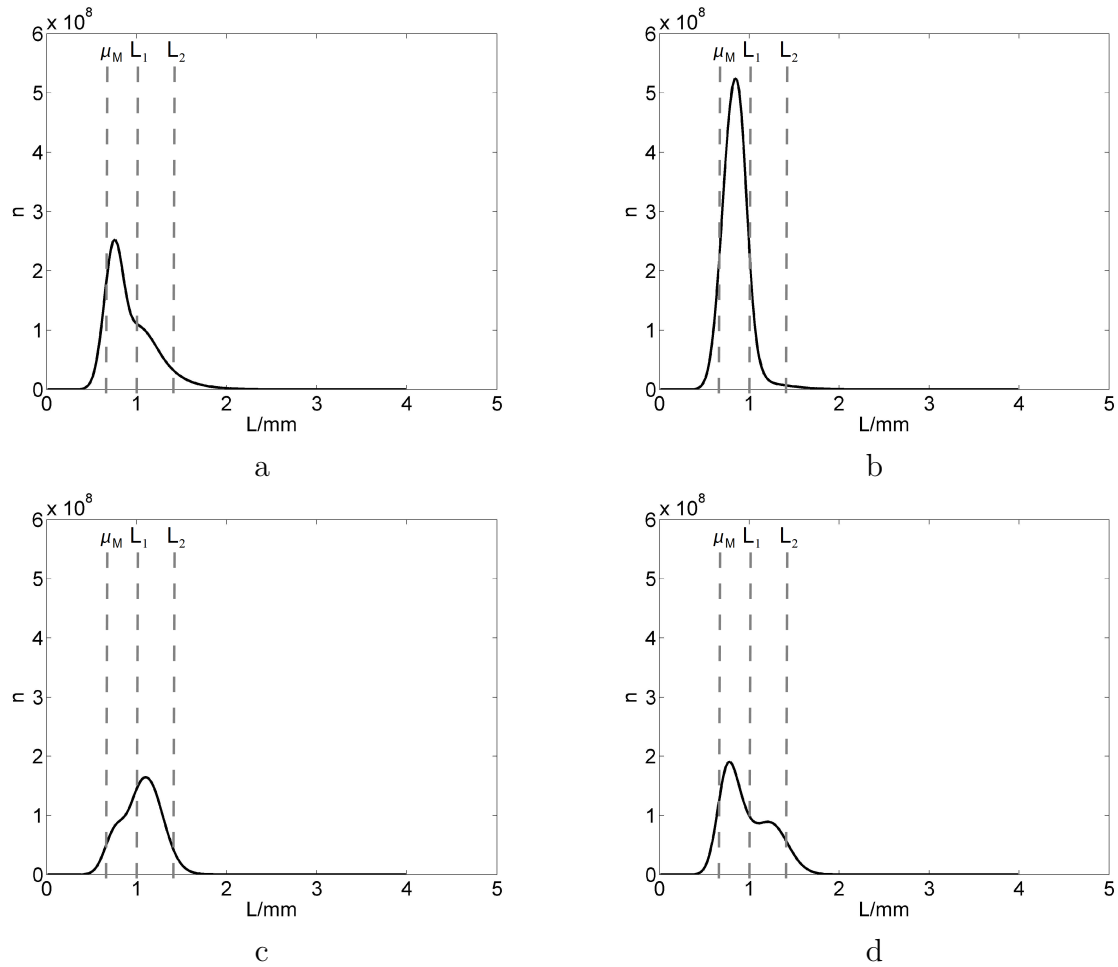
Figure 2.14: Mechanism of oscillations

The associated mechanism leading to nonlinear oscillations is as follows:

- For fine grinding the population surface excessively increases due to the smaller particles fed back from the mill. This results in a very small growth rate (Fig. 2.14 a).

- Hence, the particle flux from the oversize fraction and therefore the mill reflux are vanishing, which gives a slowly growing particle size distribution of small particles (Fig. 2.14 b).

- When the peak of this particle size distribution reaches the oversize fraction the number of small particles again increases excessively and the whole process thus repeats (Fig. 2.14 c and d).

In contrast, for a large mill grade increase in the overall particle surface is smaller preventing an excessive decrease in the growth rate. Hence, the particle flux from the oversize fraction does not vanish resulting in a constant production of nuclei.

2.3 Numerical parameter continuation and steady state calculation

It is well known, that qualitative properties as stability of equilibrium, existence of limit cycles etc., can change for a nonlinear dynamic system under parameter variations [102, 26, 9]. In particular, this phenomenon has been observed for the fluidized bed spray granulation in both configurations [9, 12]. In order to derive a complete picture of the qualitative process behavior in a certain parameter range a bifurcation analysis is useful. Here, the same semi-discretized versions of the population balance models as for the dynamic simulation are used, i.e.

$$\dot{n} = f(n, p) \tag{2.21}$$

where p is the bifurcation parameter. For the continuous fluidized bed spray granulation with external product classification the mill grade μ_M has been chosen as the bifurcation parameter [9]. For the continuous fluidized bed spray granulation with internal product classification stability has been shown to depend on the injection rate $\dot{V}_e$ [12], which is therefore chosen as the bifurcation parameter.
First, steady states $n_{p,s}$ are calculated in dependence of the bifurcation parameter $p = \{\mu_M, \dot{V}_e\}$ by continuation methods.

$$0 = f(n_{p,s}, p) \tag{2.22}$$

For this purpose an initial steady state particle size distribution $n_{s,0}$ is generated by time integration for a nominal value $p_0 = \{\mu_{M,0} = 0.9mm, \dot{V}_{e,0} = 1.67 \cdot 10^5 \frac{mm^3}{s}\}$, for which a stable steady state is found. Then, using this initial steady state solution $n_{p_0,s}$ as a prediction for a new steady state solution $n_{p_1,pred}$ for a different bifurcation parameter $p_1 = \{\mu_{M,1}, \dot{V}_{e,1}\}$,

$$n_{p_1,pred} = n_{p_0,s} \tag{2.23}$$

a steady state solution $n_{p_1,s}$ is obtained by a corrector step involving numerical minimization of the L_1-norm of the residuals of dn_i/dt. This is repeated for a successively decreasing $p = \{\mu_M, \dot{V}_e\}$ from $\mu_{M,0} = 0.9mm$ to $0.5mm$ and $\dot{V}_{e,0}$ to $0.8\dot{V}_{e,0}$, respectively. Along the branch the local stability of the computed steady states is determined by solving the eigenvalue problem for the linearized system. Here, special care has to be taken as the condition of constant hold up mass for the continuous fluidized bed spray granulation with external classification, i.e. $\dot{\mu}_3 = 0$, has to be taken explicitly into account as an additional equality constraint giving a constrained optimization problem. Whereas the steady state problem for the fluidized bed spray granulation with internal classification is an unconstrained optimization problem.

2.3.1 Bifurcation analysis - internal product classification

At a certain point $\dot{V}_{e,BP}$ two conjugate complex eigenvalues occur in the right-half plane. Beyond this point the steady states solutions are unstable. Further investigation of the time behavior in this region shows, that a stable limit cycle occurs. The described behavior is depicted in Fig. 2.15, where thick continuous lines represent stable stationary solutions, dashed lines unstable stationary solutions and dots the maximal and minimal amplitudes
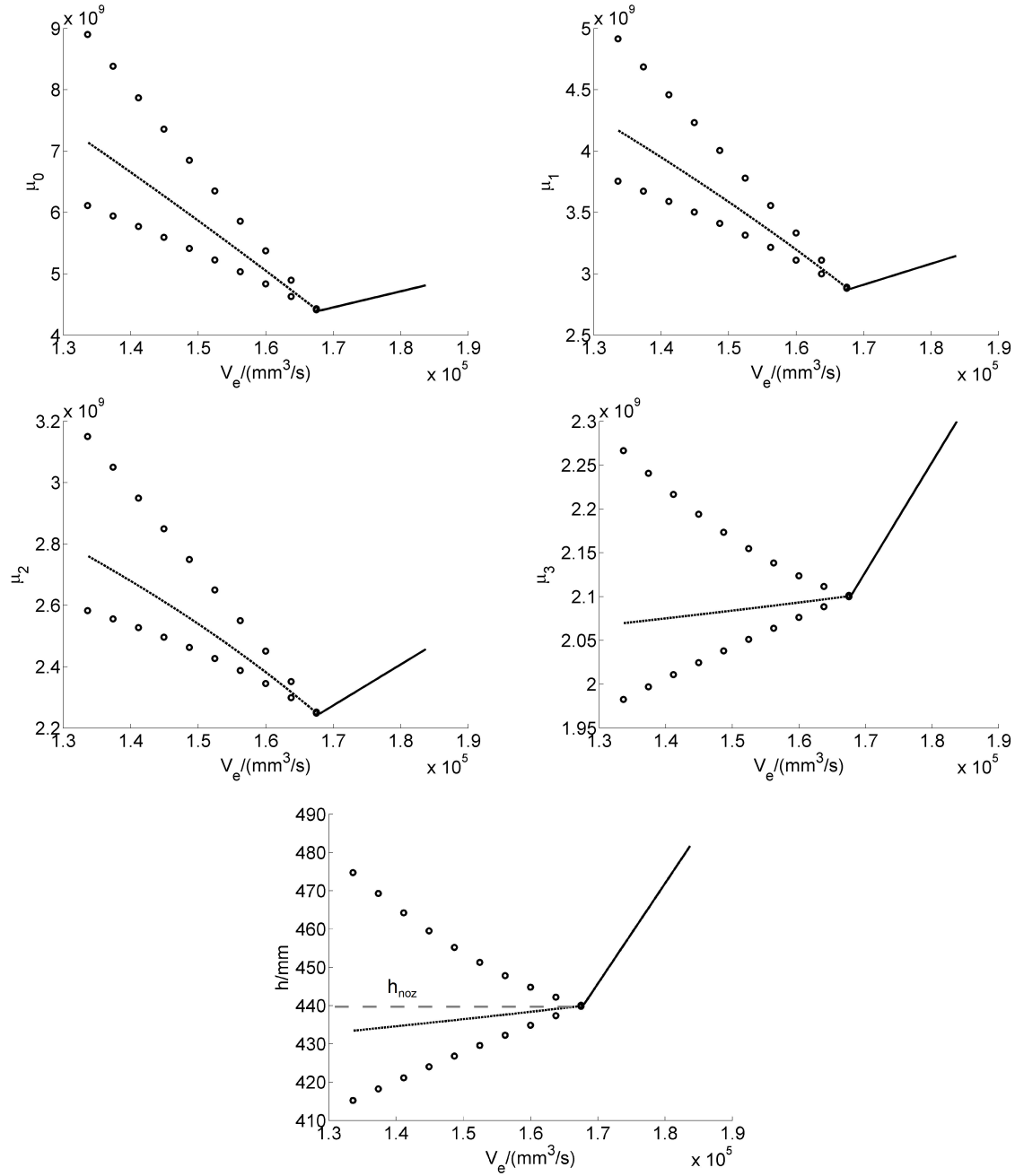
Figure 2.15: One-parameter bifurcation diagrams depending on $\dot{V}_e$

of the observed oscillations, i.e. limit cycles.

As can be seen from the bifurcation diagram in Fig. 2.15 the moments μ_0, μ_1 and μ_2 are non-monotone functions of $\dot{V}_e$, which would result in uniqueness problems when choosing $\dot{V}_e$ as a control input and one of these moments as the controlled variable. This phenomenon, i.e. the abrupt change in the slope of the bifurcation curves and the loss of monotonicity, is connected to the nozzle height h_{noz} and occurs when the bed reaches the height of the nozzle as can be seen in Fig. 2.15.
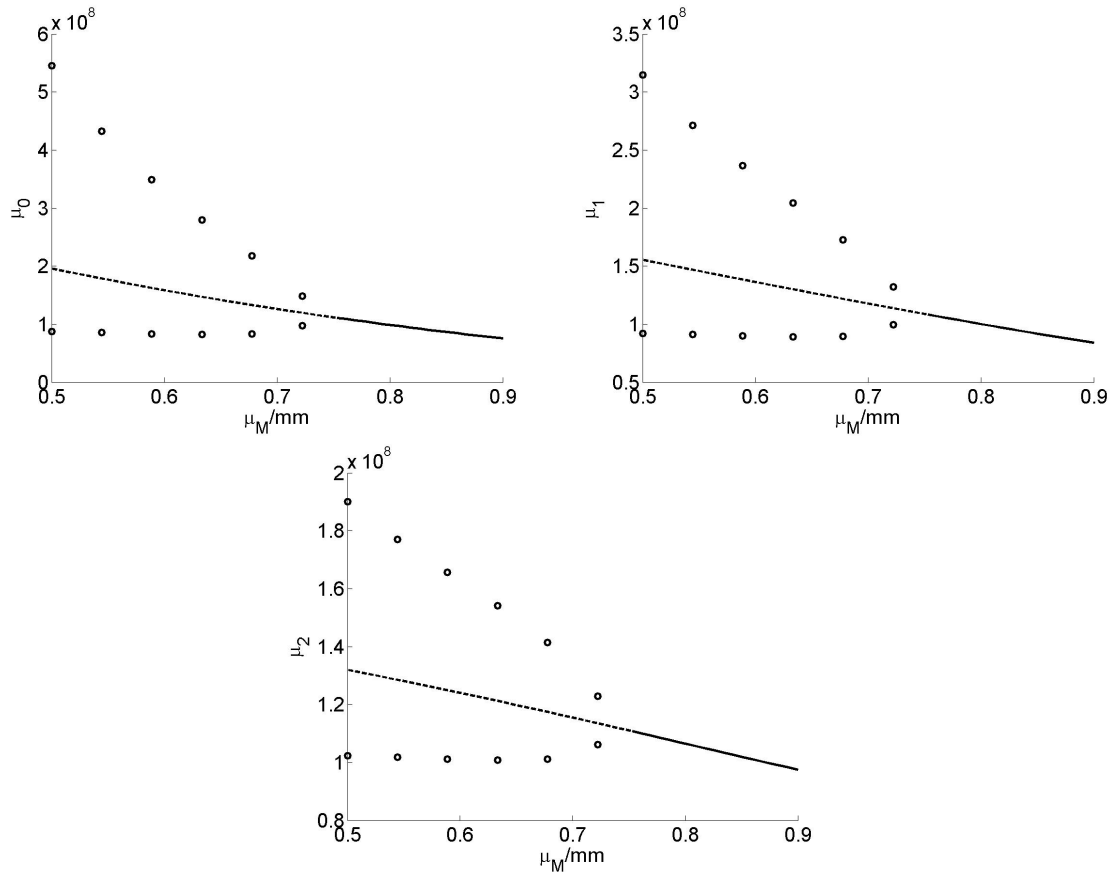
Figure 2.16: One-parameter bifurcation diagrams depending on μ_M

2.3.2   Bifurcation analysis - external product classification

At a certain point $\mu_{M,BP}$ two conjugate complex eigenvalues cross the imaginary axis and occur in the right-half plane. Beyond this point the steady states solutions are hence unstable and a stable limit cycle occurs. The described behavior is depicted in Fig. 2.16, where thick continuous lines represent stable stationary solutions, dashed lines unstable stationary solutions and dots the maximal and minimal amplitudes of the observed oscillations, i.e. limit cycles.

2.4   Analytical steady state calculation

An alternative approach to a numerical calculation of the steady state particle size distribution n_s as presented in the previous section is of course an analytical derivation. In order to derive easy to handle steady state population balances preceding model simplifications are convenient. This can be achieved by some minor changes affecting only the shape functions of the population balance equations, i.e. the full structure of the model is maintained.

2.4.1   Simplification and analytical steady state calculation - internal product classification

In order to derive a steady state solution for the particle size distribution of the fluidized bed spray granulation with internal product classification the model is to complicated and should hence be simplified. The original smooth classification function is therefore replaced by its discontinuous counterpart as shown in Fig. 2.17.

$$T = \frac{\int_0^L e^{-\frac{(L'-L_1)^2}{a^2}} dL'}{\int_0^\infty L^3 e^{-\frac{(L-L_1)^2}{a^2}} dL} \approx \sigma\left(L - L_1\right) \tag{2.24}$$
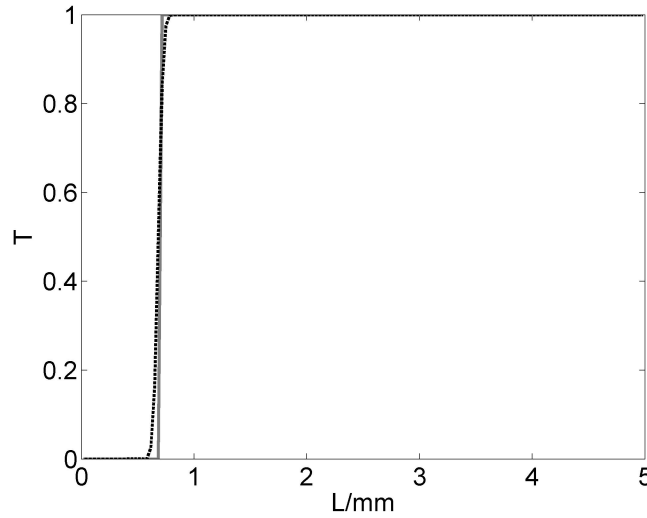
Figure 2.17: Original (dotted black) and simplified (solid gray) classification function T

The same is done for the original smooth normal distribution of nuclei particles, which is replaced by the normalized delta distribution as depicted in Fig. 2.18.

$$n_B = \frac{e^{-\frac{(L-L_0)^2}{a^2}}}{\int_0^\infty L^3 e^{-\frac{(L-L_0)^2}{a^2}} dL} \approx \frac{1}{L_0^3}\delta(L - L_0) \tag{2.25}$$

It should be mentioned that this simplified model formulation corresponds with the model presented in Vreman et. al. [12].
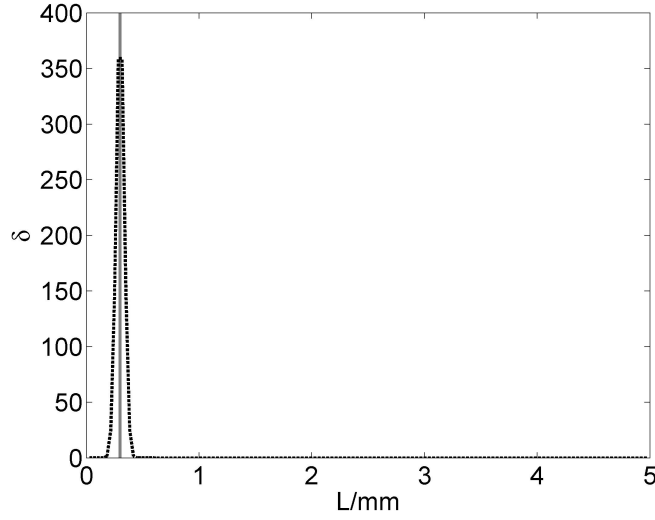
Figure 2.18: Original (dotted black) and simplified (solid gray) distribution of nuclei particles n_B

In steady state the particle size distribution is constant, i.e. $\partial n/\partial t = 0$. Therefore, the simplified population balance equation being a nonlinear partial integro-differential equation becomes a nonlinear integro-differential equation.

$$\frac{dn_s}{dL} = \frac{1}{G}\left(\frac{b\dot{V}_e}{\frac{1}{6}\pi L_0^3}\delta(L-L_0) - K\sigma(L-L_1)n_s\right) \qquad (2.26)$$

The solution of the nonlinear integro-differential equation is derived according to e.g. [128] by integration over the length L. Details are presented in Appendix B. The steady state particle size distribution $n_s(L)$

$$n_s(L) = \frac{b\dot{V}_e}{\frac{1}{6}\pi G_s L_0^3}\left[(\sigma(L-L_0) - \sigma(L-L_1)) + \sigma(L-L_1)\exp\left(-\frac{K}{G_s}(L-L_1)\right)\right], \quad (2.27)$$

depends on the steady state growth rate G_s, which can be determined by the following nonlinear equation

$$\frac{6b}{L_0^3}\left(\frac{1}{3}\left(L_1^3 - L_0^3\right) + \frac{L_1^2 G_s}{K} + 2\frac{L_1 G^2}{K^2} + 2\frac{G_s^3}{K^3}\right) = 2(1-b). \qquad (2.28)$$

Thus, solving the nonlinear equation for G_s for a given suspension injection rate $\dot{V}_e$ yields the associate steady state particle size distribution. As can been seen in Fig. 2.19 the steady state particle size distribution for the original and simplified model match well.
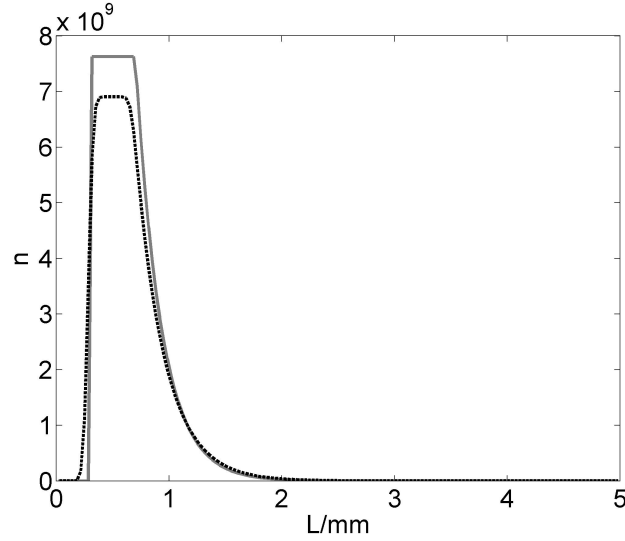
Figure 2.19: Original (dotted black) and simplified (solid gray) steady state particle size distribution n_s for $\dot{V}_e = 1.67 \cdot 10^5 \frac{mm^3}{s}$

2.4.2   Simplification and analytical steady state calculation - external product classification

In accordance with the fluidized bed spray granulation with internal product classification the model with external product classification has to be simplified. This is achieved by replacing the separation functions and the milled particle size distribution by there discontinuous counterparts.

The sieving functions T_1 and T_2 are replaced by the heaviside step functions as shown in Fig. 2.20.

$$T_{1/2} = \frac{\int_0^L e^{-\frac{\left(L'-\mu_{1/2}\right)^2}{2\sigma_{1/2}^2}} dL'}{\int_0^\infty e^{-\frac{\left(L-\mu_{1/2}\right)^2}{2\sigma_{1/2}^2}} dL} \approx \sigma\left(L - \mu_{1/2}\right) \tag{2.29}$$

The original smooth milled particle size distribution n_M is replaced by the normed rectangular function as shown in Fig. 2.4.2.

$$n_M \approx \frac{\sigma\left(L - (\mu_M - \sigma_M)\right) - \sigma\left(L - (\mu_M + \sigma_M)\right)}{\int_0^\infty L^3 \left[\sigma\left(L - (\mu_M - \sigma_M)\right) - \sigma\left(L - (\mu_M + \sigma_M)\right)\right]} \tag{2.30}$$

$$= 4\frac{\sigma\left(L - (\mu_M - \sigma_M)\right) - \sigma\left(L - (\mu_M + \sigma_M)\right)}{(\mu_M + \sigma_M)^4 - (\mu_M - \sigma_M)^4} \tag{2.31}$$

$$= \frac{\sigma\left(L - (\mu_M - \sigma_M)\right) - \sigma\left(L - (\mu_M + \sigma_M)\right)}{2\mu_M\sigma_M(\mu_M^2 + \sigma_M^2)} \tag{2.32}$$

In steady state the particle size distribution is constant, i.e. $\partial n_s/\partial t = 0$. Hence, the steady state particle size distribution is the solution of the following integro-differential
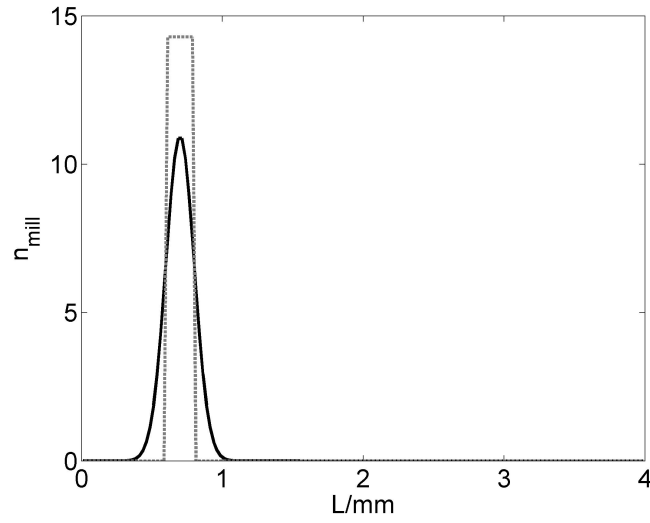
Figure 2.20: Original (solid black) and simplified (dotted gray) distribution of milled particles n_M for $\mu_M = 0.9$
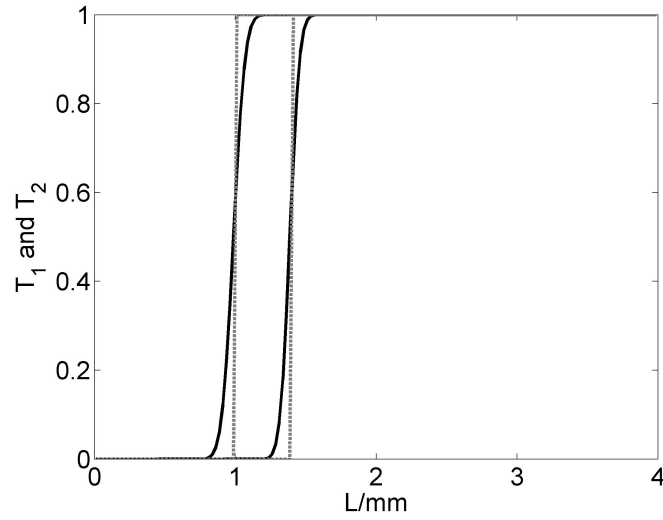
Figure 2.21: Original (solid black) and simplified (dotted gray) separation functions T_1 and T_2

equation.

$$
\begin{aligned}
\frac{\partial n_s}{\partial t} &= 0 = -G(\mu_{2,s})\frac{\partial n_s}{\partial L} - \dot{n}_{prod} - \dot{n}_{oversize} - \dot{n}_{mill} & (2.33) \\
&= -G(\mu_{2,s})\frac{dn_s}{dL} - T_2(1 - T_1)K_s n_s - T_1 K_s n + n_M(\mu_{M,s})\int_0^\infty L^3 T_1 K_s n_s dL & (2.34)
\end{aligned}
$$

Due to the ideal separation functions T_1 and T_2 the product $T_2 T_1$ is equal to T_1. Hence,

the simplified steady state population balance equation becomes

$$\frac{dn_s}{dL} = \frac{K_s}{G(\mu_{2,s})}\left(-T_2 n_s + n_M(\mu_{M,s})\int_0^\infty L^3 T_1 n_s dL\right), \quad (2.35)$$

$$= a\left(-T_2 n_s + n_M(\mu_{M,s})b\right), \quad (2.36)$$

where $a = \frac{K_s}{G(\mu_{2,s})}$ and $b = \int_0^\infty L^3 T_1 n_s dL$. The solution of the nonlinear integro-differential equation is derived by integration over the length L. Details are presented in Appendix C. The steady state particle size distribution $n_s(L)$

$$n_s(L) = abk_M\left[(L - \mu_M + \sigma_M)\sigma(L - \mu_M + \sigma_M) - (L - \mu_M - \sigma_M)\sigma(L - \mu_M - \sigma_M)\right.$$
$$\left. + 2\sigma_M(1 - \exp(-a(L - L_2)))\sigma(L - L_2)\right], \quad (2.37)$$

still depends on the two parameters a and b, where a can be determined by the following nonlinear equation

$$\frac{1}{2k_M \sigma_M} = \left(L_1^3 + \frac{3L_1^2}{a} + \frac{6L_1}{a^2} + \frac{6}{a^3}\right)e^{a(L_2 - L_1)} \quad (2.38)$$

and b is calculated from the total mass m_0.

$$b = \frac{m_0}{\frac{\rho\pi}{6}\int_0^\infty L^3 \bar{n}_s(L)dL} \quad (2.39)$$
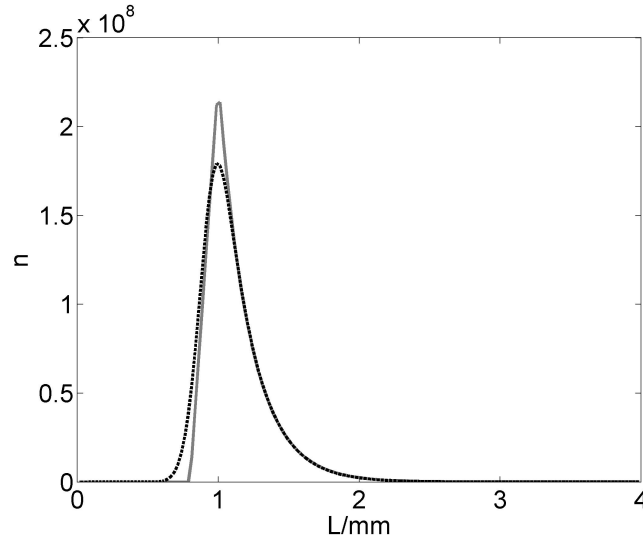
Figure 2.22: Original (dotted black) and simplified (solid gray) steady state particle size distribution n_s for $\mu_M = 0.9mm$

Chapter 3

Linear control based on discretization

This chapter deals with linear finite dimensional controller design for continuous fluidized bed spray granulation with internal and external product classification. Due to the linear control approach stability can hence be guaranteed only in a neighborhood around the steady state of the design model. Applying robust control methods this stability result can be extended to all steady states, which have been investigated by numerical parameter continuation in section 2.3. In addition, a sufficient robust stability margin allows the controller to cope with errors due to numerical discretization (Appendix A). Therefore, the linear robust controller will be able to stabilize the process, i.e. the original infinite dimensional system, in a neighborhood of its steady state particle size distribution.

For a practical implementation the proposed controllers have to be augmented by an appropriate start-up strategy. Here, the main idea is to start the process in the region of stability in open loop operation. As soon as the steady state is reached the control loop is closed. In order to achieve an open loop unstable desired steady state particle size distribution the set-point is shifted. The resulting control structure depicted in Fig. 3.1 thus consists of a feeback and feedforward component.
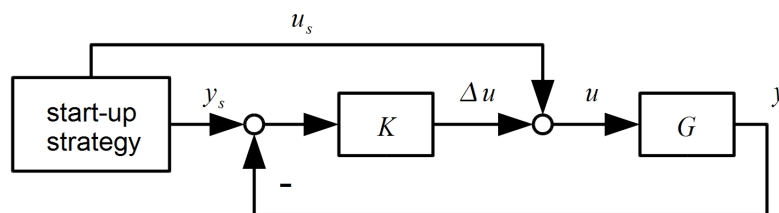
Figure 3.1: Control structure

The structure of this chapter is as follows. In section 3.1 appropriate control handles u and y are identified. In addition, reduced order design models and their associated uncertainties are derived. The error associated to the applied discretization methods is quantified in section 3.2. The linear high order design models are then reduced applying model reduction techniques. The total error and hence the required robustness margin therefore consists of three parts

1. Error due to discretization,

2. Error due to linearization at different steady states,

3. Error due to finite dimensional model reduction.

Finally, finite dimensional robust controllers are designed and tested by means of simulation on the nonlinear plants.

3.1   Finite dimensional control system analysis

3.1.1   Controllability and observability analysis

Before deriving a control law, which is capable to stabilize the steady state solution in the unstable region, the appropriate control in- and outputs have to be chosen. As a candidate for a control input one could choose the bifurcation parameter p, i.e. the mill grade μ_M for the continuous fluidized bed spray granulation with external product classification and the suspension injection rate $\dot{V}_e$ for the continuous fluidized bed spray granulation with internal product classification, which both have a direct influence on the nucleus production. A criterion to check, whether this choice is appropriate for these configurations, is to check for controllability of the state n by the input $u = \{\mu_M, \dot{V}_e\}$. Here, we use the family of linear systems derived along the steady state continuation path.

$$\dot{x} = A(p)x + B(p)u \tag{3.1}$$
$$y = C(p)x + D(p)u \tag{3.2}$$

Then, for each state space model the controllability matrix R_c has to have rank N, where N is the dimension of the A matrix.

$$rank(R_c) = rank\left(\begin{bmatrix} B & AB & A^2B & \ldots & A^{N-1}B \end{bmatrix}\right) = N \tag{3.3}$$

As the numerical rank evaluation is sensitive, the staircase algorithm has been used to transform the system into its controllability staircase form [73]

$$\dot{x} = \begin{bmatrix} A_c & A_{12} \\ 0 & A_{uc} \end{bmatrix} \begin{bmatrix} \bar{x}_c \\ \bar{x}_{uc} \end{bmatrix} + \begin{bmatrix} B_c \\ 0 \end{bmatrix} u \tag{3.4}$$

$$y = \begin{bmatrix} C_c & C_{uc} \end{bmatrix} \begin{bmatrix} \bar{x}_c \\ \bar{x}_{uc} \end{bmatrix} + Du. \tag{3.5}$$

Here, the rank of A_{uc} is equal to the number of uncontrollable states. Checking this criterion for the family of linear systems derived along the steady state continuation path yields, that the state n is linear controllable by μ_M and $\dot{V}_e$, respectively.
As the intention is to design a controller, which uses only moment measurements, one has to check for observability of the state n with respect to the candidate measurement $\mu_0, \ldots, \mu_2$ for the continuous fluidized bed spray granulation with external product classification and $\mu_0, \ldots, \mu_3$ for the continuous fluidized bed spray granulation with internal product classification. This is done again for the family of linear models using the dual criterion for observability, i.e. the observability matrix R_o has to have rank N, where N is the dimension of the A matrix.

$$rank(R_o) = rank \left(\begin{bmatrix} C \\ CA \\ CA^2 \\ \vdots \\ CA^{N-1} \end{bmatrix} \right) = N \qquad (3.6)$$

Again, the staircase algorithm has been used to transform the system into its observability staircase form [73], due to sensitivity of the numerical rank evaluation.

$$\dot{\tilde{x}} = \begin{bmatrix} A_o & 0 \\ A_{21} & A_{uo} \end{bmatrix} \begin{bmatrix} \tilde{x}_o \\ \tilde{x}_{uo} \end{bmatrix} + \begin{bmatrix} B_o \\ B_{uo} \end{bmatrix} u \qquad (3.7)$$

$$y = \begin{bmatrix} C_o & 0 \end{bmatrix} \begin{bmatrix} \tilde{x}_o \\ \tilde{x}_{uo} \end{bmatrix} + Du. \qquad (3.8)$$

Here, the rank of A_{uo} is equal to the number of unobservable states. Checking this criterion for the family of linear systems derived along the steady state continuation yields, that the state n is linear observable using an arbitrary moment measurement $\mu_0, \ldots, \mu_2$ for the fluidized bed spray granulation with external product classification and $\mu_0, \ldots, \mu_3$ for the fluidized bed spray granulation with internal product classification, respectively.

3.1.2   Uncertainty models

From a control perspective, it would be desirable if the family of linear infinite dimensional systems derived along the steady state continuation could be embedded into a set of perturbed plants, where the set of perturbed plants can be described by a nominal system G_0 and a set of bounded, stable uncertainties [70, 71, 73, 74, 72]. In the following, three different types of model uncertainties (additive, multiplicative and coprime factor uncertainty) are studied using two simple uncertain system. For a successful control design the model uncertainty should be stable and possess a finite H_∞-norm.

Example 1 [72]

The first example is an uncertain second order system with varying natural frequency. Here, the crucial point is the lack of damping. Hence, the natural frequency varies with the uncertain parameter α_1 as depicted in Fig. 3.2 (left).

$$G_1(s) = \frac{1}{s^2 + 1 + \alpha_1} \qquad (3.9)$$

The system $G(s)$ for $\alpha_1 = 0$ is called the nominal system $G_0(s)$.

$$G_{0,1}(s) = \frac{1}{s^2 + 1} \qquad (3.10)$$

Example 2

The second example is again an uncertain second order system with two conjugate complex poles. Here, the real part of the poles is uncertain resulting in a change of stability as shown in Fig. 3.2 (right). This type of uncertainty is of great importance for the processes studied in this Thesis as it reflects the situation occurring at the Hopf bifurcation.

$$G_2(s) = \frac{1}{s^2 - 2(\alpha_2 - 0.01)s + (\alpha_2 - 0.01)^2 + 1} \tag{3.11}$$

The nominal system is obtained for $\alpha_2 = 0$.

$$G_{0,2}(s) = \frac{1}{s^2 + 0.02s + 1.0001} \tag{3.12}$$
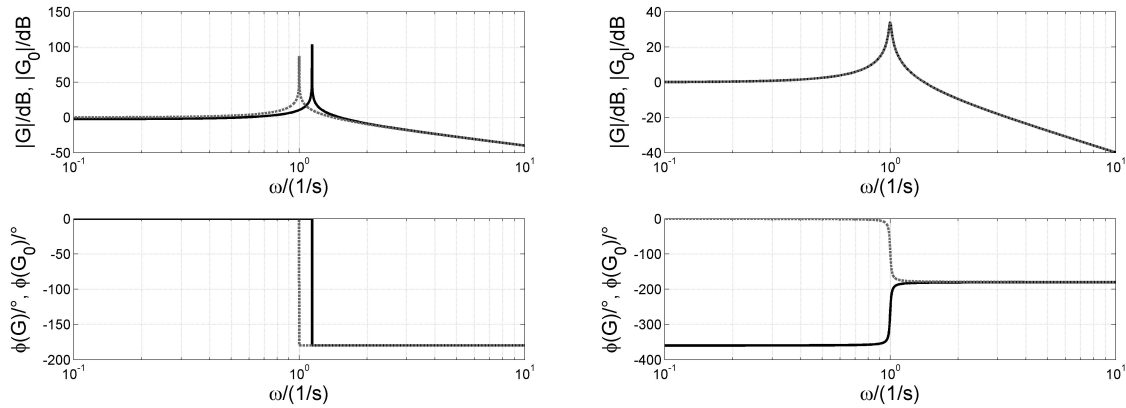
Figure 3.2: $G_1(s)$ and $G_{0,1}(s)$ - for $\alpha_1 = 0.3$ (left) and $G_2(s)$ and $G_{0,2}(s)$ for $\alpha_2 = 0.02$ (right)

Additive uncertainty

At first the uncertain system $G_1(s)$ and $G_2(s)$ are embedded into the set of the nominal system $G_{0,1}(s)$ and $G_{0,2}(s)$ and an appropriate additive uncertainty, i.e.

$$G(s) = G_0(s) + \Delta_a(s) \tag{3.13}$$

the appropriate additive uncertainty can be calculated as

$$\Delta_a(s) = G(s) - G_0(s). \tag{3.14}$$

The additive uncertainties for the first and second example are

$$\Delta_{a,1}(s) = \frac{-\alpha_1}{(s^2 + 1 + \alpha_1)(s^2 + 1)}, \tag{3.15}$$

$$\Delta_{a,2}(s) = \frac{-2\alpha_2 s + \alpha_2^2 - 0.02\alpha_2}{(s^2 - 2(\alpha_2 - 0.01)s + (\alpha_2 - 0.01)^2 + 1)(s^2 + 0.02s + 1.0001)}. \tag{3.16}$$

Obviously, as can be seen from Fig. 3.3 (left) the additive uncertainty $\Delta_{a,1}(s)$ does not have a finite H_∞-norm and hence is not an appropriate uncertainty model. For the second
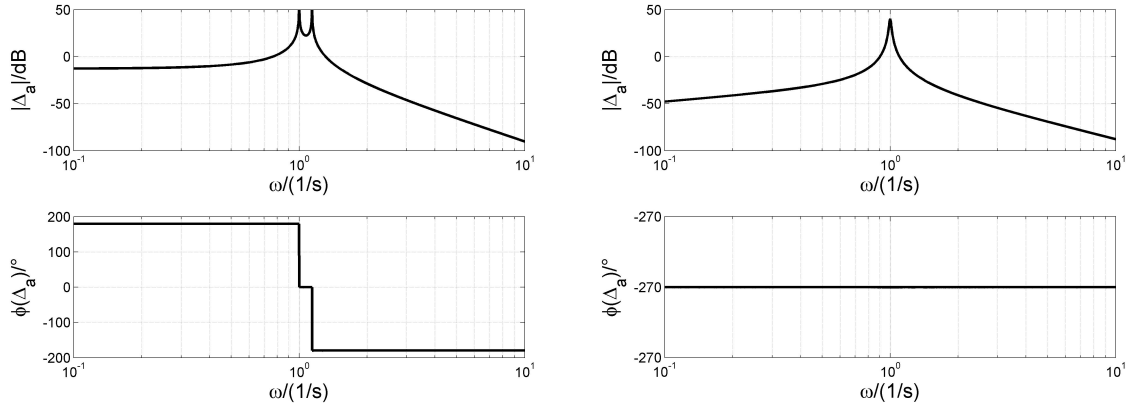
Figure 3.3: Additive uncertainty - $\Delta_{a,1}(s)$ for $\alpha = 0.3$ (left) and $\Delta_{a,2}(s)$ for $\alpha = 0.02$ (right)

example depending on the value of α_2 the stability condition for the additive uncertainty $\Delta_{a,2}(s)$ is clearly not satisfied (Fig. 3.3 (right)).

Therefore, the class of additive model uncertainties is not a feasible choice for these examples and hence for the fluidized bed spray granulation processes studied in this Thesis.

Multiplicative uncertainty

The same result holds in the case when the uncertain systems $G_1(s)$ and $G_2(s)$ are embedded into the set of the nominal systems $G_{0,1}(s)$ and $G_{0,2}(s)$ and an appropriate multiplicative uncertainty, i.e.

$$G(s) = (1 + \Delta_m(s))G_0(s). \tag{3.17}$$

The multiplicative uncertainty can be calculated as

$$\Delta_m(s) = \frac{G(s)}{G_0(s)} - 1. \tag{3.18}$$

For the first and second example the multiplicative uncertainties are

$$\Delta_{m,1}(s) = \frac{-\alpha}{(s^2 + 1 + \alpha)}, \tag{3.19}$$

$$\Delta_{m,2}(s) = \frac{2\alpha s - \alpha^2 + 0.02\alpha}{(s^2 - 2(\alpha - 0.01)s + (\alpha - 0.01)^2 + 1)}. \tag{3.20}$$

As can be seen from Fig. 3.4 (left) $\Delta_{m,1}(s)$ does not have a finite H_∞-norm and hence is not an appropriate uncertainty model for the first example. For the second example depending on the value of α_2 the stability condition for $\Delta_{m,2}(s)$ is clearly not satisfied (Fig. 3.4 (right)).

Coprime factor uncertainty

Using a coprime factorization of the nominal system $G_0(s)$, i.e. $G_0(s) = M_0(s)^{-1}N_0(s)$ where $N_0(s)$ and $M_0(s)$ are stable coprime transfer functions, the uncertain system $G(s)$
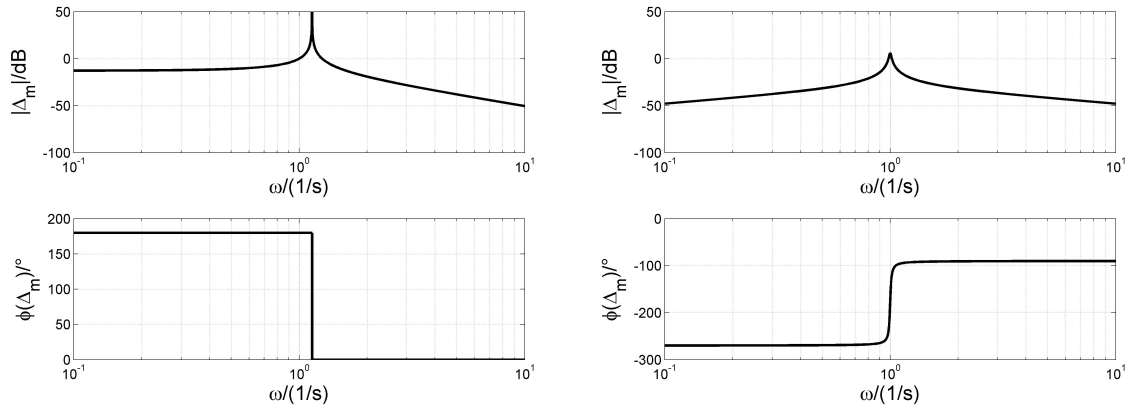
Figure 3.4: Multiplicative uncertainty - $\Delta_{m,1}(s)$ for $\alpha = 0.3$ (left) and $\Delta_{m,2}(s)$ for $\alpha = 0.02$ (right)

can be embedded into the set of the nominal system $G_0(s)$ and coprime factor uncertainties $\Delta_M(s)$ and $\Delta_N(s)$ as depicted in Fig. 3.5.

$$G(s) = (M_0(s) + \Delta_M(s))^{-1}(N_0(s) + \Delta_N(s)) \tag{3.21}$$

One possibility to calculate appropriate coprime factor uncertainties for a given coprime
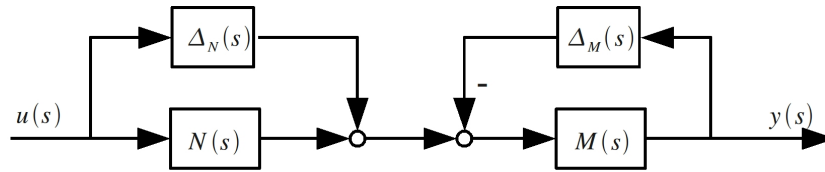
Figure 3.5: Coprime factor uncertainty

factorization of $G(s)$, i.e. $G(s) = M(s)^{-1}N(s)$ is the following

$$\Delta_N(s) = N(s) - N_0(s), \tag{3.22}$$
$$\Delta_M(s) = M(s) - M_0(s). \tag{3.23}$$

In the following, it is assumed that the coprime factors $N(s)$ and $M(s)$ are normalized, i.e. the Bezout identity

$$M(s)M^T(-s) + N(s)N^T(-s) = I \tag{3.24}$$

is fulfilled. The normalized left coprime factorization can be calculated using the state space realization of the transfer function $G(s)$ by solving the following algebraic Riccati equation in Z

$$\left(A - BS^{-1}D^TC\right)Z + Z\left(A - BS^{-1}D^TC^T\right)^T - ZC^TR^{-1}CZ + BS^{-1}B^T = 0 \tag{3.25}$$

where

$$S = I + D^TD. \tag{3.26}$$

Using the following abbreviations

$$H = -\left(BD^T + ZC^T\right)R^{-1} \qquad R = I + DD^T \tag{3.27}$$

the normalized left coprime factorization can be obtained by Laplace Transformation of the following state space model

$$\begin{bmatrix} N(s) & M(s) \end{bmatrix} \;\bullet\!\!-\!\!\circ\; \left[\begin{array}{c|cc} A + HC & B + HD & H \\ \hline R^{-\frac{1}{2}}C & R^{-\frac{1}{2}}D & R^{-\frac{1}{2}} \end{array}\right]. \tag{3.28}$$

For the nominal systems $G_{0,1}(s)$ and $G_{0,2}(s)$ and the transfer functions $G_1(s)$ and $G_2(s)$ with $\alpha_1 = 0.3$ and $\alpha_2 = 0.02$ of example 1 and 2 the normalized left coprime factorizations are

$$G_{0,1}(s) = \left(\frac{s^2 + 1}{s^2 + 0.9102s + 0.5858}\right)^{-1}\left(\frac{1}{s^2 + 0.9102s + 0.5858}\right), \tag{3.29}$$

$$G_1(s) = \left(\frac{s^2 + 1.3}{s^2 + 1.038s + 0.8858}\right)^{-1}\left(\frac{1}{s^2 + 1.038s + 0.8858}\right), \tag{3.30}$$

$$G_{0,2}(s) = \left(\frac{s^2 + 0.02s + 1}{s^2 + 0.9104s + 0.6215}\right)^{-1}\left(\frac{1}{s^2 + 0.9104s + 0.6215}\right), \tag{3.31}$$

$$G_2(s) = \left(\frac{s^2 - 0.02s + 1}{s^2 + 0.9104s + 0.5487}\right)^{-1}\left(\frac{1}{s^2 + 0.9104s + 0.5487}\right). \tag{3.32}$$

The associated coprime factor uncertainties $\Delta_M(s)$ and $\Delta_N(s)$ are

$$\Delta_{N,1}(s) = \frac{-0.12758(s + 2.351)}{(s^2 + 0.9102s + 0.5858)(s^2 + 1.038s + 0.8858)}, \tag{3.33}$$

$$\Delta_{M,1}(s) = \frac{-0.12758(s + 1.362)(s^2 - 1.362s + 0.7151)}{(s^2 + 0.9102s + 0.5858)(s^2 + 1.038s + 0.8858)}, \tag{3.34}$$

$$\Delta_{N,2}(s) = \frac{0.072832}{(s^2 + 0.9104s + 0.5487)(s^2 + 0.9104s + 0.6215)}, \tag{3.35}$$

$$\Delta_{M,1}(s) = \frac{-0.04(s - 1.411)(s^2 + 0.5s + 1.29)}{(s^2 + 0.91s + 0.5487)(s^2 + 0.9104s + 0.6215)}. \tag{3.36}$$

As depicted in Fig. 3.6, the coprime factor uncertainties $\Delta_{N,1}(s)$, $\Delta_{M,1}(s)$, $\Delta_{N,2}$ and $\Delta_{M,2}$ are all stable and have a finite H_∞-norm and are hence appropriate uncertainty models.

$$\|\Delta_{N,1}(s)\|_\infty = 0.66 \tag{3.37}$$

$$\|\Delta_{M,1}(s)\|_\infty = 0.359 \tag{3.38}$$

$$\|\Delta_{N,2}(s)\|_\infty = 0.23 \tag{3.39}$$

$$\|\Delta_{M,2}(s)\|_\infty = 0.217 \tag{3.40}$$

In contrast to multiplicative or additive model uncertainties, coprime factor uncertainties do not give a unique realization for $\Delta_M(s)$ and $\Delta_N(s)$ for a given plant $G(s)$ and nominal model $G_0(s)$. Hence, the choice of $\Delta_M(s)$ and $\Delta_N(s)$ is an additional degree of freedom. As for robust control design the H_∞-norm of a given uncertainty is crucial, a realization $\Delta_N(s)$ and $\Delta_M(s)$ with a minimal H_∞-norm should be used. This minimization problem motivates the introduction of the gap metric.
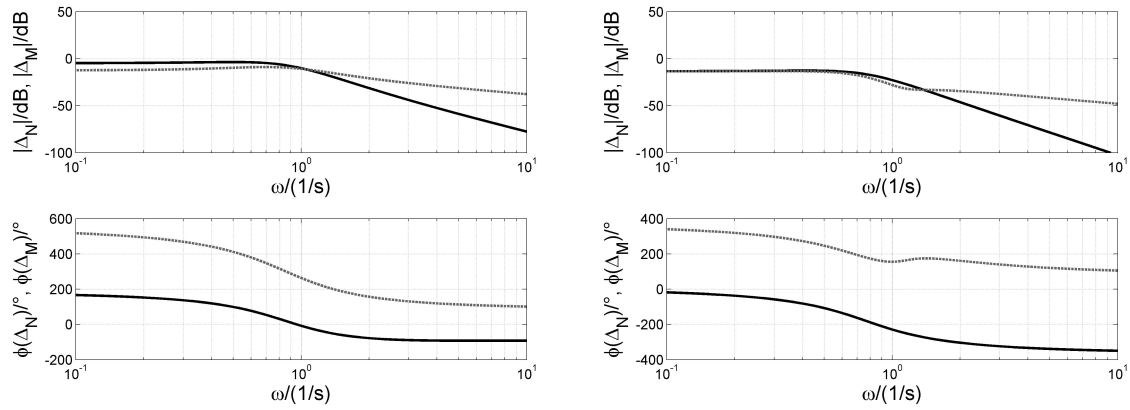
Figure 3.6: Coprime factor uncertainty $\Delta_M(s)$ and $\Delta_N(s)$ - example 1 for $\alpha = 0.3$ (left) and example 2 for $\alpha = 0.02$ (right)

3.1.3 Gap metric

For two systems $G_0(s)$ and $G(s)$ the directed gap $\vec{\delta}_g(G_0(s), G(s))$ is defined as the minimal H_∞-norm of a feasible realization of $\Delta_M(s)$ and $\Delta_N(s)$, i.e. a realization

$$G(s) = (M(s) + \Delta_M(s))^{-1} (N(s) + \Delta_N(s)) \tag{3.41}$$

where $N(s)$ and $M(s)$ are the normalized left coprime factors of $G_0(s)$.

$$\vec{\delta}_g(G_0, G) := \inf_{[\Delta_N \ \Delta_M] \in \mathcal{H}_\infty} \left\{ \|[\Delta_N \ \Delta_M]\|_\infty : G = (M + \Delta_M)^{-1} (N + \Delta_N) \right\}. \tag{3.42}$$

The directed gap $\vec{\delta}_g$ is however not a metric as it is not symmetric in its arguments, i.e. $\vec{\delta}_g(G_0(s), G(s)) \neq \vec{\delta}_g(G(s), G_0(s))$. Hence, the gap metric δ_g is introduced as the maximum of both directed gaps $\vec{\delta}_g(G_0(s), G(s))$ and $\vec{\delta}_g(G(s), G_0(s))$ [69].

$$\delta_g(G_0, G) = \max \left\{ \vec{\delta}_g(G_0, G), \vec{\delta}_g(G, G_0) \right\} \tag{3.43}$$

Using this gap metric two systems $G_1(s)$ and $G_2(s)$ are close if the associated value of the gap metric $\delta_g(G_1(s), G_2(s))$ is close to zero, implying that both can be embedded in a family of linear models using a nominal model and a, with respect to the H_∞-norm, small coprime factor uncertainty. The maximum value of the gap metric is one. It is important to note that the gap metric as any other metric satisfies the triangular inequality.

$$\delta_g(G_1, G_2) \leq \delta_g(G_1, G_3) + \delta_g(G_3, G_2) \tag{3.44}$$

Calculating the gap metric of example 1 and 2 gives the following

$$\delta_g(G_{0,1}, G_1) \quad = \quad 0.29, \tag{3.45}$$
$$\delta_g(G_{0,2}, G_2) \quad = \quad 0.043, \tag{3.46}$$

which shows, that the realizations of $\Delta_N(s)$ and $\Delta_M(s)$ chosen in the preceeding section were not optimal. This overestimation would have led to an unnecessary conservative control design.

In the following, the gap metric for the family of linear models derived along the steady state continuation with respect to a design model will be investigated for both fluidized bed spray granulation processes.

3.1.4 Analysis of the gap metric

As has been mentioned before in the case of the fluidized bed spray granulation with internal classification the third moment μ_3 is the most appropriate candidate for the controlled variable due to uniqueness problems of the moments $\mu_0, \ldots, \mu_2$ when selecting $\dot{V}_e$ as control input. Therefore, in the following a family of linear models is generated using a measurement $y = \mu_3$. Then the gap metric of each member of the family with respect to the nominal design models $G_0(s)$ associated to a suspension injection rate in the unstable region $\dot{V}_e = 14709 \frac{mm^3}{s}$ is calculated. As can be seen in Fig. 3.7 (left) the family of the associated linear systems can be embedded into a set of plants consisting of a nominal system $G_0(s)$ and a coprime factor uncertainty. The maximum gap metric $\delta_{g,lin} = \max_{\dot{V}_e}(\delta_g)$ will be used for the calculation of the required robustness margin.

$$\delta_{g,lin} = \max_{\dot{V}_e}(\delta_g) = 0.0033 \tag{3.47}$$

In the case of the fluidized bed spray granulation with external classification a family of linear models is generated using a measurement of the second moment μ_2 and the mill grade μ_M as control input. Then the gap metric of each member of the family of linear transfer functions with respect to the nominal design model $G_0(s)$ associated to the mill grade $\mu_M = 0.5$ is studied. As can be seen in Fig. 3.7 (right) the family of the associated linear systems can be embedded into a set of plants consisting of a nominal system $G_0(s)$ and a coprime factor uncertainty. Here, the maximum gap metric gives

$$\delta_{g,lin} = 0.25. \tag{3.48}$$
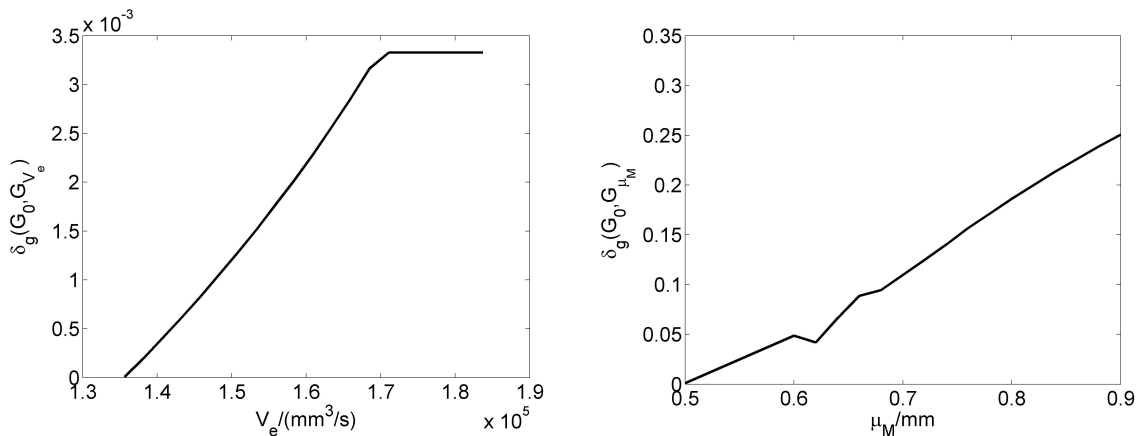
Figure 3.7: Gap metric with respect to $G_0(s)$

3.2 Quantification of the discretization error

In Appendix A convergence of the approximate solution of the particle size distribution has been studied. However, for control design this type of convergence is not sufficient. For a successful finite dimensional control design convergence should be stated in terms of certain error bounds, which can be identified with appropriate model uncertainties. The motivation is that deriving a controller with an appropriate robust stability margin closed loop stability can be guaranteed embedding the linearized population balance model into a set consisting of a nominal system $G_0(s)$ and a set of bounded, stable uncertainties. Therefore, in the following it is assumed that the population balance model has been linearized resulting in a linear distributed parameter system on a Hilbert space $\mathcal{X}$. The necessary concepts from linear infinite dimensional systems theory [81, 59, 64, 94, 96] will be shortly restated in analogy to the finite dimensional case.

3.2.1 Semigroup theory for linear distributed parameter systems

A finite dimensional linear time-invariant system in state-space representation has the following systems equation

$$\dot{x} = Ax. \tag{3.49}$$

Here, A is the system matrix. For a given initial condition x_0 at time $t = 0$ all future solutions $x(t)$ can be calculated by

$$x(t) = e^{At}x_0 \tag{3.50}$$

where e^{At} is the matrix exponential function mapping the initial state x_0 to $x(t)$. Calculating the solution in the s-domain, i.e. applying Laplace transformation, gives

$$X(s) = (sI - A)^{-1}x_0. \tag{3.51}$$

or in time-domain

$$x(t) = \mathcal{L}^{-1}\left\{(sI - A)^{-1}\right\}x_0. \tag{3.52}$$

For infinite dimensional linear time-invariant systems the situation is far more complex as the state vector x becomes infinite dimensional and the system matrix A generalizes to an operator. However, similar concepts hold. The matrix exponential function e^{At} becomes an operator $T(t)$ which is called semigroup and which maps initial states x_0 to $x(t)$. Here, we will focus only on the important class of strongly continuous semigroups, i.e. C_0-semigroups [126, 127].

Definition 1. *A strongly continuous semigroup (a C_0-semigroup) is a map $T : \mathbb{R}_+ \to L(\mathcal{X})$ with the following properties*

$$T(0) \quad = \quad I \tag{3.53}$$
$$T(t + \tau) \quad = \quad T(t)T(\tau) \text{ for all } t, \tau \geq 0 \tag{3.54}$$
$$\lim_{t \to 0} \|T(t)x - x\| \quad \to \quad 0 \text{ for all } x \in \mathcal{X}. \tag{3.55}$$

The operator A, i.e. the generalization of the system matrix, is called the infinitesimal generator of the semigroup $T(t)$.

Definition 2. *The infinitesimal generator A of a strongly continuous semigroup $T(t)$ is defined by*

$$Ax = \lim_{t \to 0} \frac{1}{t}(T(t) - I)x \tag{3.56}$$

whenever the limit exists. The set of elements $x \in \mathcal{X}$ for which the limit exists is called the domain of A, $D(A)$.

The Laplace transform of the semigroup $T(t)$, i.e. $(sI - A)^{-1}$, is called the resolvent. The subset of the domain of the infinitesimal generator A, $D(A)$, for which the resolvent exists and is bounded is called resolvent set and its complement is the spectrum of A.

Definition 3. *For an infinitesimal generator A and its associated domain $D(A)$ the resolvent set $\rho(A)$ is defined as follows*

$$\rho(A) := \left\{ s \in \mathbb{C} : (sI - A)^{-1} \text{ exists and is bounded } \right\}. \tag{3.57}$$

Its complement $\sigma(A) := \mathbb{C} \setminus \rho(A)$ is called the spectrum of A. The inverse $R(s; A) := (sI - A)^{-1}$ for $s \in \rho(A)$ is called the resolvent.

For a given infinite dimensional dynamical system

$$\dot{x} = Ax, \tag{3.58}$$

stability is defined by stability of the associated semigroup $T(t)$.

Definition 4. *A strongly continuous semigroup $T(t)$ is stable if there exist $M, \alpha > 0$ such that $\|T(t)\| \le M e^{-\alpha t}$ for all $t \ge 0$. If there exists a constant σ such that $\alpha > \sigma$ the C_0-semigroup $T(t)$ is σ-stable.*

In the following, focus will be on bounded control systems, i.e. systems with finite dimensional input and output spaces.

$$\dot{x} = Ax + Bu \tag{3.59}$$
$$y = Cx \tag{3.60}$$

Here, the operator $B \in \mathcal{L}(\mathbb{R}^p, \mathcal{X})$ maps the finite dimensional input $u \in \mathbb{R}^p$ to the state space $\mathcal{X}$ and the operator $C \in \mathcal{L}(\mathcal{X}, \mathbb{R}^q)$ maps the state space $\mathcal{X}$ to the finite dimensional output $y \in \mathbb{R}^q$. Stability for a bounded control system can then be defined by stability of the associated semigroup $T(t)$.

Definition 5. *A bounded control system (A, B, C) is called internally stable if the semigroup generated by A is stable.*

The important properties of stabilizability and detectability, well known from the finite dimensional case, can also be extended to the infinite dimensional case.

Definition 6. *A bounded control system (A, B, C) is called stabilizable if there exists a bounded linear operator $K : \mathcal{X} \to \mathbb{R}^p$ such that $A - BK$ is the generator of a stable semigroup. If there exists a bounded linear operator $F : \mathbb{R}^q \to \mathcal{X}$ such that $A - FC$ is the generator of a stable semigroup the system is called detectable.*

If in addition the semigroups generated by $A - BK$ or $A - FC$ are σ-stable the bounded control system (A, B, C) is called σ-stabilizable or σ-detectable.

Definition 7. *A bounded control system (A, B, C) is called σ-stabilizable if there exists a bounded linear operator $K : \mathcal{X} \to \mathbb{R}^m$ such that $A - BK$ is the generator of a σ-stable semigroup. If there exists a bounded linear operator $F : \mathbb{R}^n \to \mathcal{X}$ such that $A - FC$ is the generator of a σ-stable semigroup the system is called σ-detectable.*

It can be shown [61, 62] that every infinite dimensional bounded control system can be stabilized by a finite dimensional controller.

Theorem 1. *[61, 62] Every stabilizable and detectable bounded control system is stabilizable by a finite dimensional controller.*

This gives the theoretical justification for three control design procedures as depicted in Fig. 4.1:

1. *Direct finite dimensional control design.* Based on the infinite dimensional system a finite dimensional and thus implementable controller is derived.

2. *Late lumping control design.* Based on the infinite dimensional system a infinite dimensional controller is derived, which has to be discretized or lumped for an implementation.

3. *Early lumping control design.* The infinite dimensional model is discretized or lumped. Then a finite dimensional controller is derived being based on the finite dimensional system.
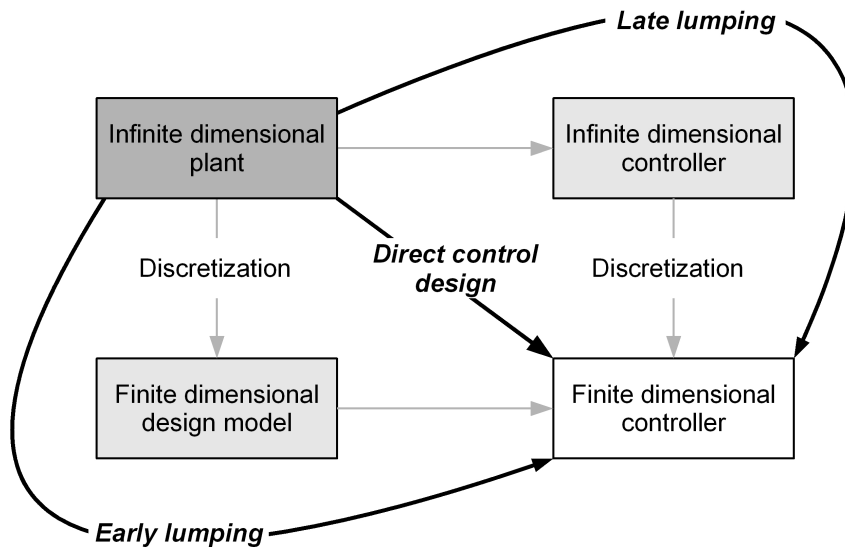
Figure 3.8: Control approaches for finite dimensional controller design

The direct control design would be the most attractive from a practical and theoretical point of view. However, in general it lacks applicability. The late lumping approach uses an approximation of the original controller for implementation, which may result in problems regarding stability and performance. In the following, the focus will be on the early lumping approach. The reason is twofold:

1. For control design a great variety of standard finite dimensional control methods can be used.

2. Assuming a converging sequence of finite dimensional approximations the discretization error can be estimated by an appropriate error bound. This error bound can be used in a finite dimensional control design approach in order to derive robust control laws.

In the following, focus will hence be on the derivation of an appropriate error bound of the discretization error.

3.2.2   Convergence in the gap metric

Consider the following system on a Hilbert space $\mathcal{X}$, where A is the generator of a strongly continuous semigroup $T(t)$ and the input/output spaces are finite dimensional, i.e. $B \in \mathcal{L}(\mathbb{R}^p, \mathcal{X})$ and $C \in \mathcal{L}(\mathcal{X}, \mathbb{R}^q)$.

$$\dot{x} = Ax + Bu \qquad (3.61)$$
$$y = Cx \qquad (3.62)$$

A discretization scheme gives a finite dimensional approximation.

$$\dot{x} = A_n x + B_n u \qquad (3.63)$$
$$y = C_n x \qquad (3.64)$$

In the following P_n will be the projection operator, which restricts C to C_n and gives $B_n = P_n B$.

Theorem 2. *[61, 62] Let (A_n, B_n, C_n) be a sequence of approximations of a σ-stabilizable/detectable bounded control system (A, B, C), satisfying the following assumptions.*

A1 *For all $x \in \mathcal{X}$, $\lim_{n \to \infty} \|P_n x - x\| = 0$*

A2 *For some $s \in \rho(A)$ and for all $x \in \mathcal{X}$*

$$\lim_{n \to \infty} \|P_n R(s; A) X(s) - R(s; A_n) P_n X(s)\| = 0 \qquad (3.65)$$

A3 *The semigroups $T_n(t)$ generated by A_n are uniformly bounded. That is, there exist M, k such that*

$$\|T_n(t)\| \le M e^{kt} \text{ for all } n \ge N \qquad (3.66)$$

A4 *The approximations are uniformly σ-stabilizable if the original system is σ-stabilizable, i.e.*

$$\lim_{n \to \infty} K_n P_n x = K x \qquad (3.67)$$

and for sufficiently large N the semigroups generated by $A_n - B_n K_n$ are uniformly bounded by $M e^{-\alpha t}$ for some $M > 0, \alpha > \sigma$ and all $n > N$.

Then the approximating systems G_n converge to the original system G in the gap metric, i.e.

$$\lim_{n \to \infty} \delta_g(G_n, G) = 0 \qquad (3.68)$$

3.2.3   Estimation of the gap metric

For a finite dimensional control design the distance between the finite dimensional approximation $G_n(s)$ and the original system $G(s)$ in the sense of the gap metric $\delta_g(G_n, G)$ is needed [63]. This is in general a very hard task, therefore in this section the estimation procedure proposed in [66] is used.
This estimation procedure is based on the fact that the gap metric satisfies the triangular inequality

$$\delta_g(G_1, G_2) \leq \delta_g(G_1, G_3) + \delta_g(G_3, G_2) \qquad (3.69)$$

or more specifically for G_1 being a finite dimensional approximation of order k of G, G_2 being the original system G and G_3 being a finite dimensional approximation of order $k+1$ of G

$$\delta_g(G_k, G) \leq \delta_g(G_k, G_{k+1}) + \delta_g(G_{k+1}, G). \qquad (3.70)$$

Using the triangular inequality and the result that the numerical approximation G_n converges to G, i.e. $\lim_{n\to\infty} G_n = G$, yields

$$\delta_g(G_n, G) \leq \sum_{k=n}^{\infty} \delta_g(G_k, G_{k+1}). \qquad (3.71)$$

This gives an estimate of the distance between the finite dimensional approximation $G_n(s)$ and the original system $G(s)$ in the sense of the gap metric $\delta_g(G_n, G)$ provided that the infinite series converges and the limit can be calculated, which in general will not be the case. Therefore, in order to derive an applicable estimation procedure, it is assumed that the gap metric $\delta_g(G_k, G_{k+1})$ can be overestimated by a sequence $\bar{\delta}_g(k)$ for which the associated series converges, then for the gap metric between the finite dimensional approximation $G_n(s)$ and the original system $G(s)$ the following holds

$$\delta_g(G_n, G) \leq \sum_{k=n}^{\infty} \delta_g(G_k, G_{k+1}) < \sum_{k=n}^{\infty} \bar{\delta}_g(k). \qquad (3.72)$$

Here, the estimate $\bar{\delta}_g(k)$ should be chosen such that the limit of the series can be easily calculated.

3.2.4   Discretization error - internal product classification

As can be seen from Fig. 3.9 the sequence of gap metrics $\delta_g(G_k, G_{k+10})$ with $k = 150, 160, \ldots$, i.e. $k = k(i) = 150 + 10(i-1)$ with $i = 1, 2, \ldots$, can be bounded from above by a sequence $\bar{\delta}_g(i) = 0.8/(i+20)^2$ with $i = \frac{k-150}{10} + 1$ for which the associated series converges.

$$\delta_g(G_{150}, G) \leq \sum_{i=1}^{\infty} \delta_g(G_k(i), G_{k(i)+10}) < \sum_{i=1}^{\infty} \frac{0.8}{(i+20)^2} \leq 0.04 \qquad (3.73)$$
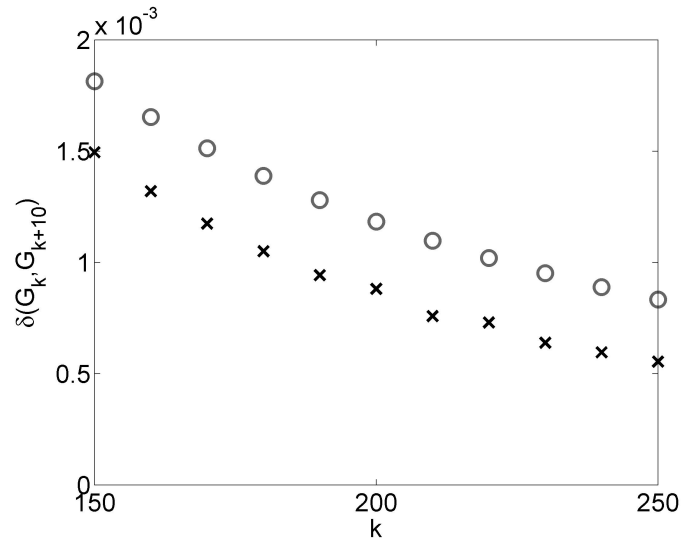
Figure 3.9: Sequence of gap metrics $\delta_g(G_k, G_{k+10})$ (black x) and $\bar{\delta}_g$ (gray o) - internal product classification

3.2.5 Discretization error - external product classification

As can be seen from Fig. 3.10 the sequence of gap metrics $\delta_g(G_k, G_{k+1})$ with $k = 160, \ldots$, i.e. $k = k(i) = 150 + 10(i-1)$ with $i = 1, 2, \ldots$, can be bounded from above by a sequence $\bar{\delta}_g(i) = 1/(i+20)^2$ with $i = \frac{k-160}{10} + 1$ for which the associated series converges.

$$\delta_g(G_{160}, G) \leq \sum_{i=1}^{\infty} \delta_g(G_{k(i)}, G_{k(i)+10}) < \sum_{i=1}^{\infty} \frac{1}{(i+20)^2} \leq 0.05 \qquad (3.74)$$
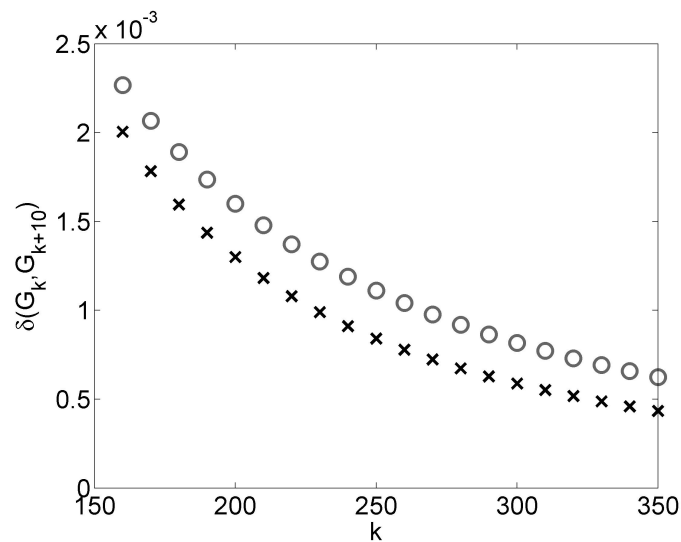

Figure 3.10: Sequence of gap metrics $\delta_g(G_k, G_{k+10})$ (black x) and $\bar{\delta}_g$ (gray o) - external product classification

3.3   Linear control design

3.3.1   Finite dimensional model reduction

So far, high order models have been used. In order to derive low order design models for control design finite dimensional model reduction techniques [65] are applied. The associated reduction error will be calculated in the gap metric.

Given a stable high order model $G(s)$ with the following state space minimal realization

$$\dot{x} = Ax + Bu, \tag{3.75}$$
$$y = Cx + Du. \tag{3.76}$$

Then the state vector $x \in \mathbb{R}^n$ can be separated into two parts $x = \begin{pmatrix} x_1 \\ x_2 \end{pmatrix}$ with $x_1 \in \mathbb{R}^r$, $x_2 \in \mathbb{R}^k$ and $n = r + k$.

$$\dot{x}_1 = A_{11}x_1 + A_{12}x_2 + B_1 u \tag{3.77}$$
$$\dot{x}_2 = A_{21}x_1 + A_{22}x_2 + B_2 u \tag{3.78}$$
$$y = C_1 x_1 + C_2 x_2 + Du \tag{3.79}$$

In order to derive a reduced order model from this representation two possibilities are via truncation and singular perturbations. Applying order reduction by truncation the states x_2 are simply left out resulting in the following reduced model

$$\dot{x}_1 = A_{11}x_1 + B_1 u, \tag{3.80}$$
$$y = C_1 x_1 + Du. \tag{3.81}$$

Investigation of the approximation error between $G_r(s)$ and $G(s)$ gives

$$G(s) - G_r(s) = C(sI - A)^{-1}B - C_1(sI - A_{11})^{-1}B_1. \tag{3.82}$$

Here, investigating the limits for $\omega \to \infty$ and $\omega \to 0$ gives that good approximation is achieved for high frequencies whereas for low frequencies the approximation error becomes high.

$$\lim_{\omega \to \infty} G(j\omega) - G_r(j\omega) = 0 \tag{3.83}$$
$$\lim_{\omega \to 0} G(j\omega) - G_r(j\omega) = -CA^{-1}B + C_1 A_{11}^{-1}B_1 \tag{3.84}$$
$$\overset{i.g.}{\neq} 0 \tag{3.85}$$

Applying order reduction by singular perturbation it is assumed that the differential equations for the states x_2 are parametrized by a small parameter μ.

$$\dot{x}_1 = A_{11}x_1 + A_{12}x_2 + B_1 u \tag{3.86}$$
$$\mu \dot{x}_2 = A_{21}x_1 + A_{22}x_2 + B_2 u \tag{3.87}$$
$$y = C_1 x_1 + C_2 x_2 + Du \tag{3.88}$$

For a vanishing parameter μ the differential equations for the states x_2 become algebraic equations

$$0 = A_{21}x_1 + A_{22}x_2 + B_2 u \tag{3.89}$$

or as an equation for x_2

$$x_2 = A_{22}^{-1}(-A_{21}x_1 - B_2 u). \tag{3.90}$$

This can be used to eliminate the states x_2 from the original model giving a reduced model $G_r(s)$.

$$\dot{x}_1 = (A_{11} - A_{12}A_{22}^{-1}A_{21})x_1 + (B_1 - A_{12}A_{22}^{-1}B_2)u, \tag{3.91}$$
$$y = (C_1 - C_2 A_{22}^{-1}A_{21})x_1 + (D - C_2 A_{22}^{-1}B_2)u. \tag{3.92}$$

Here, it can be shown that the approximation error vanishes for small frequencies, i.e. $\lim_{\omega \to 0} G(j\omega) - G_r(j\omega) = 0$.

Both methods strongly depend on the state-space realization used. A realization which has to be proven advantageous in this context is the balanced realization. A state-space realization of a stable system $G(s)$ is called balanced if its controllability and observability Gramians (W_c and W_o) are diagonal and equal, i.e.

$$W_S = \int_0^{t_e} e^{At}BB^T e^{A^T t} dt = \int_0^{t_e} e^{A^T t}C^T C e^{At} dt = W_B = \Sigma \tag{3.93}$$

where Σ is a diagonal matrix and the solution of the two Lyapunov equations

$$A\Sigma + \Sigma A^T + BB^T = 0, \tag{3.94}$$
$$\Sigma A + A^T\Sigma + C^T C = 0. \tag{3.95}$$

The elements of Σ are the so called Hankel singular values σ_i

$$\Sigma = \begin{pmatrix} \sigma_1 & & \\ & \ddots & \\ & & \sigma_n \end{pmatrix} \text{ with } \sigma_1 \geqslant \sigma_2 \geqslant \ldots \geqslant \sigma_n > 0. \tag{3.96}$$

From a model reduction point of view this realization is of great importance as dynamics associated with a high Hankel singular value are equally well controllable and observable, i.e. they have great influence on the input-output behavior, and should therefore be preserved.

Applying a reduction method (truncation or singular perturbation) to a balanced state-space model allows in addition the calculation of an explicit upper bound on the approximation error in the sense of an H_∞-norm

$$\|G(s) - G_r(s)\|_\infty \leqslant 2 \sum_{i=r+1}^{n} \sigma_i, \tag{3.97}$$

where σ_i with $i = r + 1, \ldots, n$ are the Hankel singular values associated with the reduced states x_i with $i = r + 1, \ldots, n$.

So far, stability of the original system has been assumed. In order to reduce an unstable transfer function model $G(s)$ two different approaches are possible

1. separation of the unstable system dynamics from the stable, i.e. decomposition into

$$G(s) = G_{un}(s) + G_{st}(s), \tag{3.98}$$

where $G_{st}(s)$ is the stable and $G_{un}(s)$ is the unstable part of the transfer function $G(s)$. Model reduction can then be applied to the stable part $G_{st}(s)$ only. This procedure has the disadvantage that the full unstable system dynamics are preserved in the reduced model, which may not be necessary for a control design.

2. an elegant alternative is the use of a normalized left (or right) coprime factorization of the original system $G(s)$, i.e.

$$G(s) = M^{-1}(s)N(s), \text{ with } M(s)M^T(-s) + N(s)N^T(-s) = I \qquad (3.99)$$

as here the transfer functions $M(s)$ and $N(s)$ are stable by definition irrespective on the stability behavior of the original system $G(s)$. Therefore, model reduction can be applied on each normalized coprime factors $M(s)$ and $N(s)$ separately.

$$M(s) \rightarrow M_r(s) \qquad (3.100)$$
$$N(s) \rightarrow N_r(s) \qquad (3.101)$$

The reduced system $G_r(s)$ is then formed from the reduced normalized coprime factors $M_r(s)$ and $N_r(s)$.

$$G_r(s) = M_r^{-1}(s)N_r(s) \qquad (3.102)$$

In this Thesis only the second approach has been used applying truncation of the balanced realization of each normalized left coprime factor $M(s)$ and $N(s)$ of the original plant.

Model reduction - internal product classification

As can be seen from the diagram of the Hankel singular values σ_i in Fig. 3.11 a truncation up to order 5 is reasonable. The additive approximation error $|G - G_r|$ is small over the whole frequency range of interest as shown in the Bode diagram in Fig. 3.12. The associated error in the gap metric is

$$\delta_g(G, G_r) = 1 \cdot 10^{-3}. \qquad (3.103)$$

Model reduction - external product classification

As can be seen from the diagram of the Hankel singular values σ_i in Fig. 3.13 a truncation up to order 5 is reasonable. The additive approximation error $|G - G_r|$ is small over the whole frequency range of interest as shown in the Bode diagram in Fig. 3.14. The associated error in the gap metric is

$$\delta_g(G, G_r) = 8 \cdot 10^{-3}. \qquad (3.104)$$
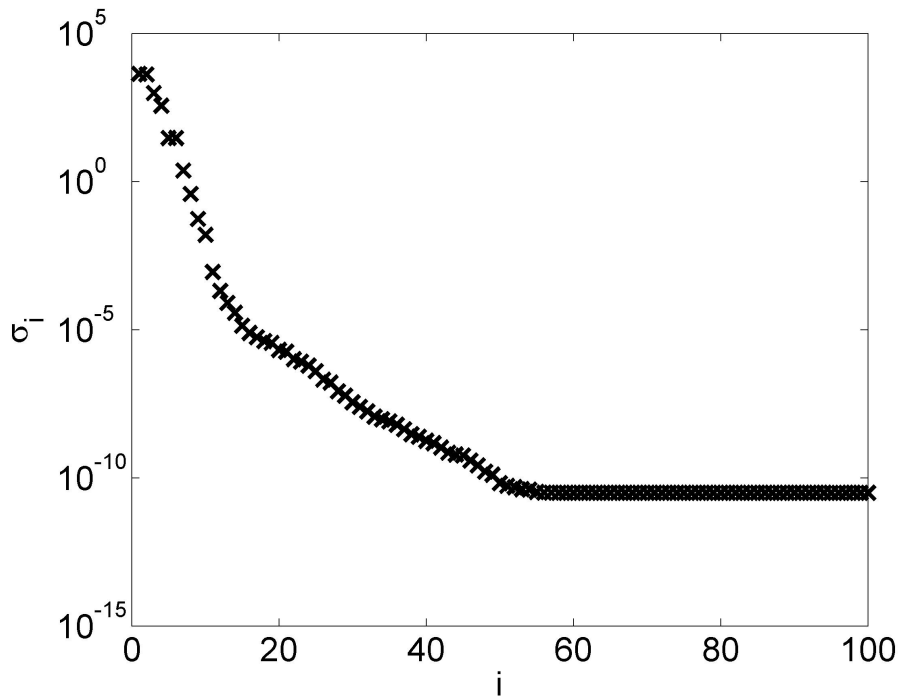
Figure 3.11: Hankel singular values of $G(s)$ - internal product classification
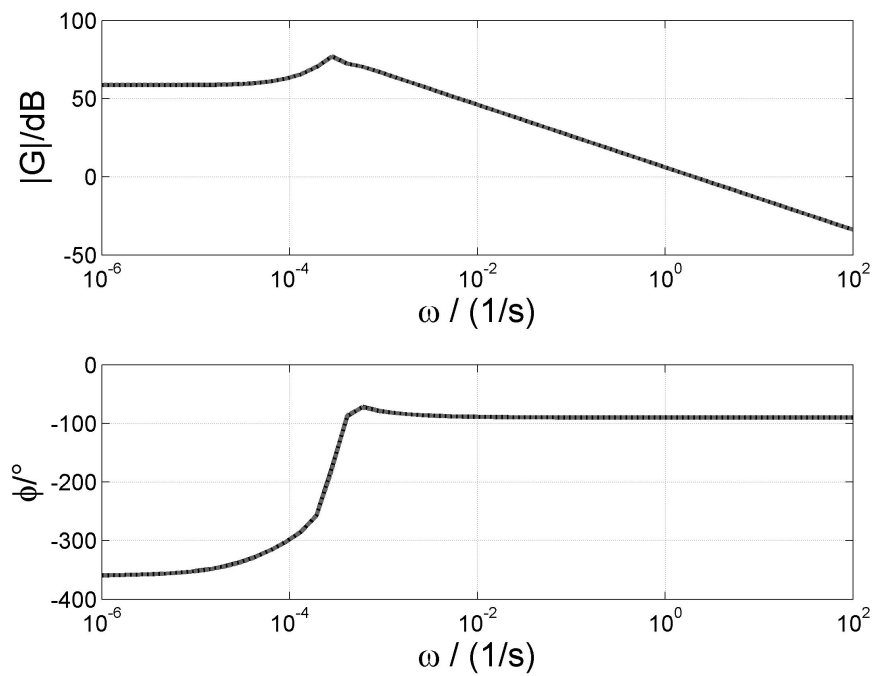
Figure 3.12: High order transfer function $G(s)$ (solid black) and reduced model $G_r(s)$ (dotted gray) - internal product classification
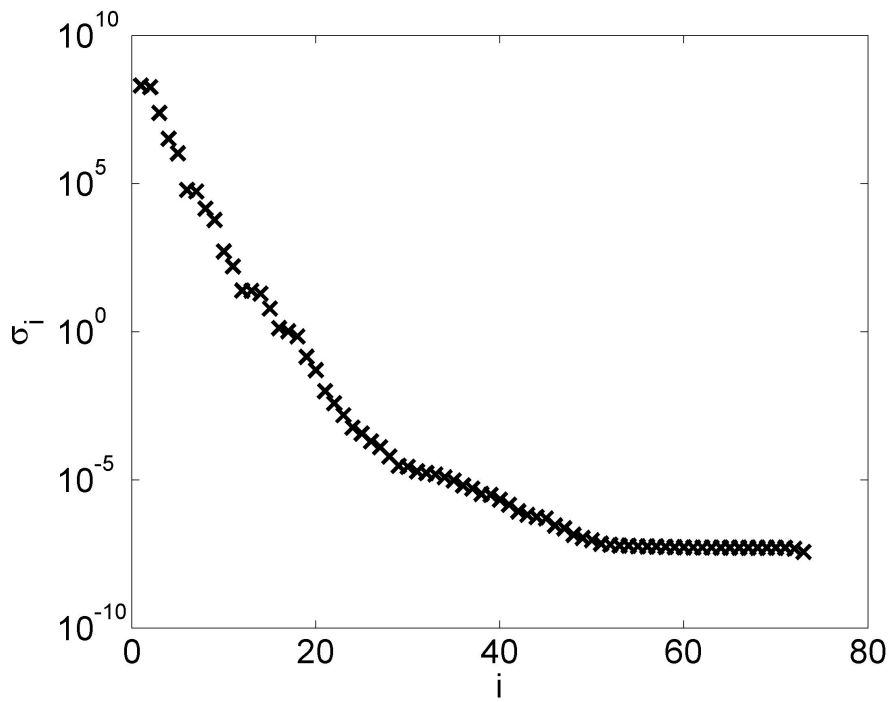
Figure 3.13: Hankel singular values of $G(s)$ - external product classification
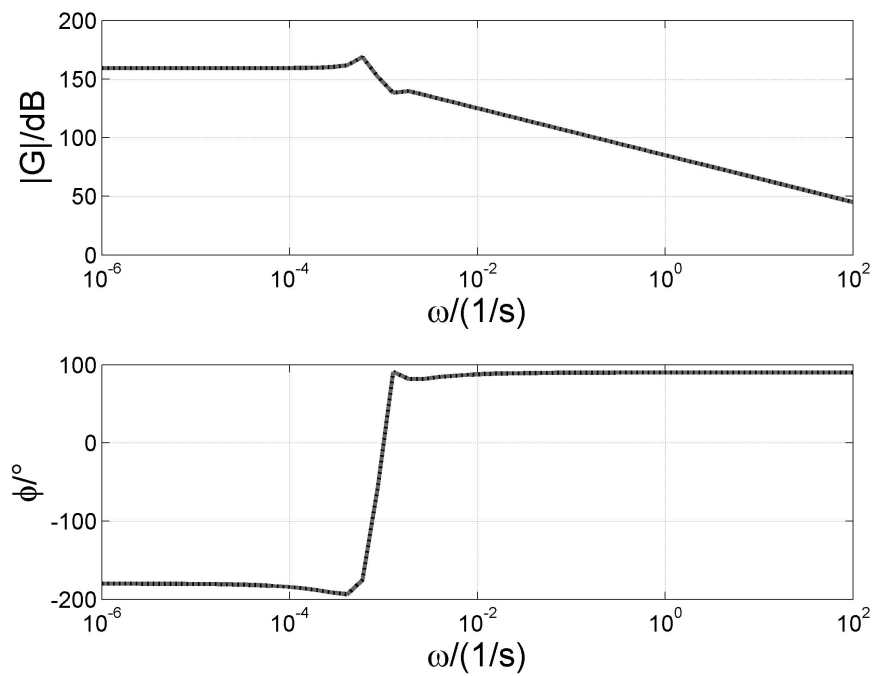
Figure 3.14: High order transfer function $G(s)$ (solid black) and reduced model $G_r(s)$ (dotted gray) - external product classification

3.3.2 Finite dimensional robust control design

In order to stabilize the particle size distribution in the whole range of $\{\dot{V}_e, \mu_M\}$, i.e. the family of linear models derived by linearization along the steady state continuation, in the following a control law is derived using H_∞-loopshaping methodology [67, 68]. Here the plant is represented by its normalized left coprime factorization with additive uncertainties $\Delta M(s), \Delta N(s)$ in each factor as depicted in Fig. 3.15.

$$G_\Delta(s) = (M(s) + \Delta_M(s))^{-1} (N(s) + \Delta_N(s)) \tag{3.105}$$
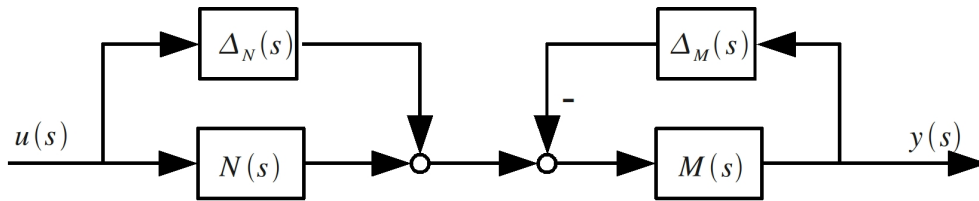
Figure 3.15: Coprime factor uncertainty

The normalized left coprime factor uncertainty is assumed to be stable with $\left\| \begin{bmatrix} \Delta_N & \Delta_M \end{bmatrix} \right\|_\infty < \epsilon$. It is well known that a controller K robustly stabilizes the perturbed feedback system (Fig. 3.3.2) if and only if it stabilizes the nominal system

$$G(s) = M(s)^{-1}N(s) \tag{3.106}$$

and

$$\left\| \begin{bmatrix} K \\ I \end{bmatrix} (I + GK)^{-1}M^{-1} \right\|_\infty \leq \frac{1}{\epsilon}. \tag{3.107}$$
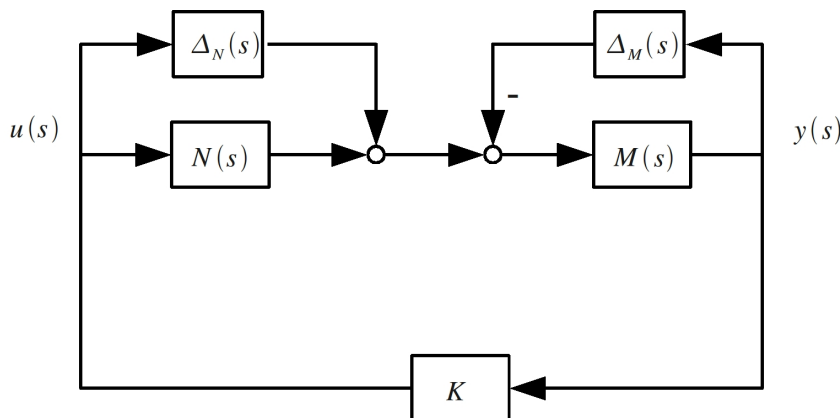
Figure 3.16: Perturbed feedback system

A coprime factor uncertainty representation is in general superior over others, e.g. additive or multiplicative uncertainties, as it is not restricted to perturbations which preserve the number of right half-plane poles of the plant. This fact is crucial for the control of

continuous fluidized bed spray granulation with internal and external product classification as stability behavior changes depending on the specific operating conditions, i.e. suspension injection rate $\dot{V}_e$ or mill grade μ_M.

For a given plant the maximal achievable stability margin ϵ_{max} is given by

$$\epsilon_{max} = (1 + \rho(XZ))^{-\frac{1}{2}} \tag{3.108}$$

where X and Z are the solutions of two algebraic Riccati equations

$$\left(A - BS^{-1}D^T C\right) Z + Z \left(A - BS^{-1}D^T C^T\right)^T - ZC^T R^{-1} CZ + BS^{-1}B^T = 0 \tag{3.109}$$

$$\left(A - BS^{-1}D^T C\right)^T X + X \left(A - BS^{-1}D^T C^T\right) - XB^T S^{-1} BX + CR^{-1}C^T = 0 \tag{3.110}$$

with

$$R = I + DD^T \qquad S = I + D^T D. \tag{3.111}$$

Moreover given an $\epsilon < \epsilon_{max}$ a controller K achieving a stability margin of ϵ can be calculated by

$$K_\infty = \left[\begin{array}{c|c} A + BF + \epsilon^{-2}(L^T)^{-1}ZC^T(C + DF) & \epsilon^{-2}(L^T)^{-1}ZC^T \\ \hline B^T X & -D^T \end{array} \right] \tag{3.112}$$

where

$$F = -S^{-1}(D^T C + B^T X) \qquad L = \left(1 - \epsilon^{-2}\right) I + XZ. \tag{3.113}$$

As the controller K_∞ gives only robust stability usually pre- and post-compensator $W_1(s)$ and $W_2(s)$ are used in order to shape the open loop singular values of the plant (Fig. 3.3.2) before calculating a robustly stabilizing controller K_∞.
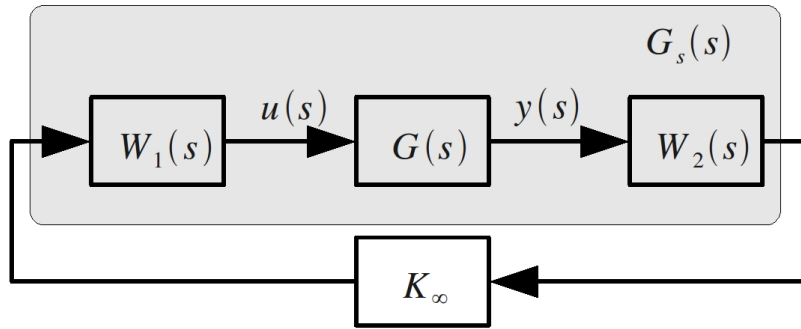
Figure 3.17: Shaped open loop

The overall controller K using the pre- and post-compensator $W_1(s)$ and $W_2(s)$ (Fig. 3.3.2) therefore reads

$$K = W_1 K_\infty W_2. \tag{3.114}$$

The application of H_∞-loopshaping design procedure for a shaped plant G_s, i.e. calculating a controller K for $G_s(s) = W_2(s)G(s)W_1(s)$ with given ϵ, results in a controller stabilizing all plants G with $\delta_g(G_s, G) < \epsilon$, where δ_g is the gap metric [69]. In the single-input single-output case the post-compensator W_2 can be set to one designing only the pre-compensator W_1. For the pre-compensator the design requirement of zero steady state error requires integral action.
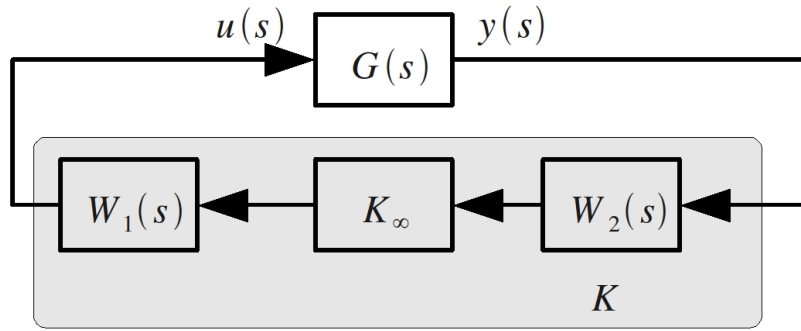
Figure 3.18: Robustly stabilizing controller

3.4 H_∞-loopshaping - internal product classification

For the fluidized bed spray granulation with internal classification the requirement of zero steady state error in the third moment μ_3 is reflected by the integral action in the pre-compensator $W_1(s)$, whereas additional poles and zeros are chosen such that a favorable shape near crossover is achieved. The pre- and post-compensator realizing the desired loop shape are therefore chosen as follows

$$W_1 = 8 \cdot 10^{-6} \frac{(500s + 1)^2}{s(200s + 1)}, \tag{3.115}$$

$$W_2 = 1. \tag{3.116}$$

The open loop Bode diagram of the original and shaped plant can be seen in Fig. 3.19.
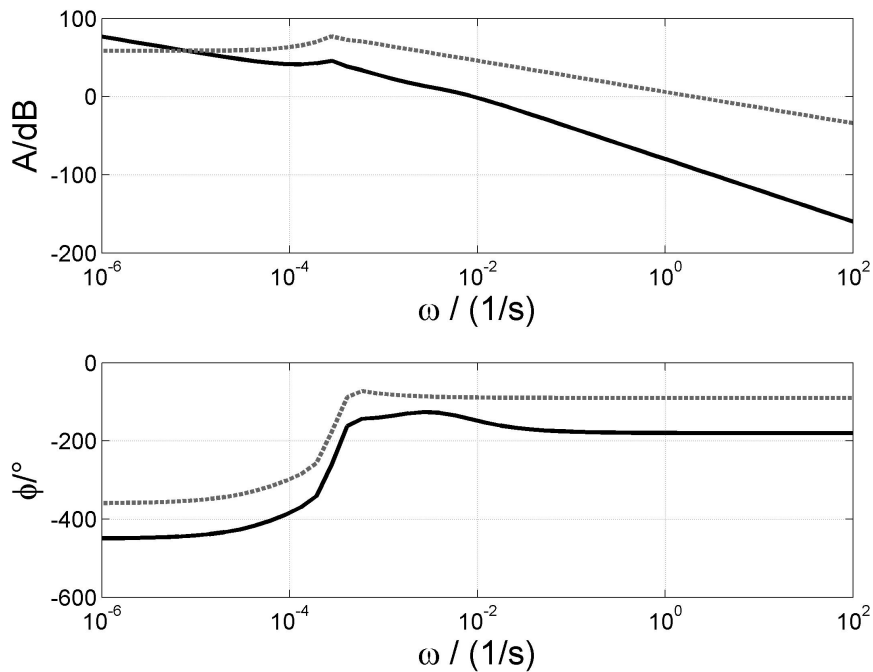
Figure 3.19: Open loop shape (dotted gray) and desired loop shape (solid black)

The required robustness margin δ_{RM} can be calculated using the triangular inequality and

the three error bounds (linearization at different set points (3.47), discretization (3.73) and finite dimensional model reduction (3.103)).

$$\delta_{RM} \leq \delta_{lin} + \delta_g(G_{150}, G) + \delta_g(G_{150}, G_r) \leq 0.045 \tag{3.117}$$

For the shaped plant $G_s = W_2 G W_1$ a robustly stabilizing controller K_∞ of order 9 is derived with $\epsilon = 0.5$. Hence, as $\epsilon > \delta_{RM}$ the derived controller guarantees robust stability. The Bode diagram of the calculated H_∞-loopshaping controller is depicted in Fig. 3.20.
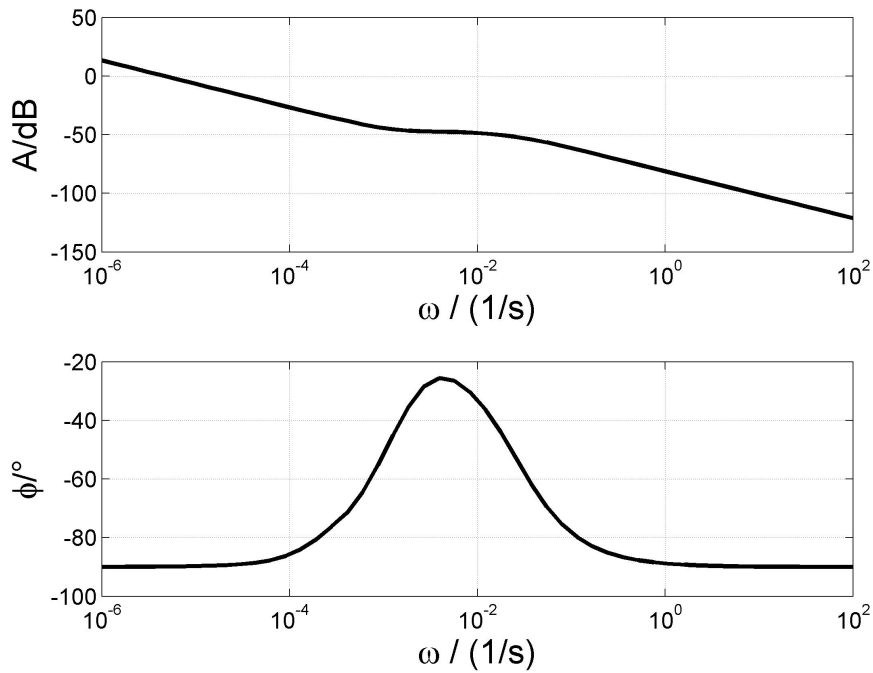
Figure 3.20: Bode plot of H_∞-loopshaping controller

As can be seen in Fig. 3.21 the difference between achieved and desired loop shape is small.

As the controller is designed for a special set point in the region of instability the remaining task is how to bring the process sufficiently near to the set point. One possibility might be to start the process with an initial particle size distribution near to the desired set point, which is obviously not favorable for a practical implementation. An alternative is to start open loop in the region of stability (for example the third moment associated to steady state distribution for $\dot{V}_{e,0} = 1.67 \cdot 10^5 \frac{mm^3}{s}$). As soon as the steady state is reached the control loop is closed and the set point is shifted slowly to the desired open loop unstable operating region (here $0.8\dot{V}_{e,0}$). The second approach has been implemented for the system without additional feedback control resulting in increasing oscillations, which would end in the associated limit cycle and for the system with the proposed H_∞-Loopshaping controller. As can be seen in Fig. 3.22 oscillations occurring during the shifting are damped in closed loop operation. The particle size distribution and all its moments $\mu_0, \mu_1, \mu_2, \mu_3$ are stabilized with reasonable control effort.

For an implementation the proposed control scheme should be robust with respect to variations in plant parameters and external disturbances. In the case of the fluidized bed
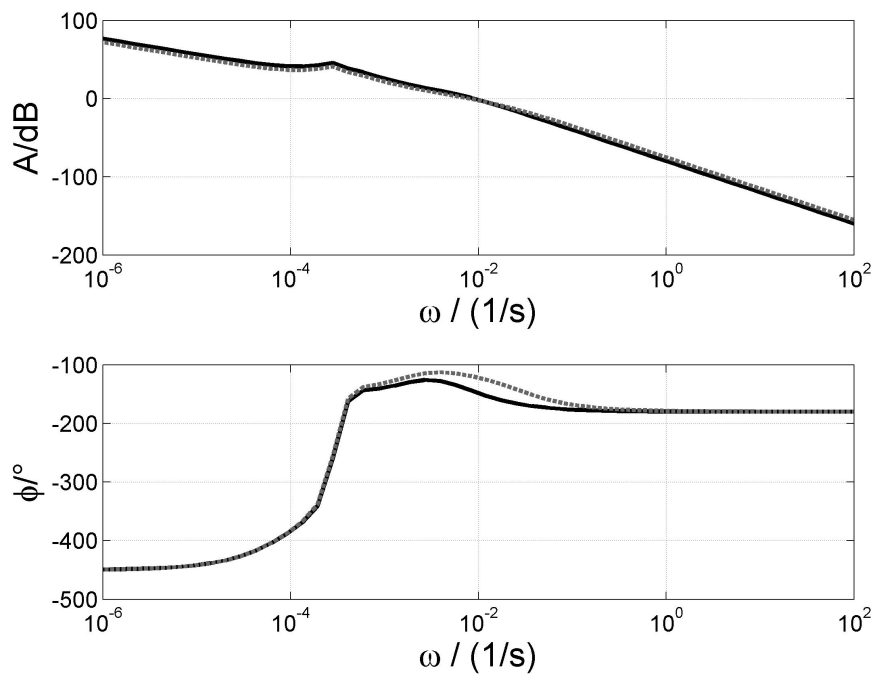
Figure 3.21: Desired (solid black) and achieved loop shape (dotted gray)

spray granulation with internal product classification a typical disturbance is a change in the drain K. Here, an increase by 10% of the product removal has been applied at $t = 2h$. As can be seen in Fig. 3.23 the controller is able to stabilize the system. Due to the integral action in the proposed H_∞-controller the error e converges to zero.
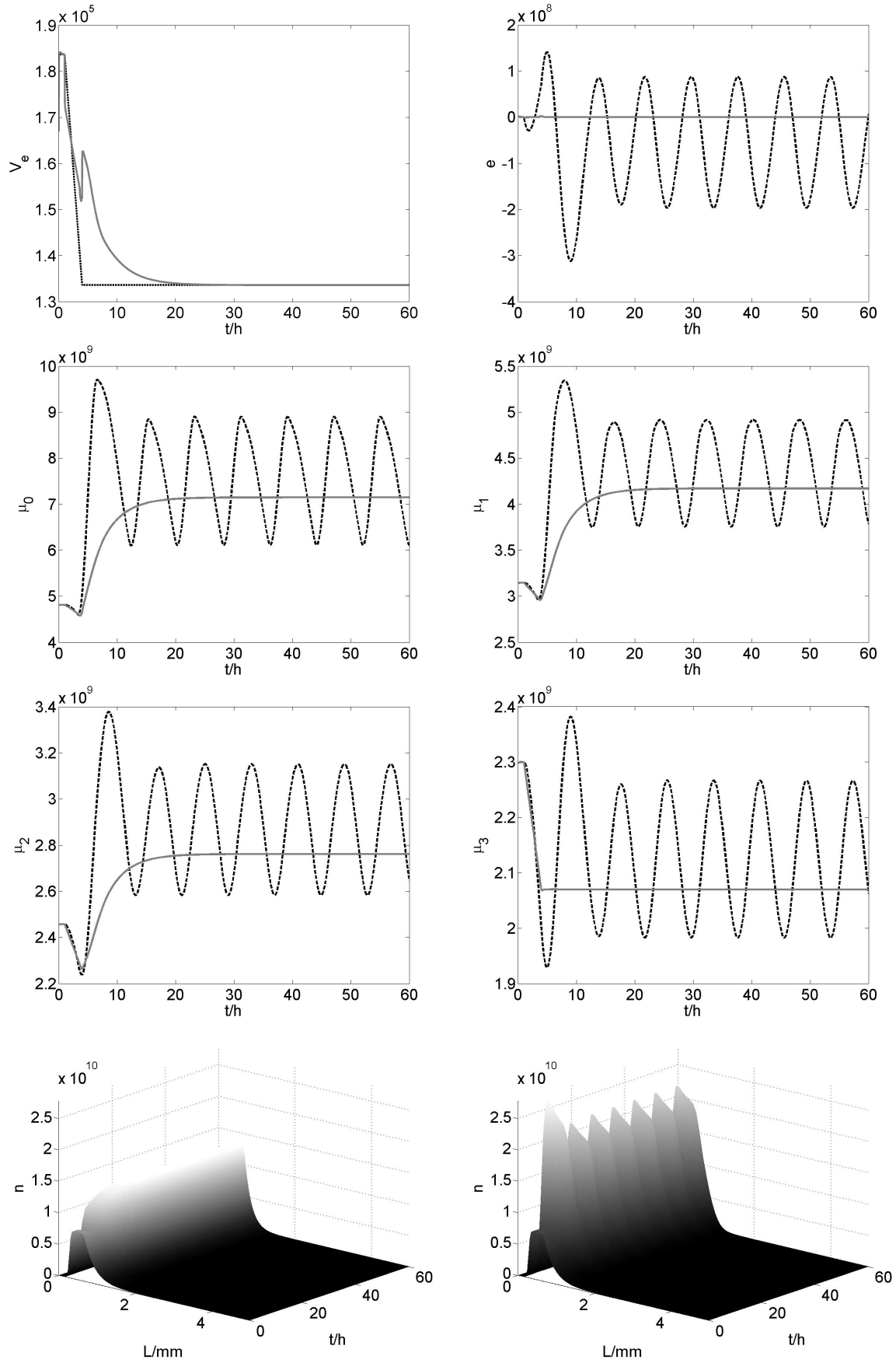
Figure 3.22: Start up with (dotted gray) and without control (solid black)
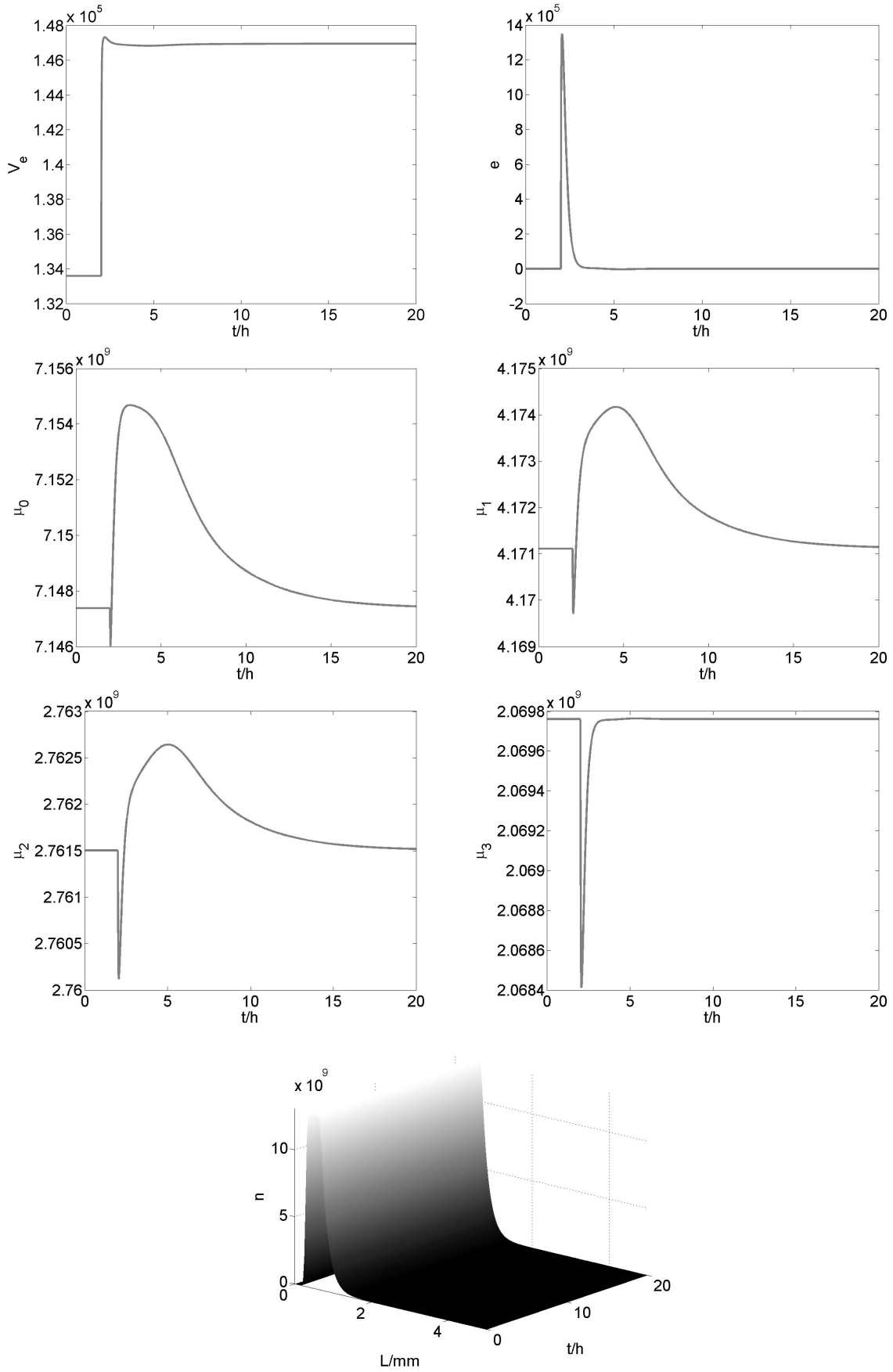
Figure 3.23: Disturbance resposense - increase of K by 10%

3.5 H_∞-loopshaping - external product classification

For the fluidized bed spray granulation with external classification again integral action is included in the pre-compensator $W_1(s)$ in order to achieve zero steady state error in the second moment μ_2. The existence of two right half plane poles and zeros suggests the use of zeros near the imaginary axis. In addition, fast left half plane poles are introduced, so that $W_1(s)$ is proper. The desired loop shape is therefore realized by choosing the following pre- and post-compensator

$$W_1 = 5 \cdot 10^{-3} \frac{(3.7 \cdot 10^3 s + 1)^4}{s(200s + 1)^4} \tag{3.118}$$

$$W_2 = 1. \tag{3.119}$$

The required robustness margin δ_{RM} can be calculated using the triangular inequality and the three error bounds (linearization at different set points (3.48), discretization (3.74) and finite dimensional model reduction (3.104)).

$$\delta_{RM} \leq \delta_{lin} + \delta_g(G_{160}, G) + \delta_g(G_{160}, G_r) \leq 0.31 \tag{3.120}$$

The open loop Bode diagram of the original and shaped plant can be seen in Fig. 3.24.
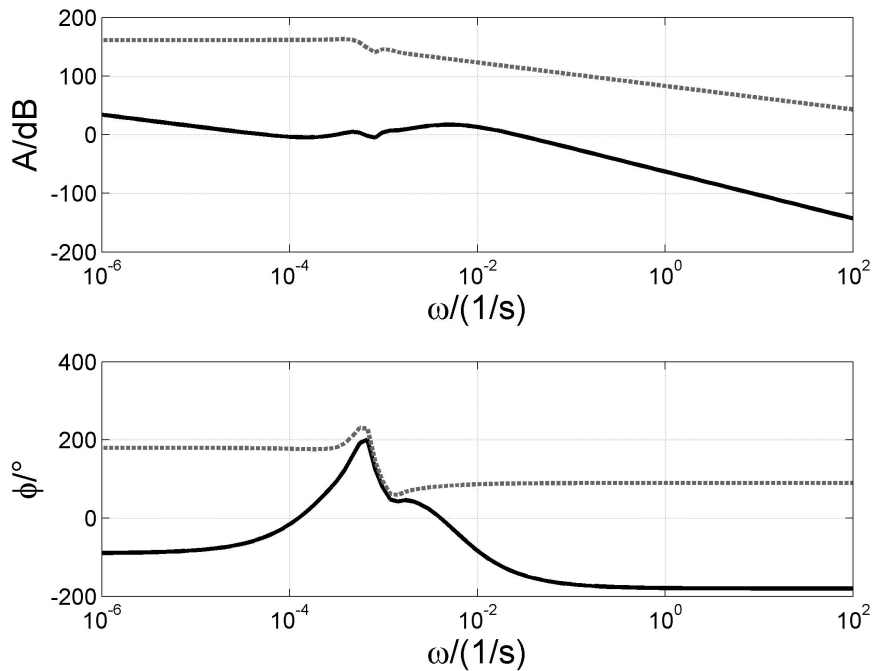
Figure 3.24: Open loop shape (dotted gray) and desired loop shape (solid black)

For the shaped plant $G_s = W_2 G W_1$ a robustly stabilizing controller K_∞ of order 10 is derived with $\epsilon = 0.4$. Hence, as $\epsilon > \delta_{RM}$ the derived controller guarantees robust stability. The Bode diagram of the calculated H_∞-loopshaping controller is depicted in Fig. 3.25. As can be seen in Fig. 3.26 the difference between achieved and desired loop shape is small.
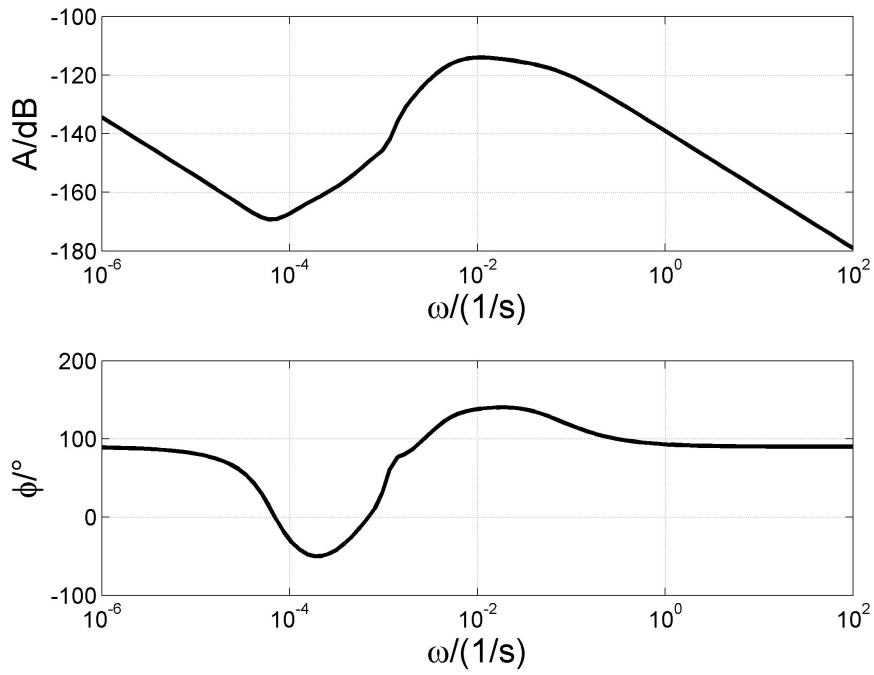
Figure 3.25: Bode plot of H_∞-loopshaping controller
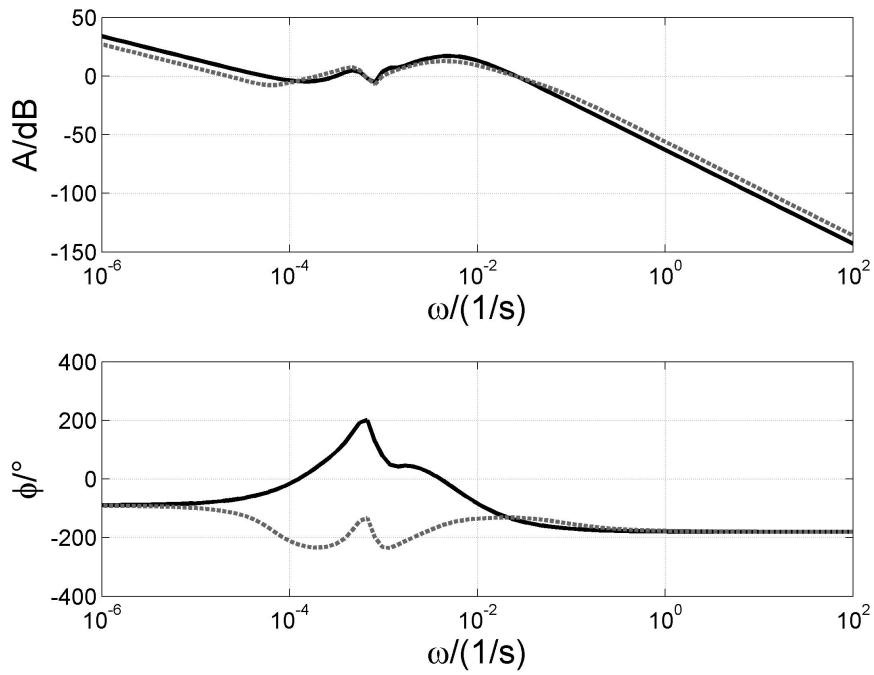
Figure 3.26: Desired (solid black) and achieved loop shape (dotted gray)

As for the fluidized bed spray granulation with internal classification the controller for the fluidized bed spray granulation with external classification has to be applied with an appropriate start-up strategy. Therefore, the processes is started open loop in the region of stability (for example $\mu_M = 0.9mm$). Reaching the steady state the control loop is closed and the set point is shifted slowly to the desired open loop unstable operating region (here the second moment associated to steady state distribution for $\mu_M = 0.5mm$). As can be seen in Fig. 3.27 oscillations occurring during the shifting are damped in closed loop operation. The particle size distribution and all its moments μ_0, μ_1, μ_2 are stabilized with reasonable control effort.

For an implementation the proposed control scheme should be robust with respect to variations in plant parameters and external disturbances. In the case of the fluidized bed spray granulation with external product classification a typical disturbance is a change in mean diameter of the sieving function T_1 and T_2 due to clogging. Here, an increase by 5% in the mean diameter L_1 and L_2 has been applied at $t = 0h$. As can be seen in Fig. 3.28 the controller is able to stabilize the system. Due to the integral action in the proposed H_∞-controller the error e converges to zero.
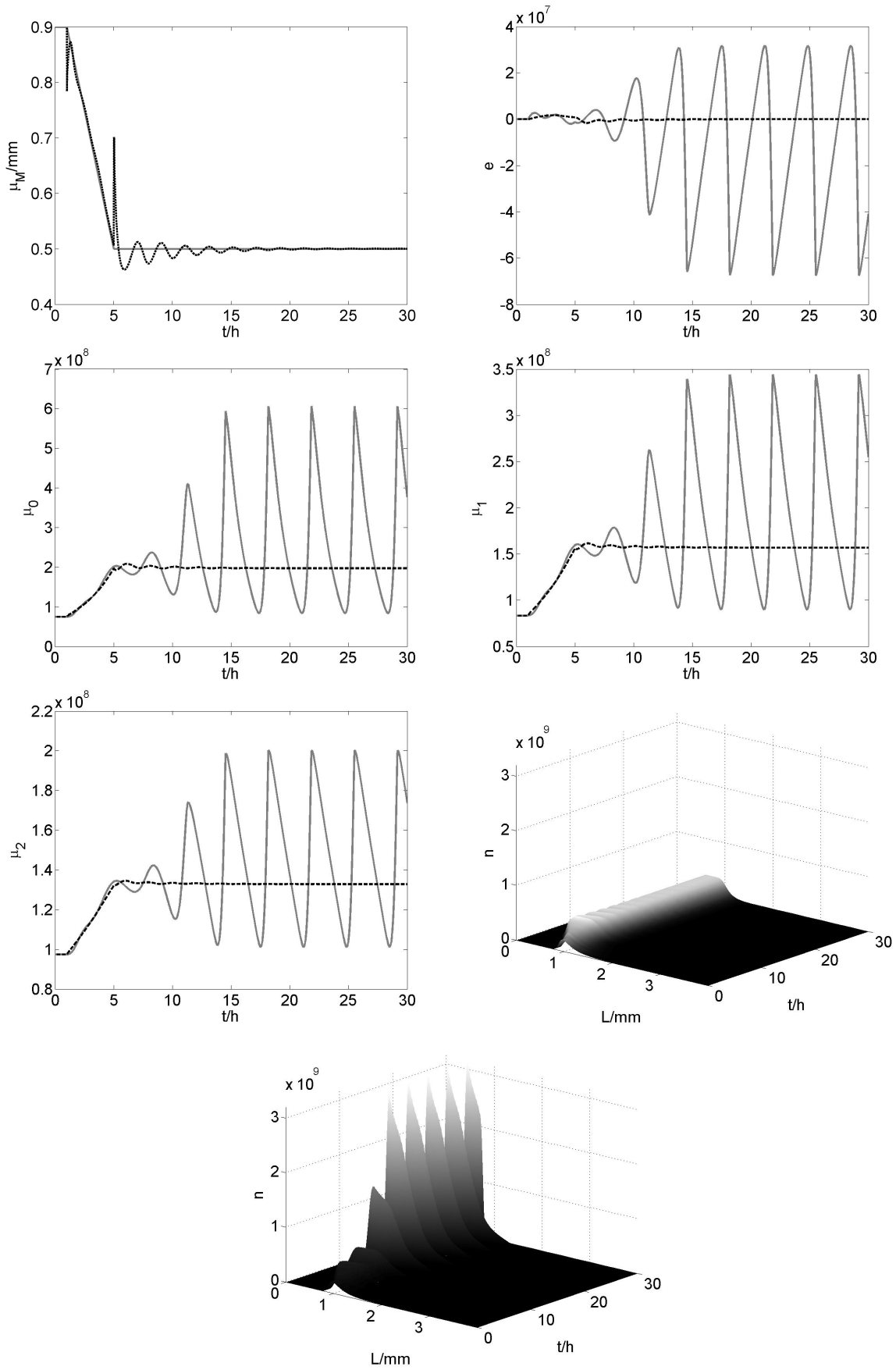
Figure 3.27: Start up with (dotted black) and without control (solid gray)
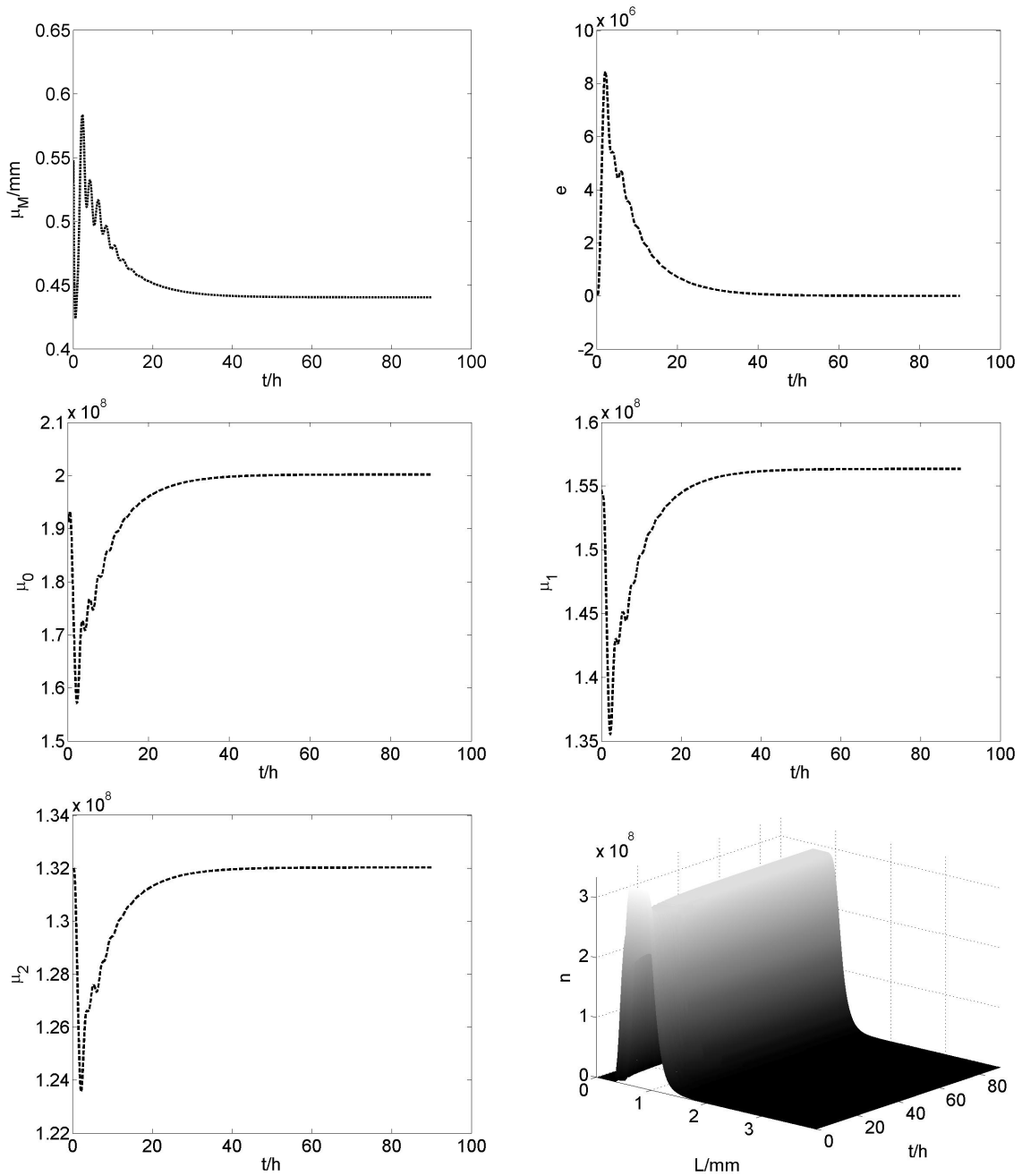
Figure 3.28: Disturbance resposense - increase of L_1 and L_2 by 5%

Chapter 4

Nonlinear analytical control design

This chapter deals with nonlinear control design for continuous fluidized bed spray granulation with internal and external product classification. The aim will be the development of an analytical control approach, i.e. without model or controller lumping. The proposed control approach is hence a direct controller design procedure with respect to the classification in Fig. 4.1.
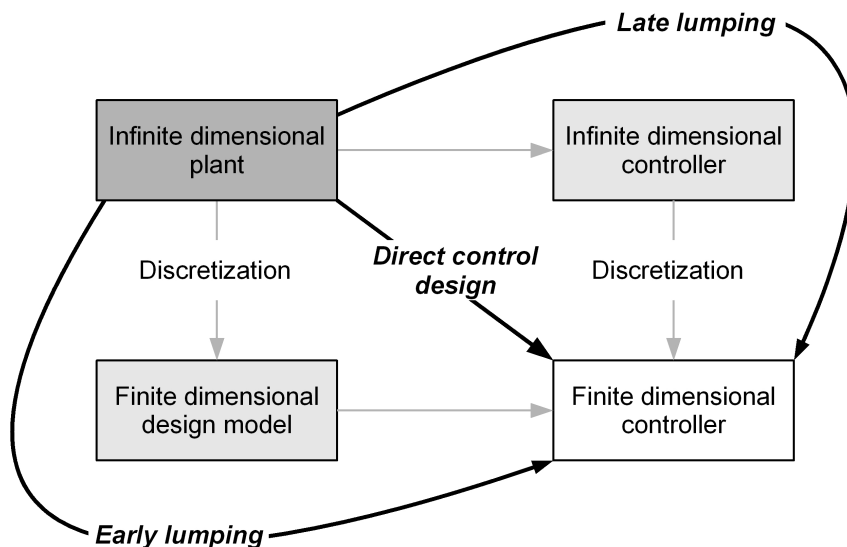
Figure 4.1: Control approaches for finite dimensional controller design

The structure of this chapter is as follows. Section 4.1 and 4.2 give a short and example based overview of standard stability theory for distributed parameter systems and its application to control design. Unfortunately, the presented theory cannot be directly applied to the class of problems studied in this Thesis. In order to overcome this problem the use of a generalized stability theory, called stability with respect to two discrepancies [76, 77, 78, 79], is motivated in section 4.3. Using this generalized stability theory two nonlinear control laws guaranteeing exponential convergence in a generalized distance measure are derived in section 4.4 and 4.5. It has to be mentioned, that the discrepancy based control approach presented in this Thesis guarantees stability of the particle size distribution in a L_p or L_∞-norm if and only if the zero dynamics associated with the chosen discrepancy, i.e. the generalized distance measure, are stable. Unfortunately,

fluidized bed spray granulations with external product classification possess in some region of operating conditions unstable zero dynamics. A solution approach, making use of an additional parallel compensator [120], is studied at the end of section 4.5.

4.1 Stability for distributed parameter systems

Before starting the analysis of distributed parameter systems, which are infinite dimensional, we take a look at finite dimensional systems [75], i.e. ordinary differential equations.

$$\dot{x} = f(t, x) \tag{4.1}$$

In the following we assume that (4.1) has an equilibrium x_0 at $x_0 = 0$, i.e. $f(t, x_0) = 0$. This is without loss of generality as we can transform any equilibrium $z_0 \neq 0$ by introducing the new state variable $x = z - z_0$ into an equilibrium $x_0 = 0$. The system (4.1) is called stable in the sense of Lyapunov if for any $\varepsilon > 0$ there exists a $\delta > 0$ such that for $|x(0)| < \delta$ follows $|x(t)| < \varepsilon$ for $t > 0$. If in addition the following inequality holds

$$\|x(t)\| \leq a\|x(0)\|e^{-bt} \tag{4.2}$$

for $t \geq 0$ and $a, b > 0$, then the system (4.1) is exponentially stable.

In order to determine stability for a given system there exist two distinct approaches

- using the solution $x(t)$ of the system,

- using Lyapunov stability theory.

In the case of a linear system

$$\dot{x} = Ax \tag{4.3}$$

the solution can be calculated up to a constant C, which is determined by the initial condition $x(t = 0)$.

$$x(t) = Ce^{At} \tag{4.4}$$

It is well known, that if the eigenvalues of A have all negative real part the system (4.3) is exponentially stable. Therefore, in the case of linear systems the solution can be used to detecte stability by solving an eigenvalue problem. In the nonlinear case the calculation of an analytical solution is in general infeasible and therefore Lyapunov stability theory has to be used. Here, the existence of a Lyapunov function $V(x)$ with the following properties

- $V(x)$ is positive definite, i.e. $V(x \neq 0) > 0$ and $V(0) = 0$,

- $\dot{V}(x)$ is negative definite, i.e. $\dot{V}(x \neq 0) < 0$ and $\dot{V}(0) = 0$,

gives stability. In the linear case an appropriate V (if exists) can be calculated by solving the following Lyapunov equation for P

$$A^T P + PA + Q = 0 \tag{4.5}$$

with an arbitrary positive definite Q. Using the solution P the associated Lyapunov function is $V(x) = x^T P x$ with $\dot{V}(x) = -x^T Q x$.

Both approaches have been extended to distributed parameter systems. In the solution

based approach semigroup theory is applied to interpret the linear infinite dimensional system as an abstract operator equation (4.6),

$$\frac{dx}{dt} = Ax(t) \tag{4.6}$$

where A is the infinitesimal generator of a semigroup $T(t)$. Stability can be tested by investigating the resolvent $R(\lambda, A)$. When applying Lyapunov stability theory to distributed parameter systems Lyapunov functionals have to be used.

One problem, when investigating stability for distributed parameter systems is that in contrast to finite dimensional systems, where all vector norms $\|\cdot\|$ are equivalent in the sense that they define the same topology, in the case of infinite dimensional systems convergence in one function norm does not imply convergence in another.

As the field of stability theory for distributed parameter systems is very broad and diverse we concentrate in the following on important case studies.

4.1.1   Parabolic partial differential equation

In the following, the stability of a parabolic partial differential equation with Dirichlet boundary conditions (4.10)-(4.12) is investigated [91]. In a first step, stability with respect to the L_2-norm,

$$\|w\|_2 = \left(\int_0^1 w^2(x)dx \right)^{1/2}, \tag{4.7}$$

is shown, then using stability with respect to the H_1-norm,

$$\|w\|_{H_1} = \left(\int_0^1 w^2(x) + \left(\frac{\partial w}{\partial x} \right)^2 dx \right)^{1/2}, \tag{4.8}$$

as an intermediate step pointwise convergence, i.e. stability in the L_∞-norm,

$$\|w\|_\infty = \max_{x \in [0,1]} |w(x)|^2 \tag{4.9}$$

is proven.

$$\frac{\partial w}{\partial t} = \frac{\partial^2 w}{\partial x^2} \tag{4.10}$$
$$w(0,t) = 0 \tag{4.11}$$
$$w(1,t) = 0 \tag{4.12}$$

Stability with respect to the L_2-norm

Using the following Lyapunov functional

$$V = \frac{1}{2} \int_0^1 w^2(x,t)dx \tag{4.13}$$

and calculating the time derivative gives

$$\dot{V} = -\int_0^1 \left(\frac{\partial w}{\partial x}\right)^2 dx. \tag{4.14}$$

Hence, V is clearly bounded by its initial value $V(0)$. However, since it depends on $\frac{\partial w}{\partial x}$ convergence of V towards zero is not obvious. Therefore we use the Poincare inequality (Appendix D) and the boundary conditions to get an estimate for $\dot{V}$.

$$\dot{V} = -\int_0^1 \left(\frac{\partial w}{\partial x}\right)^2 dx \leq -\frac{1}{4}\int_0^1 w^2 dx \leq -\frac{1}{2}V \tag{4.15}$$

This implies

$$V(t) \leq e^{-\frac{t}{2}}V(0) \tag{4.16}$$

and taking the square root exponential stability with respect to the L_2-norm follows

$$\|x(t)\|_2 \leq e^{-\frac{t}{4}}\|x(0)\|_2. \tag{4.17}$$

Stability with respect to the H_1-norm

Using the following augmented Lyapunov functional

$$V = \frac{1}{2}\int_0^1 w^2(x,t)dx + \frac{1}{2}\int_0^1 \left(\frac{\partial w}{\partial x}\right)^2 dx \tag{4.18}$$

and calculating the time derivative gives

$$\dot{V} = -\int_0^1 \left(\frac{\partial w}{\partial x}\right)^2 dx + \int_0^1 \frac{\partial w}{\partial x}\frac{\partial}{\partial x}\left(\frac{\partial w}{\partial t}\right), \tag{4.19}$$

$$\overset{P.I.}{=} -\int_0^1 \left(\frac{\partial w}{\partial x}\right)^2 dx + \frac{\partial w}{\partial x}\frac{\partial^2 w}{\partial x^2}\Big|_0^1 - \int_0^1 \left(\frac{\partial^2 w}{\partial x^2}\right)^2 dx. \tag{4.20}$$

Due to the fact that $\frac{\partial^2 w}{\partial x^2}$ is equal to $\frac{\partial x}{\partial t}$ and w is constant at the boundary, i.e. $w(0) = w(1) = 0$, the second term is equal to zero.

$$\dot{V} = -\int_0^1 \left(\frac{\partial w}{\partial x}\right)^2 dx - \int_0^1 \left(\frac{\partial w}{\partial x}\right)^2 dx \tag{4.21}$$

$$\leq -\int_0^1 \left(\frac{\partial w}{\partial x}\right)^2 dx \tag{4.22}$$

Again V is bounded by its initial value $V(0)$. In order to show exponential stability the Poincare inequality (Appendix D) is used to derive the following estimate of $\dot{V}$.

$$\dot{V} \leq -\int_0^1 \left(\frac{\partial w}{\partial x}\right)^2 dx \leq -\frac{1}{2}\int_0^1 \left(\frac{\partial w}{\partial x}\right)^2 dx - \frac{1}{2}\int_0^1 \left(\frac{\partial w}{\partial x}\right)^2 dx \tag{4.23}$$

$$\leq -\frac{1}{8}\int_0^1 w^2 dx - \frac{1}{2}\int_0^1 \left(\frac{\partial w}{\partial x}\right)^2 dx \tag{4.24}$$

$$\leq -\frac{1}{8}\int_0^1 w^2 dx - \frac{1}{8}\int_0^1 \left(\frac{\partial w}{\partial x}\right)^2 dx \tag{4.25}$$

$$\leq -\frac{1}{4}V \tag{4.26}$$

This implies

$$V(t) \leq e^{-\frac{t}{4}} V(0) \tag{4.27}$$

and therefore exponential stability with respect to the H_1-norm immediately follows

$$\|x(t)\|_{H_1} \leq e^{-\frac{t}{4}} \|x(0)\|_{H_1}. \tag{4.28}$$

Stability with respect to the L_∞-norm - pointwise convergence

In order to show stability with respect to the L_∞-norm the boundary condition and Young's and Agmon's inequalities (Appendix D) are used.

$$
\begin{aligned}
\|w\|_\infty = \max_{x \in [0,1]} |w(x,t)|^2 &\leq 2\|w(t)\|_2 \left\| \frac{\partial w}{\partial x} \right\|_2 & (4.29) \\
&\leq \|w\|_2 + \left\| \frac{\partial w}{\partial x} \right\|_2 & (4.30) \\
&\leq e^{-\frac{t}{2}} \left(\|w(0,t)\|_2^2 + \left\| \frac{\partial w(0,t)}{\partial x} \right\|_2^2 \right) & (4.31)
\end{aligned}
$$

Therefore $w(x,t) \to 0$ as $t \to \infty$.

4.1.2   Hyperbolic partial differential equation

Consider the following first order hyperbolic partial differential equation.

$$
\begin{aligned}
\frac{\partial w}{\partial t} &= \frac{\partial w}{\partial x} & (4.32) \\
w(1) &= 0 & (4.33)
\end{aligned}
$$

Stability can be shown by using the following Lyapunov-Krasovskii functional

$$V = \frac{1}{2} \int_0^1 (1+x) w(x,t)^2 dx \tag{4.34}$$

Evaluating the time derivate and applying integration by parts gives

$$\dot{V} \quad = \quad \int_0^1 (1+x)ww_t dx \tag{4.35}$$

$$= \quad \int_0^1 (1+x)ww_x dx = \int_0^1 (1+x)\frac{1}{2}\frac{\partial w^2}{\partial x}dx \tag{4.36}$$

$$\overset{P.I.}{=} \quad \left.\frac{1+x}{2}w^2\right|_0^1 - \frac{1}{2}\int_0^1 w^2 dx \tag{4.37}$$

$$= \quad w(1,t)^2 - \frac{1}{2}w(0,t)^2 - \frac{1}{2}\int_0^1 w^2 dx \tag{4.38}$$

$$\leq \quad -\frac{1}{2}\int_0^1 w^2 dx = -\frac{1}{4}\int_0^1 w^2 dx - \frac{1}{4}\int_0^1 w^2 dx \tag{4.39}$$

$$\leq \quad -\frac{1}{4}\int_0^1 xw^2 dx - \frac{1}{4}\int_0^1 w^2 dx \leq -\frac{1}{4}\int_0^1 (x+1)w^2 dx \tag{4.40}$$

$$\leq \quad -\frac{1}{2}V \tag{4.41}$$

Therefore, the system is exponentially stable in the sense of the norm

$$\left(\frac{1}{2}\int_0^1 (1+x)w(x,t)^2 dx\right)^{\frac{1}{2}}. \tag{4.42}$$

4.1.3   Stability of a general PBE

In the following, the stability of the equilibrium $n_d = 0$ of a general population balance equation (4.43) with length independent growth rate G is investigated.

$$\frac{\partial n}{\partial t} = G\frac{\partial n}{\partial L} + F(n,L) \tag{4.43}$$

Choosing the candidate Lyapunov functional as follows

$$V = \frac{1}{2}\int_0^\infty (1+L)n^2 dL \tag{4.44}$$

and taking the time derivative of V along equation (4.43) yields

$$\dot{V} \quad = \quad \int_0^\infty (1+L)n\frac{\partial n}{\partial t}dL, \tag{4.45}$$

$$= \quad \int_0^\infty (1+L)n\left[G\frac{\partial n}{\partial L} + F(n,L)\right]dL, \tag{4.46}$$

$$= \quad \int_0^\infty \left[G(1+L)n\frac{\partial n}{\partial L} + (1+L)nF(n,L)\right]dL. \tag{4.47}$$

As the growth rate G is length independent, i.e. $G \neq f(L)$, the time derivative of the

candidate Lyapunov functional $\dot{V}$ can be written as follows

$$
\begin{aligned}
\dot{V} &= G \int_0^\infty (1+L)n\frac{\partial n}{\partial L}dL + \int_0^\infty (1+L)nF(n,L)dL, & (4.48) \\
&= G \int_0^\infty \frac{(1+L)}{2}\frac{\partial n^2}{\partial L}dL + \int_0^\infty (1+L)nF(n,L)dL, & (4.49) \\
&\overset{P.I.}{=} \frac{G}{2}\left[\lim_{L\to\infty}(1+L)n(L,t)^2 - n(0,t)^2\right] - \frac{G}{2}\int_0^\infty n^2 dx \\
&\quad + \int_0^\infty (1+L)nF(n,L)dL. & (4.50)
\end{aligned}
$$

However, in this general setting stability strongly depends on the present source term $F(n,L)$, growth rate G and the boundary conditions $n(0,t)$ and $\lim_{L\to\infty} n(L,t)$. Therefore, stability analysis, irrespective of the norm underlying the chosen Lyapunov functional, is at least very difficult, if not infeasible, for the fluidized bed spray granulation with external and internal product classification.

4.2 Stabilization of distributed parameter systems

Over the last decades different methods for stabilization of systems with distributed parameters have been developed. Most of them are based on the solution of the system itself or at least the desired error system, i.e. the system in closed loop operation. In the backstepping approach [80, 91, 92, 100] for example the control input is designed such that it maps the original system onto a desired stable error system. In the works of Bastin et. al. [87, 88, 84, 97] stability is proven using the solution derived by the method of characteristics. For infinite dimensional electromechanical systems a stabilizing control law can be derived using the associated Hamiltonian [98, 101, 99].

In order to clarify the problems of control design for fluidized bed spray granulation with external and internal product classification, stabilization of a general population balance equation in a L_2-norm is investigated. Further, a reformulation of the stabilization problem is motivated being crucial for solvability.

4.2.1 Stabilization of a general PBE in L^2-norm

In the following, the stabilitzation of the equilibrium n_d of a general population balance equation (4.51) by a control u will be investigated. In view of generalization a length dependent growth rate is considered.

$$
\frac{\partial n}{\partial t} = \frac{\partial G(L)n}{\partial L} + F(n,L)u \tag{4.51}
$$

Choosing the candidate Lyapunov functional as follows

$$
V = \frac{1}{2}\int_0^\infty (n-n_d)^2 dL \tag{4.52}
$$

and taking the time derivate of V along equation (4.51) yields

$$\dot{V} = \int_0^\infty (n - n_d)\frac{\partial n}{\partial t}dL \tag{4.53}$$

$$= \int_0^\infty (n - n_d)\left[\frac{\partial G(L)n}{\partial L} + F(n, L)u\right]dL. \tag{4.54}$$

A typical Lyapunov design procedure would choose the control u such that

$$\dot{V} = -2cV. \tag{4.55}$$

However, in this case the control u would read

$$u = F(n, L)^{-1}\left(-c(n - n_d) - \frac{\partial G(L)n}{\partial L}\right) \tag{4.56}$$

which is clearly infeasible unless we are dealing with a distributed control action. As the control input u is in most cases a concentrated input this approach is impossible. In order to overcome this problem the deviation n_e of a particle size distribution n to a desired particle size distribution n_d, i.e. $n_e = n - n_d$, will not be measured in a L^p-norm but in the sense of a moment of n_e for example the second moment. The associated candidate Lyapunov functional is hence defined as follows

$$V = \frac{1}{2}\left(\int_0^\infty L^2(n_d - n)dL\right)^2. \tag{4.57}$$

Calculating the time derivate $\dot{V}$ gives

$$\dot{V} = -\int_0^\infty L^2(n_d - n)dL \int_0^\infty L^2\left(\frac{\partial G(L)n}{\partial L} + F(n, L)u\right)dL \tag{4.58}$$

or equivalently for a concentrate control input u

$$\dot{V} = -\int_0^\infty L^2(n_d - n)dL\left[\int_0^\infty L^2\left(\frac{\partial G(L)n}{\partial L}\right)dL + \int_0^\infty L^2 F(n, L)dLu\right]. \tag{4.59}$$

In this case the design requirement of an exponentially converging Lyapunov functional, i.e.

$$\dot{V} = -2cV \tag{4.60}$$

can be realized by choosing the following control law

$$u = \frac{c\int_0^\infty L^2(n_d - n)dL - \int_0^\infty L^2\frac{\partial G(L)n}{\partial L}dL}{\int_0^\infty L^2 F(n, L)dL}. \tag{4.61}$$

This motivates the use of moments for control design. Before deriving control laws for the fluidized bed spray granulation with internal and external classifications, the connection between the moment $\Delta\mu_i$ of a particle size distribution n and the particle size distribution n itself have to be investigated. It will be shown, that a moment $\Delta\mu_i$ or a norm of $\Delta\mu_i$ is not a norm for the particle size distribution n. Therefore, stabilizing an arbitrary moment $\Delta\mu_i$ of a particle size distribution n does not automatically yield stabilization of n in any norm.

A norm is a real-valued function mapping an element of a space (here the particle size distribution n) onto the set of positive real number. It has to fulfill the following three conditions:

1. $\|n\| = 0 \Rightarrow n = 0$, i.e. the norm vanishes only for the zero element,

2. $\|\alpha n\| = |\alpha|\|n\|$ for an arbitrary $\alpha \in \mathbb{K}$ (homogeneity),

3. $\|n_1 + n_2\| \le \|n_1\| + \|n_2\|$ (triangle inequality).

The moment $\Delta\mu_i$ of a particle size distribution n is a real-valued function mapping n onto the set of real numbers. As long as n is positive $\Delta\mu_i$ even maps n onto the set of positive real numbers. However, as we are interested in the deviation n_e of a particle size distribution n to a desired particle size distribution n_d, i.e. $n_e = n - n_d$, the moment $\Delta\mu_i = \int_0^\infty L^i(n-n_d)dL$ can also be negative. Thus, norms of the moment $\Delta\mu_i$ are studied. As we are dealing with a one-dimensional quantity for which all p-norms are equivalent we restrict ourselves to the 1-norm, i.e.

$$\|\Delta\mu_i\|_1 = |\Delta\mu_i| = \left| \int_0^\infty L^i n dL \right|. \tag{4.62}$$

If $\|\Delta\mu_i\|_1$ would be a norm for the deviation n_e of the particle size distribution n from a desired particle size distribution n_d it should satisfy the three norm conditions:

1. $\|n_e\| = 0 \Rightarrow n_e = 0$, taking a look at the following counter example depicted in Fig. 4.2 with $\|n_e\| = 0$ and $n_e \ne 0$ shows that the first condition is clearly not satisfied.

$$n_e = (\sigma(L - L_0) - \sigma(L - (L_1 + L0)))\frac{1}{L^i} - (\sigma(L - (L_1 + L_0)) - \sigma(L - (2L_1 + L_0)))\frac{1}{L^i} \tag{4.63}$$

Here, $\sigma(L)$ is the Heaviside step function.

2. the second condition is satisfied, i.e.

$$\left| \int_0^\infty L^i \alpha n_e dL \right| = |\alpha| \left| \int_0^\infty L^i n_e dL \right| \tag{4.64}$$

3. the third condition is satisfied, i.e.

$$\left| \int_0^\infty L^i (n_{e,1} + n_{e,2}) dL \right| = \left| \int_0^\infty L^i n_{e,1} dL + \int_0^\infty L^i n_{e,2} dL \right| \tag{4.65}$$

$$\le \left| \int_0^\infty L^i n_{e,1} dL \right| + \left| \int_0^\infty L^i n_{e,2} dL \right|. \tag{4.66}$$

Therefore, the norm of any moment $\Delta\mu_i$ of $n_d - n$ is not a norm of $n_d - n$. Consequently, convergence of the moment $\Delta\mu_i$ does not automatically imply convergence of the deviation in the particle size distribution $n_d - n$. Hence, from a stability theory point of view, stability has to be interpreted in a generalized setting. This will be achieved by identifying norms of moments with discrepancies, generalized distance measures, and applying the concept of stability with respect to two discrepancies.
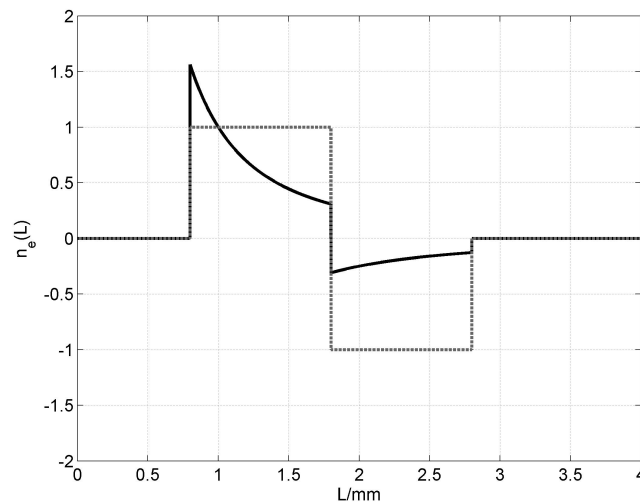
Figure 4.2: Counter example $n_e(L)$ for $L_0 = 0.8mm$ and $L_1 = 1mm$ with $i = 0$ (solid black) and $i = 2$ (dotted gray)

4.3 Stability with respect to two discrepancies

In the following, the most important properties and facts on stability with respect to two discrepancies are stated in accordance to [76, 77, 78, 79]. Here, the process $\varphi(.,t)$ is a solution of the distributed parameter system and $\varphi_0 = 0$ an equilibrium of the system.

Definition 8. *Discrepancy*
A discrepancy is a real valued functional $\rho = \rho[\varphi(.,t),t]$ *with the following properties*

  1. $\rho(\varphi,t) \geq 0$

  2. $\rho(0,t) = 0$

  3. *for an arbitrary process* $\varphi = \varphi(.,t)$ *the real valued functional* $\rho(\varphi(.,t),t)$ *is continuous with respect to* t.

The discrepancy $\rho(\varphi(.,t),t)$ is a measure of the distance between the process $\varphi(.,t)$ and the equilibrium φ_0. Any measure of distance with the above described properties can be used. Of great importance is the fact that a discrepancy has not all properties of a metric, e.g. symmetry $d(x,y) = d(y,x)$ or triangular inequality $d(x,y) \leq d(x,z) + d(z,y)$ are not satisfied. In addition, it has not to satisfy the important property of definiteness, i.e. a vanishing discrepancy $\rho(\varphi,t) = 0$ does not automatically imply $\varphi = 0$. Therefore, the discrepancy is an extension of the distance measures normally used in stability theory for distributed parameter systems like L_p and L_∞- norms.
In the context of stability with respect to two discrepancies besides the discrepancy $\rho(\varphi(.,t,t))$ measuring the distance between $\varphi(.,t)$ and the equilibrium φ_0, a second time independent discrepancy ρ_0 is used describing the distance between the initial state $\varphi(.,0)$ and the equilibrium φ_0. The two discrepancies ρ and ρ_0 have to satisfy, that the discrepancy $\rho(\varphi(.,t),t)$ is continuous at time $t = t_0$ with respect to ρ_0 at $\rho_0 = 0$, i.e. for every $\varepsilon > 0$ and $t_0 > 0$ there exists a $\delta(\varepsilon, t_0) > 0$, such that from $\rho_0 \leqslant \delta(\varepsilon, t_0)$ it follows that $\rho < \varepsilon$.

Definition 9. *Stability with respect to two discrepancies ρ and ρ_0*
The equilibrium $\varphi_0 = 0$ is stable in the sense of Lyapunov with respect to the two discrepancies ρ and ρ_0 for all $t \geq t_0$ if for every $\varepsilon > 0$ and $t_0 \geq 0$ there exists a $\delta = \delta(\varepsilon, t_0) > 0$ such that for every process $\varphi(.,t)$ with $\rho_0 < \delta(\varepsilon, t_0)$ it follows that $\rho < \varepsilon$ for all $t \geq t_0$. If in addition $\lim_{t \to \infty} \rho = 0$, than the equilibrium φ_0 is called asymptotically stable in the sense of Lyapunov with respect to the two discrepancies ρ and ρ_0.

The basis of many nonlinear control methods is the stability theory of Lyapunov [106, 107, 111, 113, 114, 115]. The knowledge of a control Lyapunov function for example immediately allows the design of a stabilizing control [115, 116, 117]. In order to achieve a comparable situation for the stability with respect to two discrepancies a relationship between the existence of a Lyapunov functional V and stability with respect of two discrepancies has to be established. For this purpose the notions of positivity and positive definiteness of a functional with respect to a discrepancy are introduced.

Definition 10. *Positivity with respect to a discrepancy ρ*
The functional $V = V[\varphi, t]$ is called positive with respect to the discrepancy ρ, if $V \geq 0$ and $V[0, t] = 0$ for all φ with $\rho(\varphi, t) < \infty$.

Definition 11. *Positive definiteness with respect to a discrepancy ρ*
The functional $V = V[\varphi, t]$ is positive definite with respect to a discrepancy ρ, if $V \geq 0$ and $V[0, t] = 0$ for all φ with $\rho(\varphi, t) < \infty$ und for every $\varepsilon > 0$ there exists a $\delta = \delta(\varepsilon) > 0$, such that $V \geq \delta(\varepsilon)$ for all φ with $\rho[\varphi, t] \geq \varepsilon$.

The following two theorems state the conditions for a function V guaranteeing (asymptotic) stability with respect to two discrepancies. For convenience (the reference is in russian) the proofs of both theorems are stated.

Theorem 3. *[78] The process φ with the equilibrium $\varphi_0 = 0$ is stable with respect to the two discrepancies ρ and ρ_0 if and only if there exists a functional $V = V[\varphi, t]$ positive definite with respect to the discrepancy ρ, continuous at time $t = t_0$ with respect to ρ_0 at $\rho_0 = 0$ and not increasing along the process φ, i.e. $\dot{V} \leq 0$.*

Proof. [78] For a process φ the following functional is defined:

$$V[\varphi, t] = \sup_{\tilde{t} \in [t, \infty)} \rho\left[\varphi(., \tilde{t}), \tilde{t}\right] \text{ with } t \geq t_0. \tag{4.67}$$

From (4.67) directly follows:

- $V(0, t) = 0$, $V \geq 0$, $V \geq \rho$ implies that for every ε from $\rho \geq \varepsilon$ it follows that $V \geq \varepsilon =: \delta(\varepsilon)$, i.e. functional V is positive definite with respect to the discrepancy ρ,

- $V[\varphi(., t_1), t_1] \geq V[\varphi(., t_2), t_2]$ for $t_1 \leqslant t_2$, i.e. V is nonincreasing along the perturbed process φ.

Let the equilibrium $\varphi_0 = 0$ be stable with respect to the two discrepancies ρ and ρ_0, i.e. $\rho < \varepsilon \; \forall t > t_0$ if $\rho_0 < \delta(\varepsilon, t_0)$ for a given ε. Then $V[\varphi, t] = \sup_{\tilde{t} \in [t, \infty)} \rho < \varepsilon$ if $\rho_0 < \delta(\varepsilon, t_0)$ for a given ε. Therefore the discrepancy ρ and the functional $V = \sup_{\tilde{t} \in [t, \infty)} \rho$ are continuous at the moment $t = t_0$ with respect to ρ_0 at $\rho_0 = 0$.

Given a functional $V = V[\varphi, t]$ positive definite with respect to the discrepancy ρ and $\varepsilon > 0$, there exists $\varepsilon_1(\varepsilon) > 0$ such that $V \geq \varepsilon_1(\varepsilon) > 0$ if $\rho \geq \varepsilon > 0$ at $t = t_0$. With $V = V[\varphi, t]$ being continuous at the moment $t = t_0$ with respect to ρ_0 at $\rho_0 = 0$ for every $\varepsilon_1 > 0$ there exists a $\delta_1 = \delta_1(\varepsilon_1) > 0$ such that $V < \varepsilon_1$ for $\rho_0 < \delta_1(\varepsilon_1)$.
(As ρ is continuous in ρ_0 at $\rho_0 = 0$, $t = t_0$ for a given $\varepsilon > 0$ there exists a $\delta_2 = \delta_2(\varepsilon)$ such that $\rho < \varepsilon$ at $t = t_0$ if $\rho_0 < \delta_2(\varepsilon)$.)
Assuming that at $T \in [t, \infty)$ $\rho \geq \varepsilon$. Then, as V is a functional positive definite with respect to the discrepancy ρ, $V \geq \varepsilon_1(\varepsilon)$. Which is in contradiction with $V < \varepsilon_1(\varepsilon)$ for arbitrary $t \geq t_0$. Therefore $\rho < \varepsilon$.

$\square$

Theorem 4. *[78] The process φ with the equilibrium $\varphi_0 = 0$ is asymptotically stable with respect to the two discrepancies ρ and ρ_0 if and only if there exists a functional $V = V[\varphi, t]$ positive definite with respect to the discrepancy ρ, continuous at time $t = t_0$ with respect to ρ_0 at $\rho_0 = 0$ and not increasing along the process φ, i.e. $\dot{V} \leq 0$, with $\lim\limits_{t \to \infty} V = 0$.*

Proof. [78] As the process $\varphi = 0$ is asymptotically stable $\lim_{t \to \infty} \rho = 0$, i.e. for an arbitrary $\varepsilon > 0$ there exists a T such that for $t \geq T$ $\rho < \varepsilon$. Therefore with $V = \sup_{\tilde{t} \in [t, \infty)} \rho < \varepsilon$ for $t \geq T$ follows that $\lim_{t \to \infty} V = 0$. $\square$

4.3.1 Relative degree and zero dynamics - finite dimensional case

In order to state conditions, when convergence in two discrepancies yields convergence of the deviation n_e of the particle size distribution n to a desired particle size distribution n_d, the following well known results from finite dimensional systems theory [103, 104, 105, 109, 110] are restated and than generalized to the infinite dimensional case.
Given an affine nonlinear single-input single-output system of order n.

$$\dot{x} = f(x) + g(x)u \tag{4.68}$$
$$y = h(x) \tag{4.69}$$

Time derivative of the output y yields

$$\dot{y} = L_f h(x) + L_g h(x)u, \tag{4.70}$$

with the Lie derivatives

$$L_f h(x) = \frac{\partial h}{\partial x} f(x), \tag{4.71}$$

$$L_g h(x) = \frac{\partial h}{\partial x} g(x). \tag{4.72}$$

Higher order Lie derivatives are defined recursively, e.g.

$$L_f^2 h(x) = \frac{\partial}{\partial x} (L_f h) f(x) \tag{4.73}$$

$$L_g L_f h(x) = \frac{\partial}{\partial x} (L_f h) g(x). \tag{4.74}$$

If the Lie derivatives $L_g L_f^k h(x)$ are equal to zero for $k = 0, 1, \ldots, r - 2$ and $L_g L_f^{r-1} h(x)$ is nonzero, then the r-th time derivative of the output y is obtained as

$$y^{(r)} = L_f^r h(x) + L_g L_f^{r-1} h(x) u. \tag{4.75}$$

The first index r for which at a point x_0 the Lie derivative $L_g L_f^{r-1} h(x_0)$ does not vanish, i.e. $L_g L_f^{r-1} h(x_0) \neq 0$, is called the relative degree r of the system. For all indexes k smaller than the relative degree r the Lie derivative $L_g L_f^{k-1} h(x)$ vanishes at a point x_0 and its neighborhood, i.e. $L_g L_f^k h(x) = 0$. If the relative degree r is equal to the system order n, i.e. $r = n$, then the system is said to have full relative degree.

For a system of relative degree $r < n$ a coordinate transformation $z = \Phi(x)$ can be constructed such that the new states $z_1, \ldots, z_r$ are equal to the associated time derivatives of the output y, i.e. $y, \dot{y}, \ldots, y^{(r-1)}$.

$$z = \begin{pmatrix} z_1 \\ z_2 \\ \vdots \\ z_r \end{pmatrix} = \begin{pmatrix} y \\ \dot{y} \\ \vdots \\ y^{(r-1)} \end{pmatrix} = \begin{pmatrix} h(x) \\ L_f h(x) \\ \vdots \\ L_f^{r-1} h(x) \end{pmatrix} \tag{4.76}$$

In these new coordinates the system can be represented as:

$$\begin{pmatrix} \dot{z}_1 \\ \dot{z}_2 \\ \vdots \\ \dot{z}_r \\ \dot{z}_{r+1} \\ \vdots \\ \dot{z}_n \end{pmatrix} = \begin{pmatrix} z_2 \\ z_3 \\ \vdots \\ 0 \\ l_{r+1}(z) \\ \vdots \\ l_n(z) \end{pmatrix} + \begin{pmatrix} 0 \\ 0 \\ \vdots \\ L_f^r h(x) + L_g L_f^{r-1} h(x) u \\ m_{r+1}(z) u \\ \vdots \\ m_n(z) u \end{pmatrix} \tag{4.77}$$

where $l_{r+1}(z), \ldots, l_n(z)$ and $m_{r+1}(z), \ldots, m_n(z)$ are associated nonlinear functions. Separating the state variable z into two parts $\xi = \begin{pmatrix} z_1 & \ldots & z_r \end{pmatrix}^T$ and $\eta = \begin{pmatrix} z_{r+1} & \ldots & z_n \end{pmatrix}^T$ the system can be represented as:

$$\dot{\xi} = \begin{pmatrix} 0 & 1 & 0 & \ldots & 0 \\ 0 & 0 & 1 & \ldots & 0 \\ \vdots & \vdots & \vdots & \ddots & \vdots \\ 0 & 0 & 0 & \ldots & 1 \\ 0 & 0 & 0 & \ldots & 0 \end{pmatrix} \xi + \begin{pmatrix} 0 \\ 0 \\ \vdots \\ 1 \end{pmatrix} (L_f^r h(x) + L_g L_f^{r-1} h(x) u), \tag{4.78}$$

$$\dot{\eta} = l(\xi, \eta) + m(\xi, \eta) u. \tag{4.79}$$

For this system representation choosing the control input u as follows

$$u = -(L_g L_f^{r-1} h(x))^{-1} (L_f^r h(x) + v(\xi) \tag{4.80}$$

results in a linear system for ξ

$$\dot{\xi} = \begin{pmatrix} 0 & 1 & 0 & \ldots & 0 \\ 0 & 0 & 1 & \ldots & 0 \\ \vdots & \vdots & \vdots & \ddots & \vdots \\ 0 & 0 & 0 & \ldots & 1 \\ 0 & 0 & 0 & \ldots & 0 \end{pmatrix} \xi + v(\xi) \tag{4.81}$$

where stability can be guaranteed for an appropriate choice of $v(\xi)$. Therefore, applying the above control law the output y is stabilized. The remaining internal dynamics associated with the states η, called zero dynamics, are rendered unobservable from the output y by the control law. It is important to mention, that stability of the zero dynamics is not guaranteed a priori and has to be checked. Hence, applying the linearizing control law yields stability of the whole system if and only if the zero dynamics are stable. For a system with full relative degree, no zero dynamics exist and stabilizing the output implies stability for the whole system.

For a linear single-input single-output system of order n:

$$\dot{x} = Ax + Bu, \tag{4.82}$$
$$y = Cx, \tag{4.83}$$

the relative degree is also well defined and equal to the difference on the number of poles n and zeros m, i.e. $r = n - m$, of the associated transfer function $G(s)$. In the linear case the Lie derivatives are simply:

$$L_f^k h(x) = CA^k x, \tag{4.84}$$
$$L_g L_f^k h(x) = CA^k B. \tag{4.85}$$

Thus, the relative degree r is given by the following conditions:

$$CA^k B = 0 \text{ for all } k < r - 1, \tag{4.86}$$
$$CA^{r-1} B \neq 0. \tag{4.87}$$

For a linear system having a relative degree r smaller than its order n a flat output z, i.e. a new output resulting in a full relative degree [119, 124, 125], can be constructed using the following ansatz for a general output equation:

$$z = C_f x, \tag{4.88}$$

where C_f is an output vector to be derived. The conditions for a full relative degree are:

$$C_f A^i B = 0 \text{ for } i = 0, \ldots, n - 2, \tag{4.89}$$
$$C_f A^{n-1} B \neq 0, \tag{4.90}$$

or equivalently

$$C_f [B, AB, \ldots, A^{n-1} B] = [0, 0, \ldots, k], \tag{4.91}$$

with $k \neq 0$ and $[B, AB, \ldots, A^{n-1}B]$ is the controllability matrix. If the system is controllable, i.e. the controllability matrix $[B, AB, \ldots, A^{n-1}B]$ has full rank n, choosing $k = 1$ the output vector C_f can be calculated.

$$C_f = [0, \ldots, 1][B, AB, \ldots, A^{n-1}]^{-1} \tag{4.92}$$

In the case of a linear system the order of the zero dynamics corresponds to the number of zeros of the associated transfer function. In addition, instability of the zero dynamics is directly connected to the presence of right-half plane zeros [122].
The calculation of the zero dynamics for a given finite dimensional nonlinear system is not an easy task and often demands for the use of computational algebra systems.

4.3.2 Relative degree and zero dynamics - infinite dimensional case

The notions of relative degree and zero dynamics can be easily extended to distributed parameter systems (e.g. [83]). Consider for example the following first-order partial differential equation.

$$\frac{\partial w}{\partial t} = A(z)\frac{\partial w}{\partial z} + B(z)u \tag{4.93}$$

$$y = C(z)w \tag{4.94}$$

Taking successively time derivatives of the output y yields:

$$y = C(z)w, \tag{4.95}$$

$$\dot{y} = C(z)A(z)\frac{\partial w}{\partial z} + \underbrace{C(z)B(z)}_{=0}u, \tag{4.96}$$

$$y^{(2)} = C(z)\left(A(z)\frac{\partial}{\partial z}\right)^2 w + \underbrace{C(z)A(z)\frac{\partial}{\partial z}B(z)}_{=0}u, \tag{4.97}$$

$$\vdots$$

$$y^{(j)} = C(z)\left(A(z)\frac{\partial}{\partial z}\right)^j w + C(z)\left(A(z)\frac{\partial}{\partial z}\right)^{j-1}B(z)u. \tag{4.98}$$

In analogy with the definition of the relative degree for finite dimensional systems the relative degree is defined as the first index j for which $C(z)\left(A(z)\frac{\partial}{\partial z}\right)^{j-1}B(z)$ does not vanish, i.e. $C(z)\left(A(z)\frac{\partial}{\partial z}\right)^{j-1}B(z) \neq 0$. As a separation of the state variables is inconvenient for a distributed parameter system, the zero dynamics are defined by constraining the output to zero by applying the appropriate control law, e.g. the discrepancy based control law. Therefore, applying the discrepancy based control law guarantees stability of the whole system if and only if the zero dynamics associated with the discrepancy ρ are stable. Unfortunately, this condition is very hard to check. For the fluidized bed spray granulation with internal and external product classification only the conditions related to the finite dimensional linear case, i.e. the presence of right-half plane zeros, will be checked. This will at least give a local result, guaranteeing stability in a neighborhood of a steady state.

4.4 Discrepancy based control - internal product classification

In the following a stabilizing control is derived for the fluidized bed spray granulation with internal classification (2.7). As has been shown earlier in section 3.4 the third moment of the particle size distribution μ_3 as the controlled variable and the suspension injection rate $\dot{V}_e$ as the control variable are appropriate handles in order to stabilize the process. The error therefore is

$$e = \int_0^\infty L^3 \left(n_d - n\right) dL. \tag{4.99}$$

In order to derive a stabilizing controller the above presented stability concept is applied. Here, we choose the discrepancy ρ as follows

$$\rho = \frac{1}{2} \left(\int_0^\infty L^3 \left(n_d - n\right) dL \right)^2. \tag{4.100}$$

Obviously, the above requirements on a discrepancy are met. It is important to note that using the third moment μ_3 important norm properties as homogeneity, definiteness and the triangular inequality are not satisfied. In order to guarantee continuity at time $t = t_0$ at $\rho_0 = 0$ the second discrepancy ρ_0 is chosen as follows

$$\rho_0 = \rho(t = 0). \tag{4.101}$$

According to Theorem 4, existence of an appropriate functional V is sufficient to guarantee asymptotic stability with respect to the two discrepancies ρ and ρ_0. For this purpose the following candidate Lyapunov functional is introduced

$$V = \frac{1}{2} \left(\int_0^\infty L^3 \left(n_d - n\right) dL \right)^2. \tag{4.102}$$

In order to achieve stability in the sense described above the control variable has to be chosen such that the time derivative of V along the system trajectories (2.7) is negative definite for all times and vanishes only for $V = 0$.

$$\dot{V} = \begin{cases} < 0 \text{ for } V \neq 0 \\ \\ = 0 \text{ for } V = 0. \end{cases} \tag{4.103}$$

Calculating the time derivative $\dot{V}$ yields

$$\dot{V} = e\dot{e} = -e \int_0^\infty L^3 \frac{\partial n}{\partial t} dL, \tag{4.104}$$

$$= -e \left[\int_0^\infty L^3 \left(-G \frac{\partial n}{\partial L} - \dot{n}_{prod} + B \right) dL \right] \tag{4.105}$$

$$= -e \left[\int_0^\infty L^3 \left(-\frac{2(1-b)\dot{V}_e}{\pi \mu_2} \frac{\partial n}{\partial L} - \dot{n}_{prod} + \frac{b\dot{V}_e}{\frac{1}{6}\pi L_0^3} \delta(L - L_0) \right) dL \right] \tag{4.106}$$

$$= -e \left[\int_0^\infty L^3 \left[\left(-\frac{2(1-b)}{\pi \mu_2} \frac{\partial n}{\partial L} + \frac{b}{\frac{1}{6}\pi L_0^3} \delta(L - L_0) \right) \dot{V}_e - \dot{n}_{prod} \right] dL \right]. \tag{4.107}$$
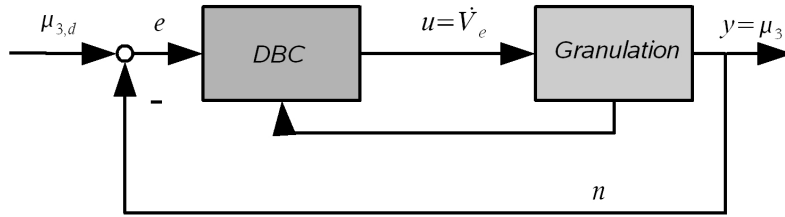
Figure 4.3: Control scheme

Using (4.113) the negative definiteness of the time derivative of the candidate Lyapunov functional V can be guaranteed choosing the following control law.

$$\dot{V}_e = \frac{1}{\int_0^\infty L^3 \left(-\frac{2(1-b)}{\pi \mu_2} \frac{\partial n}{\partial L} + \frac{b}{\frac{1}{6}\pi L_0^3} \delta(L - L_0) \right) dL} \left[ce + \int_0^\infty L^3 \dot{n}_{prod} dL \right] \qquad (4.108)$$

In addition to stability the control law (4.108) even guarantees exponential convergence of V.

$$\dot{V} = -ce^2 = -2cV \qquad (4.109)$$

The proposed control scheme (Fig. 4.4) is tested for a shift of the desired third moment $\mu_{3,d}$ from a value in the region of stability ($\mu_{3,d} = 2.3 \cdot 10^9$) to a third moment associated with the open-loop unstable operating region ($\mu_{3,d} = 2.07 \cdot 10^9$). It should be noted that this simulation scenario spans the whole region studied in the bifurcation analysis. As can be seen in Fig. 4.4 the proposed control scheme is able to stabilize the particle size distribution n and all its moments $\mu_0, \ldots, \mu_3$ with reasonable control effort.

Because of the nonlinear control approach the proposed discrepancy based control law can be applied without any start up strategy, i.e. starting directly from the stable limit cycle. As depicted in Fig. 4.5 closing the feedback loop at $t = 38h$ the discrepancy based controller is able to stabilize the system with reasonable control effort. In order to test the disturbance behavior the product removal, i.e. the drain K, is increased by 10% at $t = 2h$. As can be seen in Fig. 4.6 the controller is able to stabilize the system. However, due to the missing integral action the error e does not converge to zero.
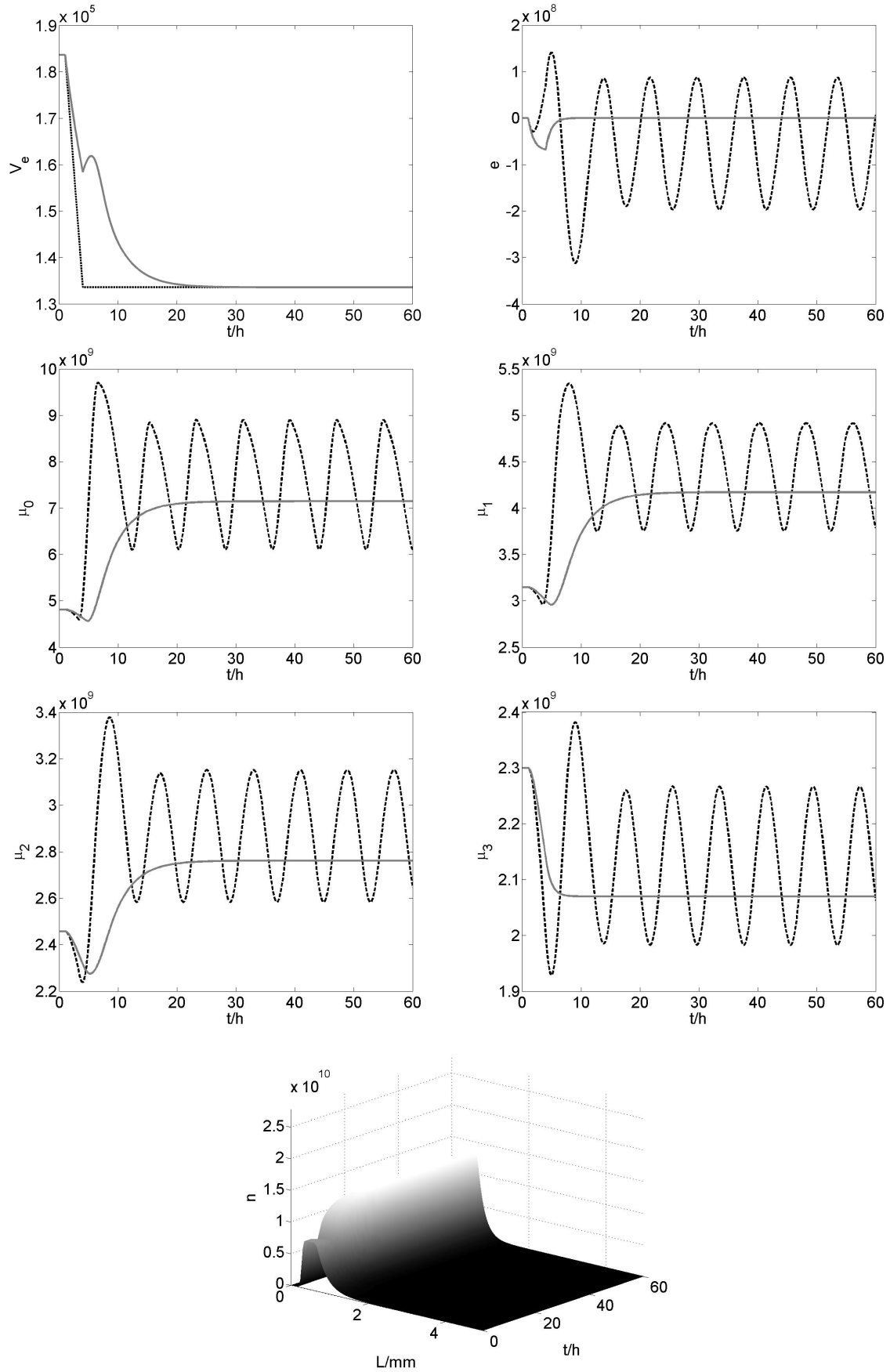
Figure 4.4: Start up with (solid gray) and without control (dotted gray)
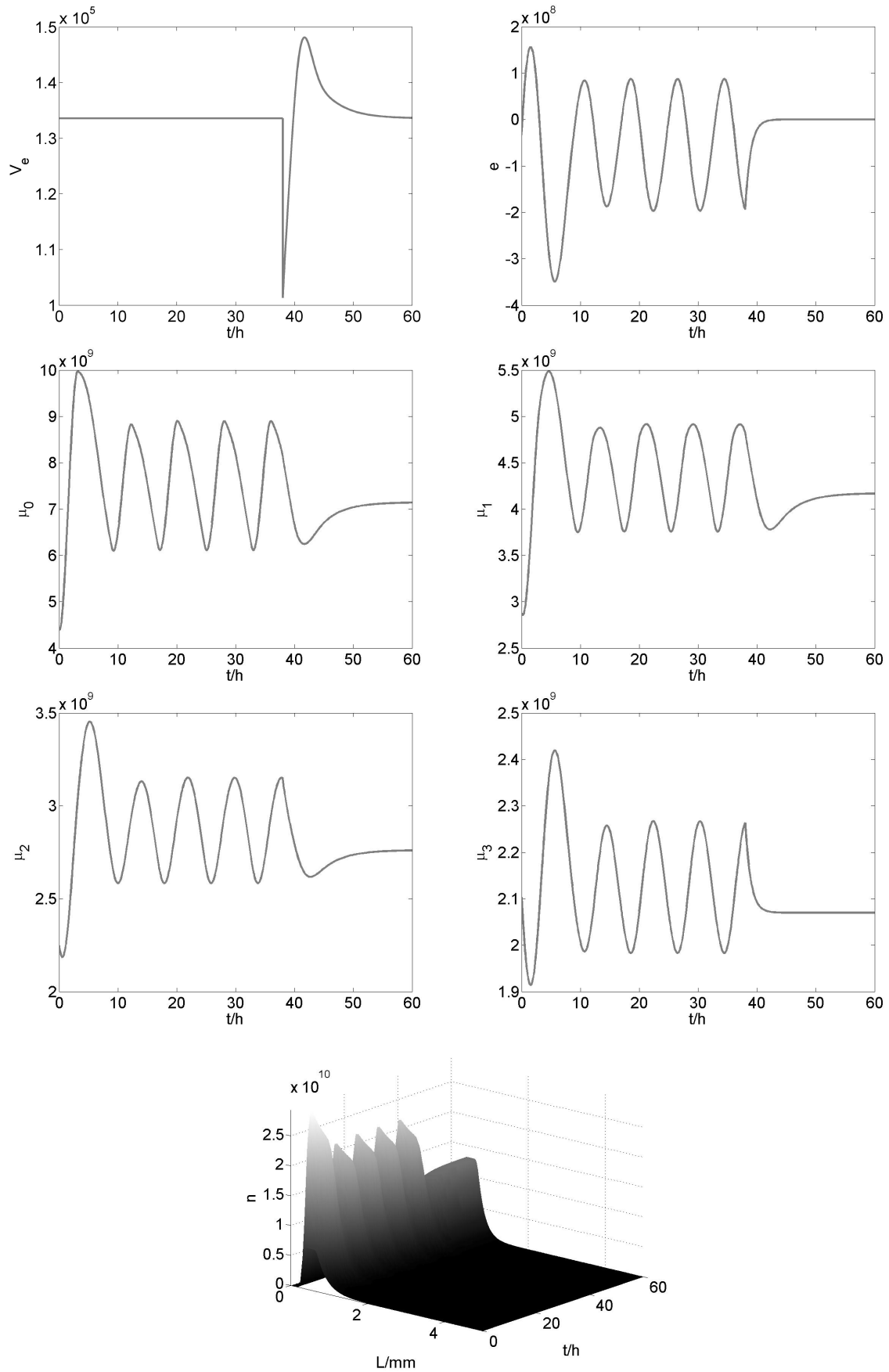
Figure 4.5: Starting from the limit cycle for $\dot{V}_e = 1.336 \cdot 10^5 \frac{mm^3}{s}$
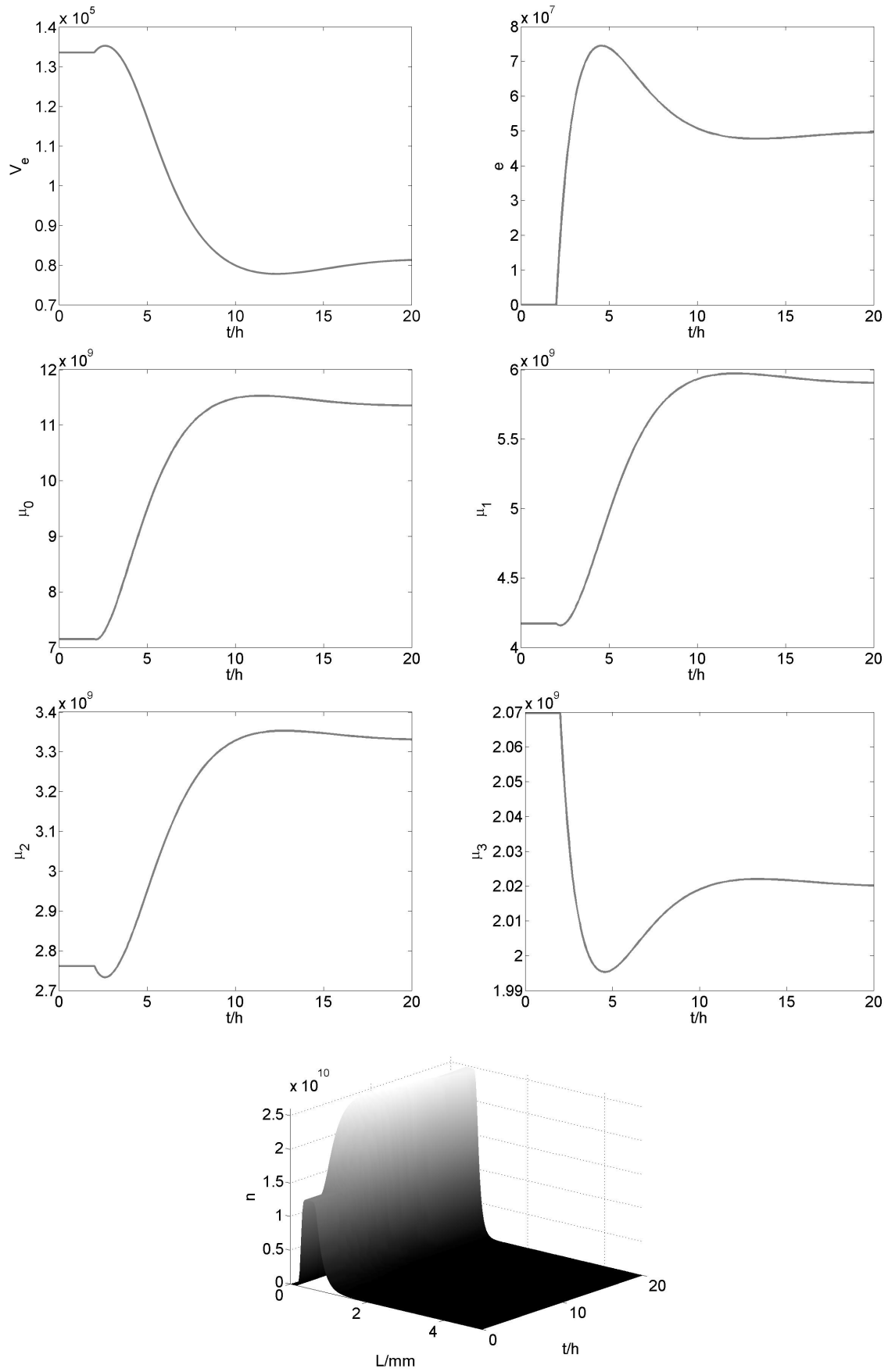
Figure 4.6: Disturbance resposense - increase of K by 10%

4.5 Discrepancy based control - external product classification

In the following a stabilizing control is derived for the fluidized bed spray granulation with external classification (2.14). As has been shown earlier in section 3.5 the second moment of the particle size distribution μ_2 as the controlled variable and the mill grade μ_M as the control variable are appropriate handles in order to stabilize the process. The error therefore is In order to design a control law the error e is defined as:

$$e = \int_0^\infty L^2 \left(n_d - n\right) dL. \tag{4.110}$$

It should be mentioned, that the error is an integral quantity of the difference between desired particle size distribution n_d and the process particle size distribution. The choice is motivated by the fact, that the particle growth depends on the surface area of the particle size distribution, which is strongly connected to its second moment. To derive a controller the following candidate Lyapunov functional is introduced

$$V = \frac{1}{2}e^2. \tag{4.111}$$

The time derivative of V along the system trajectories (2.14) is

$$\dot{V} = e\dot{e} = -e \int_0^\infty L^2 \frac{\partial n}{\partial t} dL, \tag{4.112}$$

$$= -e \left[\int_0^\infty 2LGn - L^2 \left(T_1 Kn + T_2(1 - T_1)Kn\right) dL \right.$$

$$\left. + \int_0^\infty L^3 T_1 Kn dL \int_0^\infty L^2 n_{mill} dL \right]. \tag{4.113}$$

Here, n_{mill} is the shape of the particle size distribution generated by the mill depending on the mill grade μ_M.

$$n_{mill} = 6 \frac{e^{-\frac{\left(L - \mu_M\right)^2}{2\sigma_M^2}}}{\sqrt{2\pi\pi}\varrho\sigma_M} \tag{4.114}$$

As the second moment of n_{mill} cannot be directly solved for the mill grade μ_M the characteristic curve $\mu_M \to \int_0^\infty n_{mill}(\mu_M)dL$ (Fig. 4.7 (left)) has been inverted pointwise (Fig. 4.7 (right)).

In the following, the second moment of n_{mill} will thus be used as a virtual control u_{virt}.

$$u_{virt} = \int_0^\infty L^2 n_{mill}(\mu_M)dL \tag{4.115}$$

Using (4.113) the negative definiteness of the time derivative of the candidate Lyapunov functional V can be guaranteed choosing the following virtual control law.

$$u_{virt} = \frac{1}{\int_0^\infty L^3 T_1 Kn dL} \left[ce - \int_0^\infty 2LGn \right.$$

$$\left. -L^2 \left(T_1 Kn + T_2(1 - T_1)Kn\right) dL \right] \tag{4.116}$$
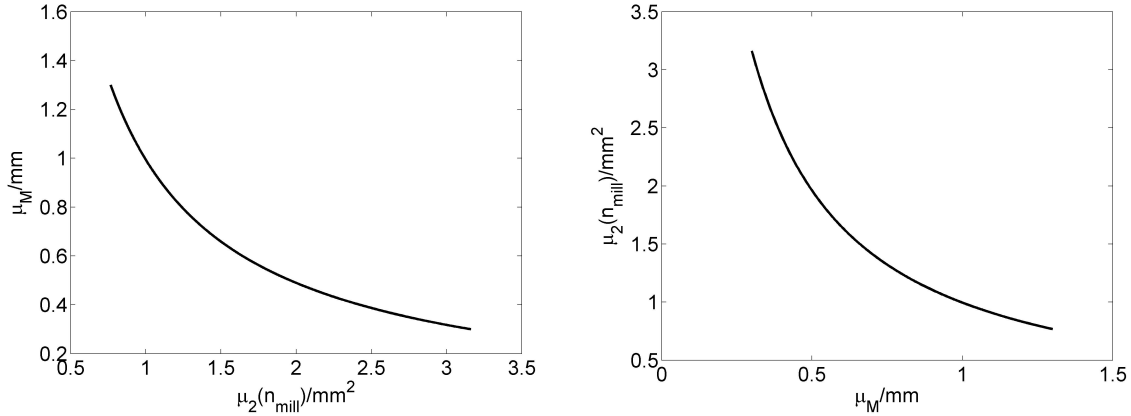
Figure 4.7: Characteristic curve $\mu_M \to \int_0^\infty n_{mill}(\mu_M)dL$ (left) and $\int_0^\infty n_{mill}(\mu_M)dL \to \mu_M$ (right)

In addition to stability the control law (4.116) even guarantees exponential convergence of V.

$$\dot{V} = -ce^2 = -2cV \tag{4.117}$$

The resulting control scheme (Fig. 4.5) therefore consists of the control law (4.116) using the virtual control u_{virt} and an inversion of the characteristic curve from $\int_0^\infty L^2 n_{mill}(\mu_M)dL$ to μ_M.
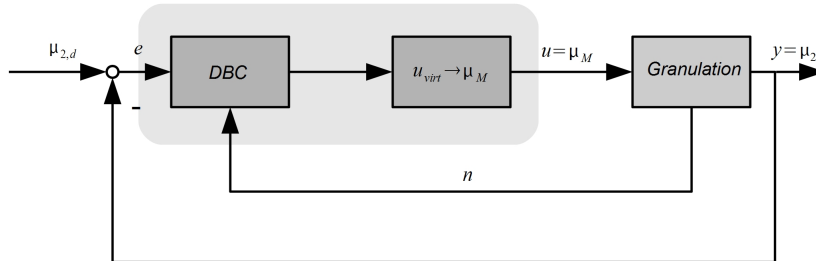
Figure 4.8: Control scheme

The proposed control scheme is tested for a shift of the desired second moment $\mu_{2,d}$ from a value in the region of stability ($\mu_{2,d} = 5.1 \cdot 10^7$) to a second moment associated with the open-loop unstable operating region ($\mu_{2,d} = 6.05 \cdot 10^7$). It should be noted that this simulation scenario spans only the first half of the region studied in the bifurcation analysis. As can be seen in Fig. 4.10 the proposed control scheme is able to stabilize the particle size distribution n and all its moments $\mu_0, \ldots, \mu_2$ with reasonable control effort. In addition, even in the region of stability, where the desired steady state distribution could be derived by shifting the mill grade μ_M, the transition behavior is significantly improved comparing to the open-loop system as depicted in Fig. 4.11 for shift from $\mu_M = 0.9mm$ to $\mu_M = 0.8mm$ or $\mu_2 = 5.1 \cdot 10^7$ to $\mu_2 = 5.58 \cdot 10^7$ respectively. Because of the nonlinear control approach the proposed discrepancy based control law can be applied without any start up strategy, i.e. starting directly from the stable limit cycle. As depicted in Fig. 4.12 closing the feedback loop at $t = 6h$ the discrepancy based controller is able to stabilize the system with reasonable control effort.

However, shifting the desired second moment $\mu_{2,d}$ further into the region of instability the proposed control scheme does not stabilize the particle size distribution n and its moments μ_0 and μ_1 but only μ_2 as depicted in Fig. 4.13. This interesting behavior is strongly connected to aforementioned zero dynamics. In the first scenario, i.e. in the first half of the region studied by the bifurcation analysis, the zero dynamics have been stable resulting in a stable closed loop. Whereas, for the second half the zero dynamics are unstable.

For a rigorous analysis the stability behavior of the zero dynamics with respect to $\mu_{2,d}$ has to be studied, i.e. the stability of the following distributed parameter system.

$$\frac{\partial n}{\partial t} = -G\frac{\partial n}{\partial L} - T_1 Kn - T_2(1-T_1)Kn + n_{mill}(\mu_M)\int_0^\infty L^3 T_1 Kn dL \quad (4.118)$$

$$u_{virt} = \int_0^\infty L^2 n_{mill}(\mu_M)dL \quad (4.119)$$

$$u_{virt} = \frac{1}{\int_0^\infty L^3 T_1 Kn dL}\left[c(\mu_{2,d}-\mu_2) - \int_0^\infty 2LGn\right.$$
$$\left. -L^2\left(T_1 Kn + T_2(1-T_1)Kn\right)dL\right] \quad (4.120)$$

This is, as has been motivated earlier, an infeasible task. However, studying the linear discretized approximation of the process gives at least a local information. As can be seen in Fig. 4.9 decreasing the mill grade below $0.7mm$ two zeros cross the imaginary axis and enter the right half plane resulting in unstable zero dynamics and the associated loss of stability.
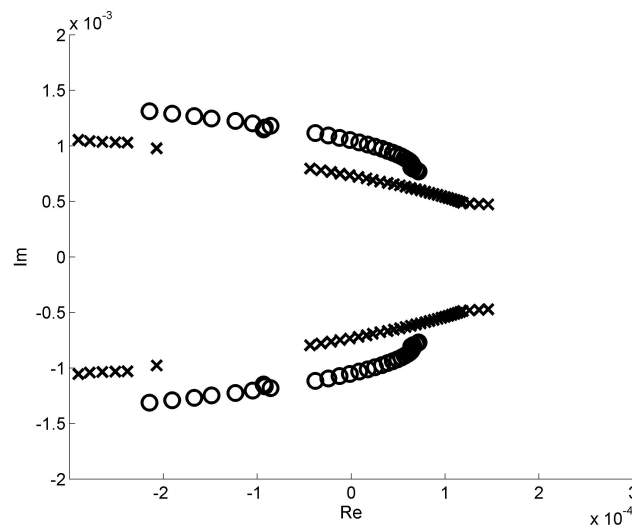

Figure 4.9: Evolution of plant roots (x) and zeros (o) with decreasing mill grade μ_M
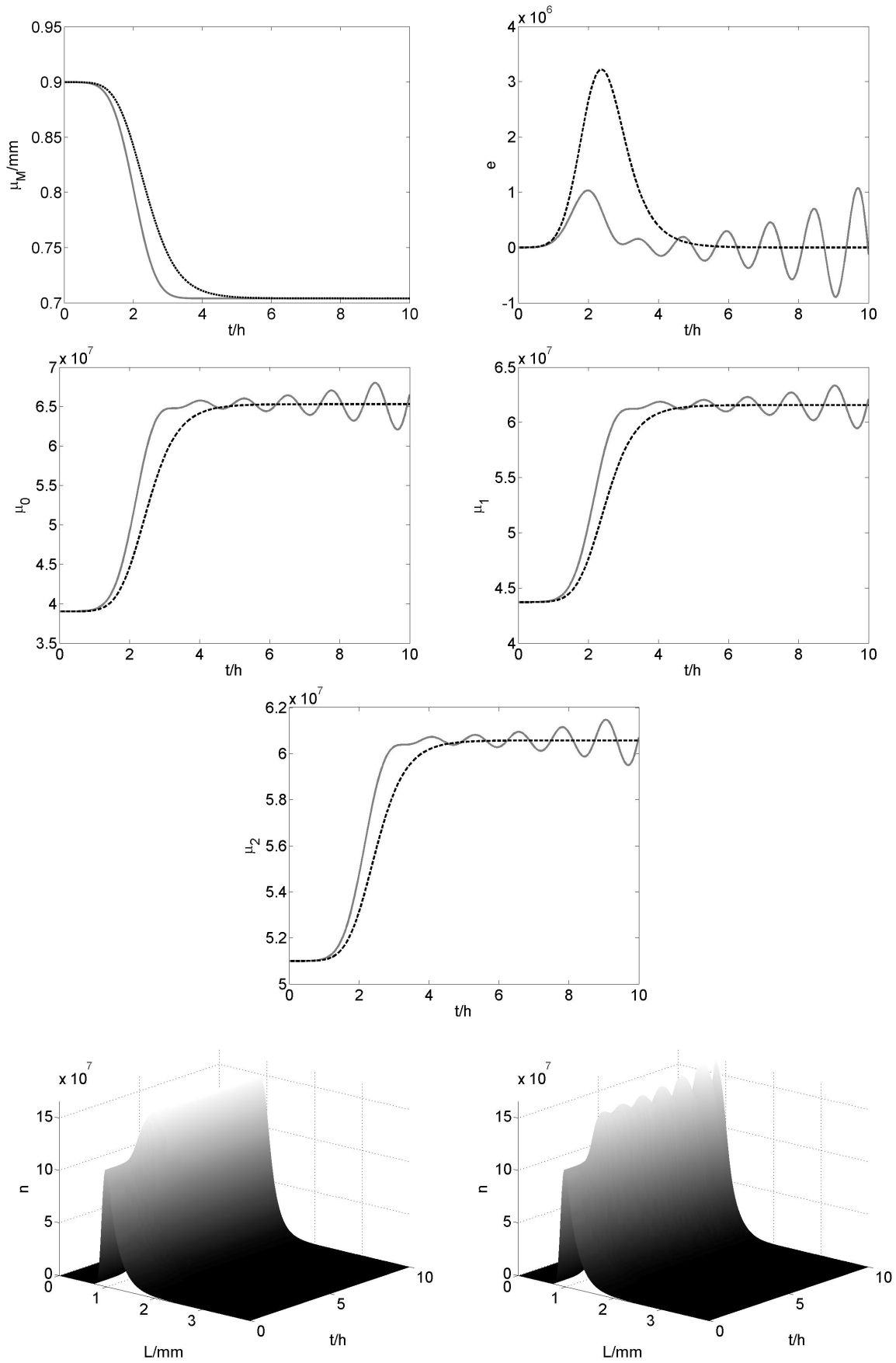
Figure 4.10: Start up with control (dotted black) and without control (solid gray)
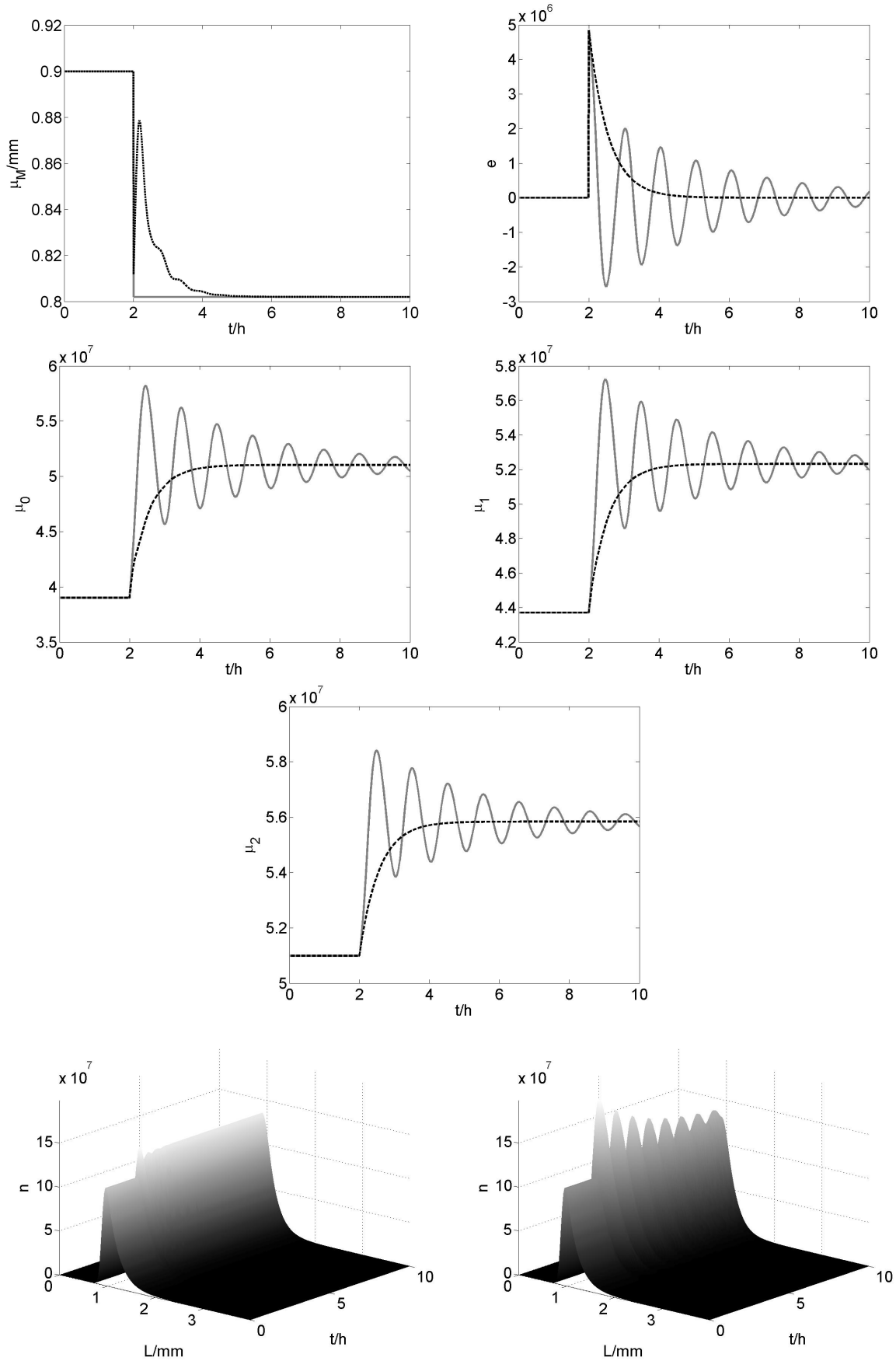
Figure 4.11: Step response with control (dotted black) and without control (solid gray)
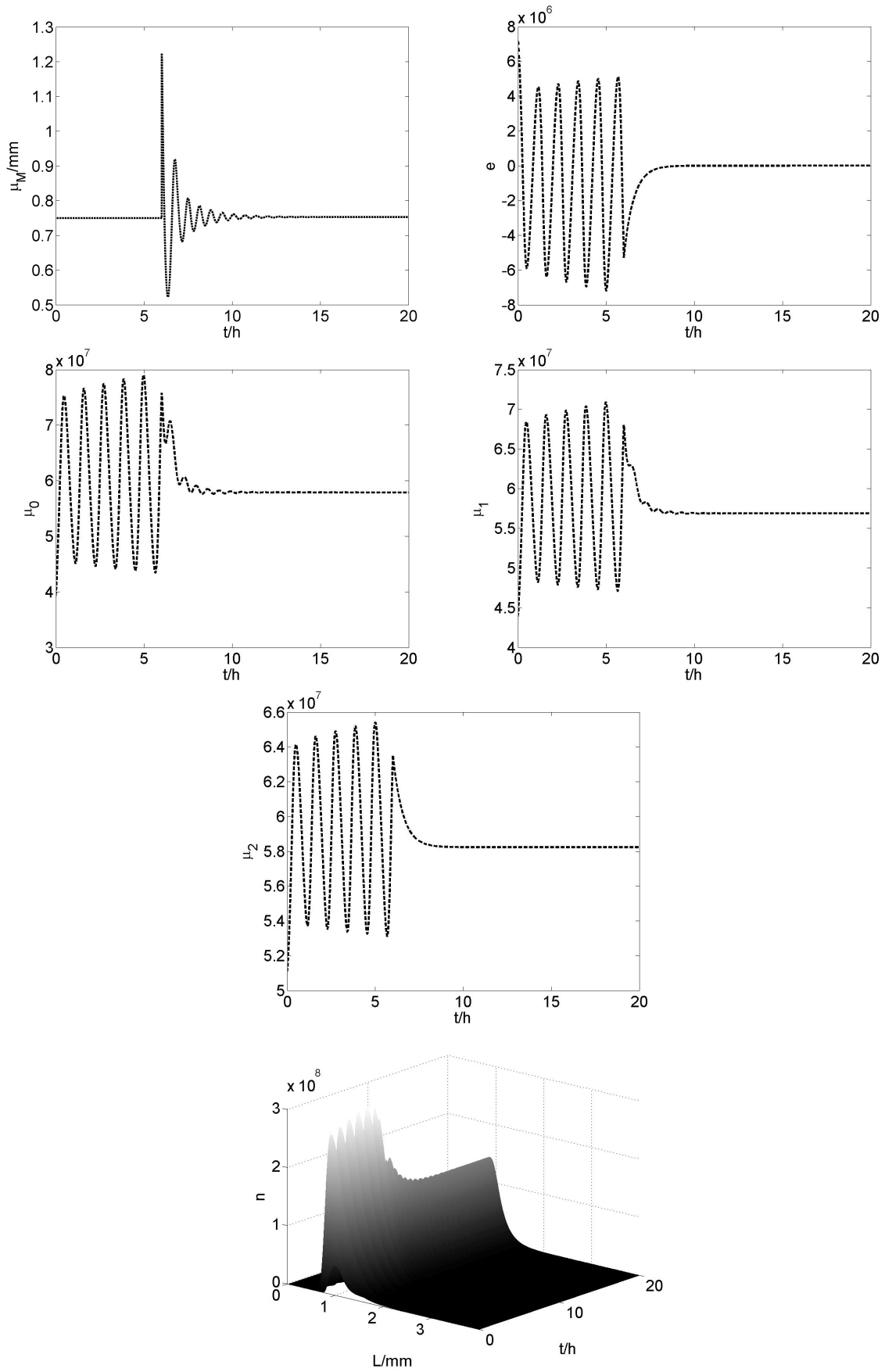
Figure 4.12: Starting from the limit cycle for $\mu_M = 0.75mm$
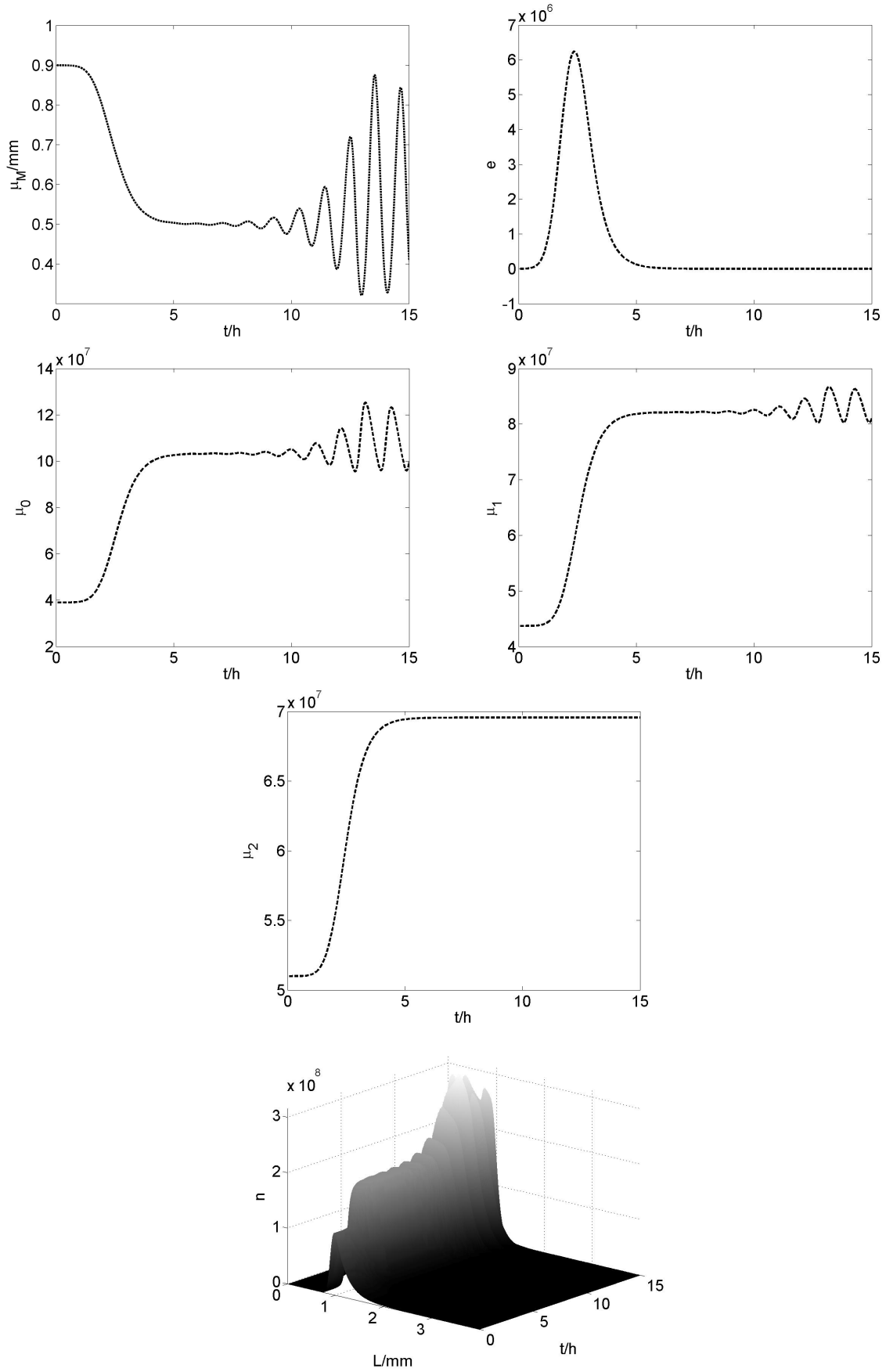
Figure 4.13: Start up with control

In order to overcome the problem of unstable zero dynamics for the continuous fluidized bed spray granulation with external product classification at least four approaches can be applied:

1. Choice of a new control input, which gives stable zero dynamics or completely eliminates the zero dynamics [123]. This approach is of course limited in its applicability for the continuous fluidized bed spray granulation with external product classification.

2. Choice of a different discrepancy and therefore different control variable with stable zero dynamics. However, as has been investigated, for the given continuous fluidized bed spray granulation with external classification the use of a different moment μ_0 or μ_1 or a mean diameter, i.e. μ_1/μ_0, μ_2/μ_0 or μ_1/μ_2, does not change the stability behavior of the zero dynamics.

3. Construction of a flat output. As has been discussed earlier in the case of a linear finite dimensional system a discrepancy resulting in a full relative degree and therefore no zero dynamics can be directly calculated. Whether this new discrepancy yields a favorable behavior of the zero dynamics for the original system at least in a neighborhood of the steady state solutions has to be checked afterwards. However, for the continuous fluidized bed spray granulation with external classification the controllability matrix $[B, AB, \ldots, A^{n-1}B]$ is bad conditioned and therefore numerically not invertible.

4. Design of a parallel compensator. The stability behavior of the zero dynamics can also be influenced by designing an appropriate parallel compensator [120, 121] as depicted in Fig. 4.14. This approach seems to be the most promising as here robust control methods can be applied in order to design a parallel compensator, which gives stable zero dynamics for all linear discretized approximation.
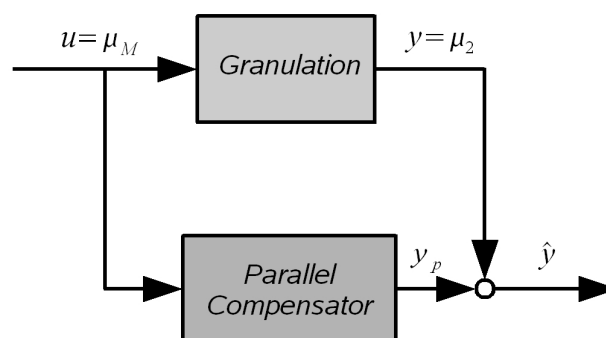

Figure 4.14: Parallel compensator for changing the zero dynamics

In the following, the fourth approach, i.e. stabilization of the zero dynamics by parallel compensator design, is investigated. It will be shown, that applying robust linear control methods allows the design of an appropriate parallel compensator, which solves the aforementioned problem.

4.5.1 Compensator design for zero dynamics stabilization - simple example

In order to introduce the basic concept a simple example is investigated first. Given the following nonlinear state space model of second order with an equilibrium at $u_s = x_{1,s} = x_{2,s} = 0$.

$$\begin{pmatrix} \dot{x}_1 \\ \dot{x}_2 \end{pmatrix} = \begin{pmatrix} x_2 \\ 9\sin(x_1) \end{pmatrix} + \begin{pmatrix} 0 \\ 1 \end{pmatrix} u \tag{4.121}$$

$$y = x_2 - x_1 \tag{4.122}$$

As can be easily seen the nonlinear system has a relative degree of one and therefore zero dynamics of order one. Taking the first time derivative of the controlled variable y

$$\dot{y} = \dot{x}_2 - \dot{x}_1 \tag{4.123}$$

$$= 9\sin(x_1) + u - x_2 \tag{4.124}$$

a linearizing control law can be constructed.

$$u = -9\sin(x_1) + x_2 - c(x_2 - x_1) \tag{4.125}$$

This control would result in the following error equation for the controlled variable y and hence exponentially stabilize the output.

$$\dot{y} = -cy \tag{4.126}$$

However, in order to guarantee stability of the whole system, i.e. all internal states x_1 and x_2, stability of the zero dynamics has to be guaranteed. Here, the stability analysis will be provided using only the linearized system equations although this simple example can be handled by nonlinear analysis methods, too. This is due to the fact that for the stability analysis of the fluidized bed spray granulation with external classification only linear finite dimensional methods are applicable.

Linearizing the nonlinear state space model yields the following linear state space model.

$$\begin{pmatrix} \Delta\dot{x}_1 \\ \Delta\dot{x}_2 \end{pmatrix} = \begin{pmatrix} 0 & 1 \\ 9 & 0 \end{pmatrix} \begin{pmatrix} \Delta x_1 \\ \Delta x_2 \end{pmatrix} + \begin{pmatrix} 0 \\ 1 \end{pmatrix} u \tag{4.127}$$

$$y = \begin{pmatrix} -1 & 1 \end{pmatrix} \begin{pmatrix} \Delta x_1 \\ \Delta x_2 \end{pmatrix} \tag{4.128}$$

For convenience the linear state space model is thus transformed to its zero-pole transfer function representation.

$$G(s) = \frac{s-1}{(s+3)(s-3)} \tag{4.129}$$

Here, the zero $s = 1$ in the right half plane suggests that the zero dynamics of the system are unstable. This can also be seen from closed loop simulation results depicted in Fig. 4.15 for the initial condition $x_1 = 0.2$, $x_2 = 0.1$ and the control gain $c = 10$. Although, the controlled variable y shows the desired exponential convergence, the states x_1 and x_2 are not stabilized applying the proposed control law.
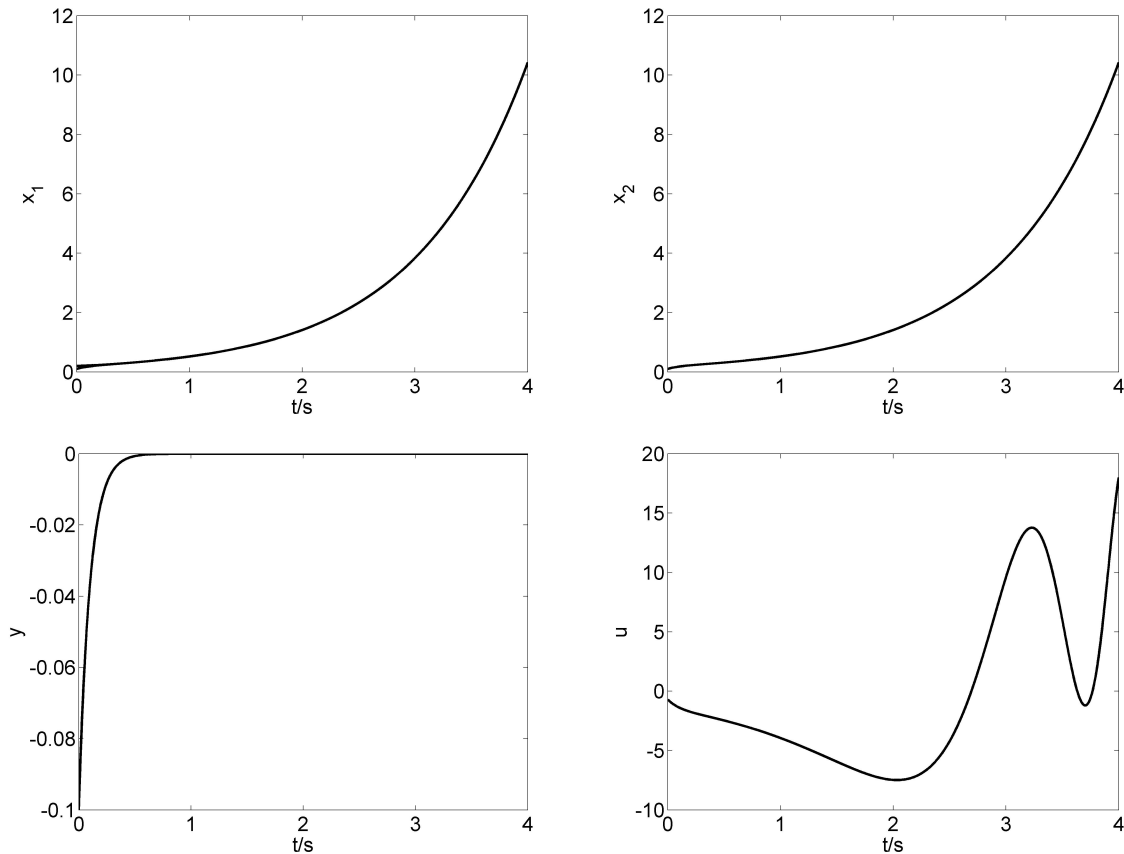
Figure 4.15: Output stabilization with unstable zero dynamics

It should be stressed that the zero dynamics and therefore the instability of the states x_1 and x_2 are invariant with respect to any feedback law. This is in contrast to the eigendynamics, which can be altered by feedback. Hence, in order to derive a system with stable zero dynamics a system augmentation with an parallel compensator as depicted in Fig. 4.14 has been suggested in [118]. This approach has been later extended to nonlinear systems [120] yielding stable zero dynamics at least in a neighborhood of the equilibrium. In order to design an appropriate parallel compensator for a single-input single-output system the associated transfer function $G(s)$ is separated into four fractions

$$G(s) = \frac{N^+(s)N^-(s)}{D^+(s)D^-(s)} \tag{4.130}$$

where the superscript $^+$ represents the fractions with zeros in the left half plane and $^-$ the fractions with zeros in the right half plane. The parallel compensator is constructed in a similar way and contains the fraction $N^+(s)$ and $D^+(s)$ from the original plant plus two additional fractions $N_c(s)$ and $D_c(s)$.

$$G_c(s) = \frac{N^+(s)N_c(s)}{D^+(s)D_c(s)} \tag{4.131}$$

The parallel connection of the plant $G(s)$ and the parallel compensator $G_c(s)$ yields

$$G_s(s) = G(s) + G_c(s) = \frac{N^+(s)\left[N^-(s)D_c(s) + N_c(s)D^-(s)\right]}{D^+(s)D^-(s)D_c(s)}. \tag{4.132}$$

For an unstable plant, i.e. $D^-(s)$ not empty, the new system $G_s(s)$ still has to be stabilized by feedback irrespective of the chosen parallel compensator. However, designing an appropriate parallel compensator the zero dynamics of the new system $G_s(s)$ can be altered. Because of $N^+(s)$ having only zeros in the left half plane, stability of the zero dynamics of the augmented system $G_s(s)$ can be achieved if and only if the fraction

$$\left[N^-(s)D_c(s) + N_c(s)D^-(s) \right] \tag{4.133}$$

has no zeros in the right half plane. From a design point of view this condition is not very convenient and should therefore be restated. As can be easily seen an equivalent condition would be that

$$1 + \frac{N_c(s)D^-(s)}{N^-(s)D_c(s)} = 0 \tag{4.134}$$

has no zeros in the right half plane. This condition resembles the closed loop stability requirement for the inverse virtual plant

$$G^-(s) = \frac{N^-(s)}{D^-(s)} \tag{4.135}$$

and

$$\tilde{G}_c(s) = \frac{N_c(s)}{D_c(s)} \tag{4.136}$$

being the controller to be designed, i.e. derive a controller $\tilde{G}_c(s)$ such that

$$1 + \tilde{G}_c(s)\frac{1}{G^-(s)} \tag{4.137}$$

has no zeros in the right half plane. Using this equivalent condition the compensator can be designed by any control design method.
The example system can be separated into the following fractions

$$
\begin{aligned}
N^-(s) &= s - 1 & (4.138) \\
D^-(s) &= s - 3 & (4.139) \\
D^+(s) &= s + 3 & (4.140)
\end{aligned}
$$

with $N^+(s)$ being empty. The condition for stable zero dynamics of the augmented system therefore is that

$$(s - 1)D_c(s) + N_c(s)(s - 3) \tag{4.141}$$

or equivalently

$$1 + \tilde{G}_c(s)\frac{(s - 3)}{s - 1} \tag{4.142}$$

has no zeros in the right half plane. An appropriate compensator $\tilde{G}_c(s)$ can be designed, e.g. by root locus methods as depicted in Fig. 4.16.

$$\tilde{G}_c(s) = \frac{-0.5}{0.1s + 1} \tag{4.143}$$

The parallel compensator hence reads

$$G_c(s) = \frac{N^+(s)N_c(s)}{D^+(s)D_c(s)} = \frac{-0.5}{(0.1s + 1)(s + 3)}. \tag{4.144}$$
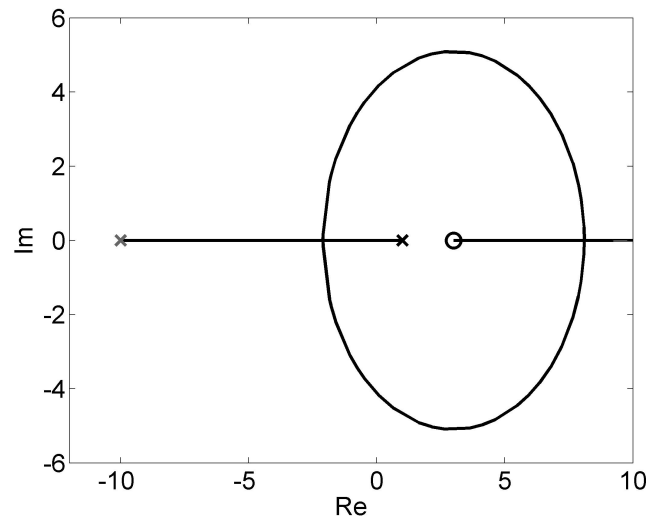
Figure 4.16: Compensator design $\tilde{G}_c(s)$ by root locus methods

Using the designed parallel compensator in the proposed structure therefore yields a new system with at least locally stable zero dynamics. In order to derive a feedback linearizing control law the first time derivative of the new output $\tilde{y} = y + y_c$ is calculated.

$$
\begin{align}
\dot{\tilde{y}} &= \dot{y} + \dot{y}_c && (4.145) \\
&= 9\sin(x_1) - x_2 + u + \dot{y}_c && (4.146)
\end{align}
$$

The linearizing control law is

$$
u = -9\sin(x_1) + x_2 - \dot{y}_c - c\tilde{y} \tag{4.147}
$$

and guarantees exponential convergence for the new output $\tilde{y}$. The derivative of the compensator output $\dot{y}_c$ can be derived by numerical differentiation or by including an additional zero in the transfer function of $G_c(s)$. From a simulation point of view the inclusion of additional zeros may cause problems due to algebraic loops, which may be counter acted by introducing sufficiently fast stable poles.

Testing the controller consisting of a nonlinear control law and a parallel compensator (Fig. 4.17) closed loop operation gives the simulation results depicted in Fig. 4.18. As can be seen the controlled variable y_s shows the desired exponential convergence and the states x_1 (black) and x_2 (gray dotted) are now stabilized.
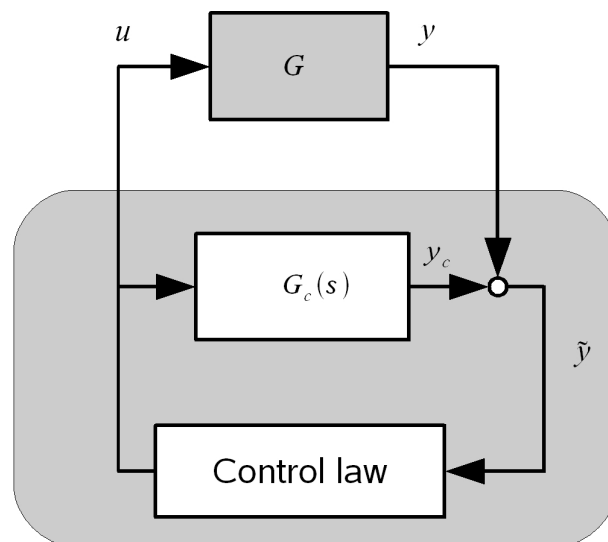
Figure 4.17: Extended control structure
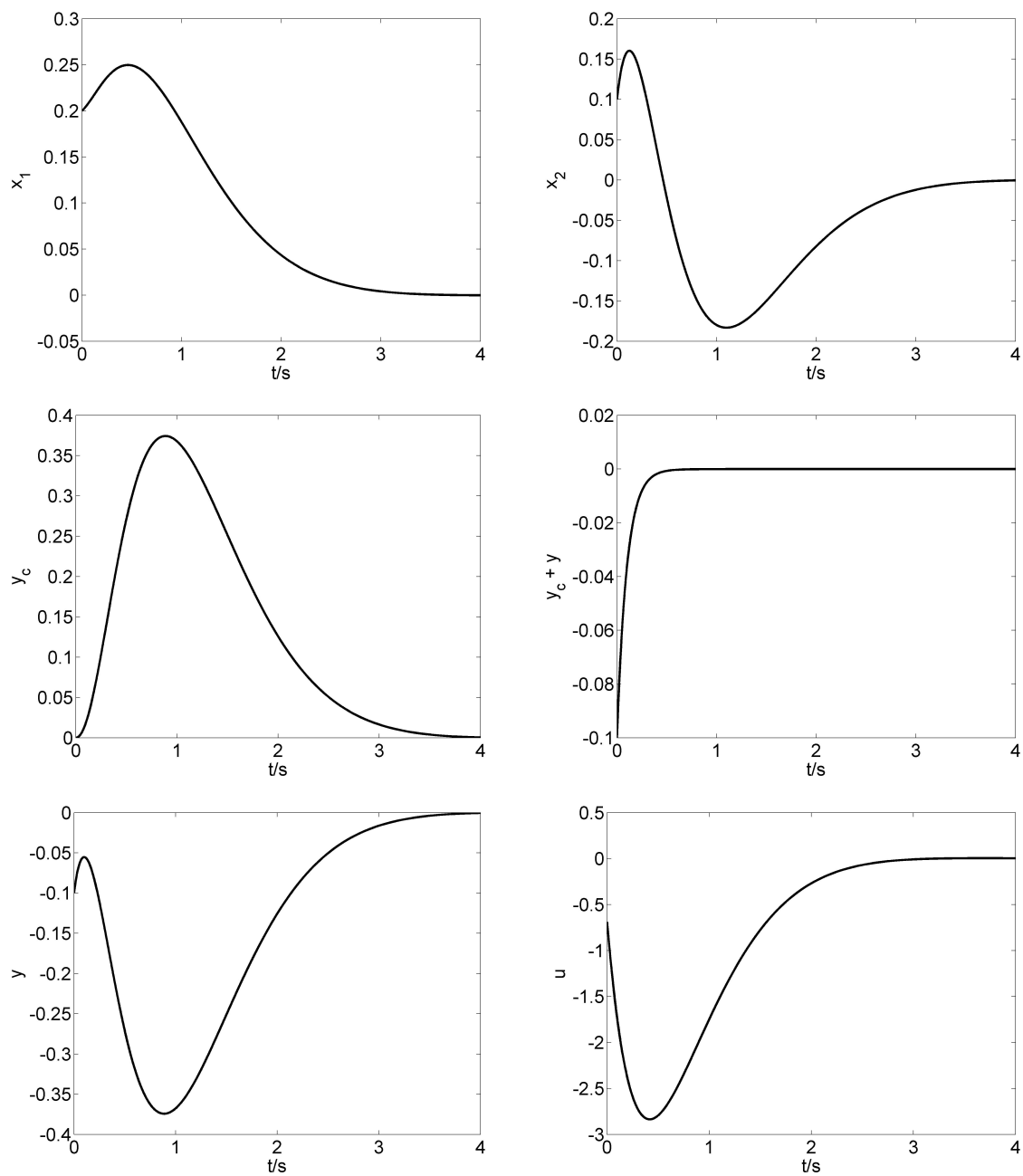
Figure 4.18: Output stabilization with parallel compensator

4.5.2 Compensator design for zero dynamics stabilization - continuous fluidized bed spray granulation with external classification

In order to stabilize the fluidized bed spray granulation with external classification by applying discrepancy based control theory the zero dynamics have to be stabilized in the full region of interest, i.e. in the neighborhood of steady state solutions for $\mu_M \in [0.9mm, 0.5mm]$. Therefore, in the following a linear parallel compensator is derived applying the proposed design procedure. After that a discrepancy based control law is derived for the augmented system, i.e. the population balance model of the fluidized bed spray granulation with external classification and the parallel compensator. The final controller thus consists of the nonlinear feedback law and the linear parallel compensator. The parallel compensator will be designed for the linear finite dimensional approximation of the continuous fluidized bed spray granulation with external classification at the steady state for $\mu_M = 0.5mm$. At this set point the fractions $N^{-1}(s)$ and $D^-(s)$ are as follows

$$
\begin{aligned}
N^-(s) &= s^2 - 0.0004301s + 2.627 \cdot 10^{-6}, & \text{(4.148)} \\
D^-(s) &= s^2 - 0.0005115s + 1.032 \cdot 10^{-6}. & \text{(4.149)}
\end{aligned}
$$

The condition for stable zero dynamics of the augmented system therefore is that

$$
1 + \tilde{G}_c(s)\frac{s^2 - 0.0005115s + 1.032 \cdot 10^{-6}}{s^2 - 0.0004301s + 2.627 \cdot 10^{-6}} \tag{4.150}
$$

has no zeros in the right half plane. In order to guarantee robust stability of the zero dynamics the compensator $\tilde{G}_c(s)$ is calculated by solving the following H_∞-problem for $G(s) = D^-(s)/N^-(s)$, where M is the nominator of the normalized left coprime factorization of $G(s)$.

$$
\left\| \begin{bmatrix} \tilde{G}_c \\ I \end{bmatrix} (I + G\tilde{G}_c)^{-1} M^{-1} \right\|_\infty \leq \frac{1}{\epsilon_{max}}. \tag{4.151}
$$

This control problem resembles the H_∞-Loopshaping design for $W_1(s) = W_2(s) = 1$ and gives therefore a maximal robust stabilizing control with respect to coprime plant uncertainties. The calculated compensator $\tilde{G}_c(s)$ and the resulting parallel compensator $G_c(s)$ are depicted in Fig. 4.19 and Fig. 4.20. As can be seen in Fig. 4.21 the compensator $\tilde{G}_c(s)$ alters the location of the systems zeros and therefore stabilizes the zero dynamics. In addition, as the compensator has been designed by robust control methods this property is preserved for different set points (Fig. 4.22). It should be mentioned that in order to avoid problem with numerical simulations the compensator $\tilde{G}_c(s)$ has been augmented by a fast pole at -10. This guarantees that the derivative being used in the discrepancy based control law, i.e $\dot{e}_c \,\circ\!\!-\!\!\bullet\, sG_c(s)\Delta M u_M(s)$, does not cause an algebraic loop.
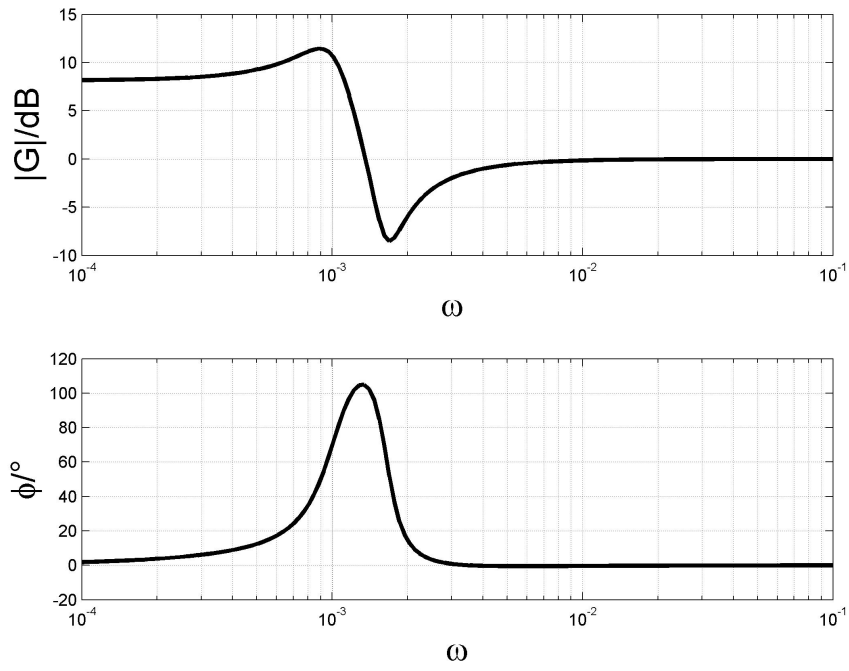
Figure 4.19: Bode diagram $\tilde{G}_c(s)$
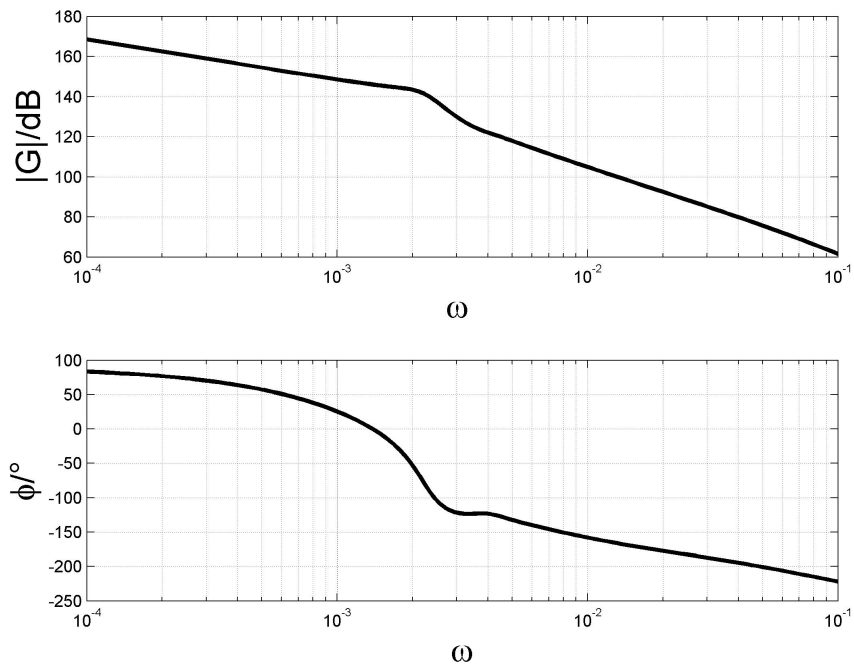
Figure 4.20: Bode diagram of the parallel compensator $G_c(s)$
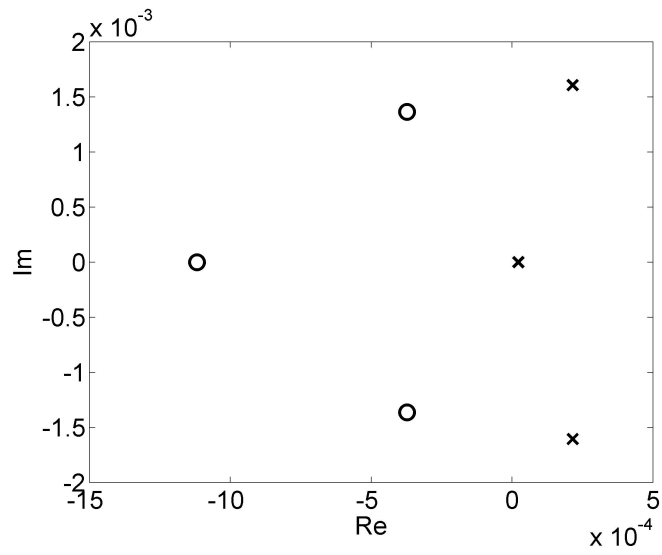
Figure 4.21: Pole/zero map of $N^-(s)D_c(s) + N_c(s)D^-(s)$
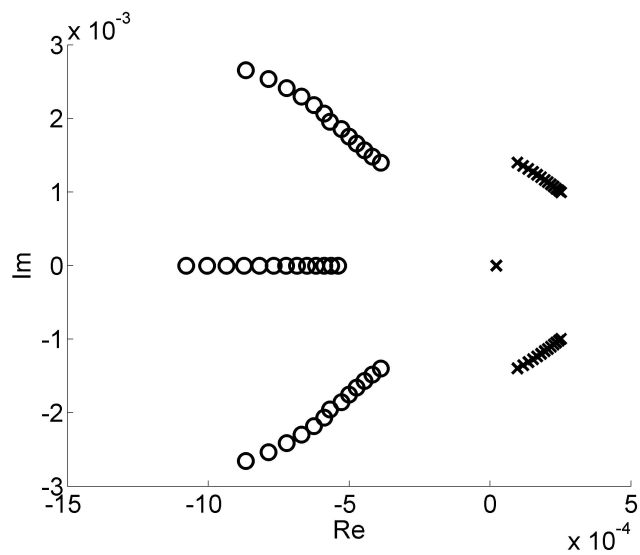
Figure 4.22: Pole/zero map of $N^-_{\mu_M}(s)D_c(s) + N_c(s)D^-_{\mu_M}(s)$ for varying mill grade

For the augmented plant, i.e. the continuous fluidized bed spray granulation with external classification plus the designed parallel compensator, a redesign of the discrepancy based control law has to be done. Therefore, the proposed control Lyapunov functional is extended including the augmented error $\tilde{e} = e + e_c$.

$$\tilde{V} = \frac{1}{2}\tilde{e}^2 \tag{4.152}$$

The time derivative of $\tilde{V}$ along the system trajectories is

$$
\begin{aligned}
\dot{\tilde{V}} &= \tilde{e}(-\dot{\mu}_2 + \dot{e}_c) \tag{4.153}\\
&= \tilde{e}\dot{e}_c + \tilde{e}\left[\int_0^\infty 2LGn - L^2\left(T_1 Kn + T_2(1-T_1)Kn\right)dL\right.\\
&\quad \left. + \int_0^\infty L^3 T_1 Kn dL \int_0^\infty L^2 n_{mill} dL\right] \tag{4.154}\\
&= \tilde{e}\dot{e}_c + \tilde{e}\left[\int_0^\infty 2LGn - L^2\left(T_1 Kn + T_2(1-T_1)Kn\right)dL\right.\\
&\quad \left. + \int_0^\infty L^3 T_1 Kn dL\right]u_{virt} \tag{4.155}
\end{aligned}
$$

Here, the second moment of n_{mill} has been used as a virtual control u_{virt}. The negative definiteness of the time derivative of the candidate Lyapunov function $\tilde{V}$ can be guaranteed choosing the following virtual control law.

$$
\begin{aligned}
u_{virt} &= \frac{1}{\int_0^\infty L^3 T_1 Kn dL}\left[c\tilde{e} + \dot{e}_c - \int_0^\infty 2LGn\right.\\
&\quad \left. -L^2\left(T_1 Kn + T_2(1-T_1)Kn\right)dL\right] \tag{4.156}
\end{aligned}
$$

In addition to stability the control law (4.156) guarantees exponential convergence of $\tilde{V}$.

$$\dot{\tilde{V}} = -c\tilde{e}^2 = -2c\tilde{V} \tag{4.157}$$

The resulting augmented control scheme (Fig. 4.5.2) therefore consists of the control law (4.156) using the virtual control u_{virt} and an inversion of the characteristic curve from $\int_0^\infty L^2 n_{mill}(\mu_M)dL$ to μ_M and the designed parallel compensator.

The proposed control scheme is tested for a shift of the desired second moment $\mu_{2,d}$ from a value in the region of stability ($\mu_{2,d} = 5.1 \cdot 10^7$) to a second moment associated with the open-loop unstable operating region ($\mu_{2,d} = 6.95 \cdot 10^7$). It should be noted that this simulation scenario spans now the full region studied in the bifurcation analysis and therefore includes the region of unstable zero dynamics. As can be seen in Fig. 4.24 the proposed control scheme is able to stabilize the particle size distribution n and all its moments $\mu_0, \ldots, \mu_2$ with reasonable control effort.

In order to test the disturbance behavior the the mean diameter L_1 and L_2 are increased by 5% at $t = 0h$. As can be seen in Fig. 4.25 the controller is able to stabilize the system. However, due to the missing integral action the error e does not converge to zero.
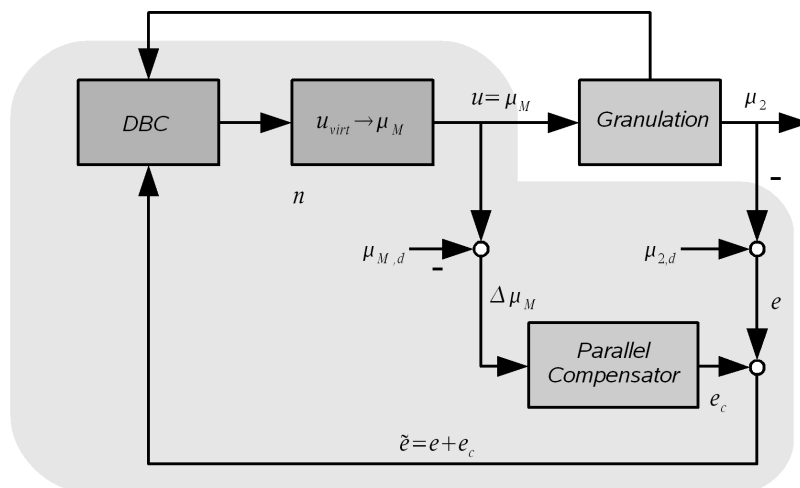
Figure 4.23: Control scheme
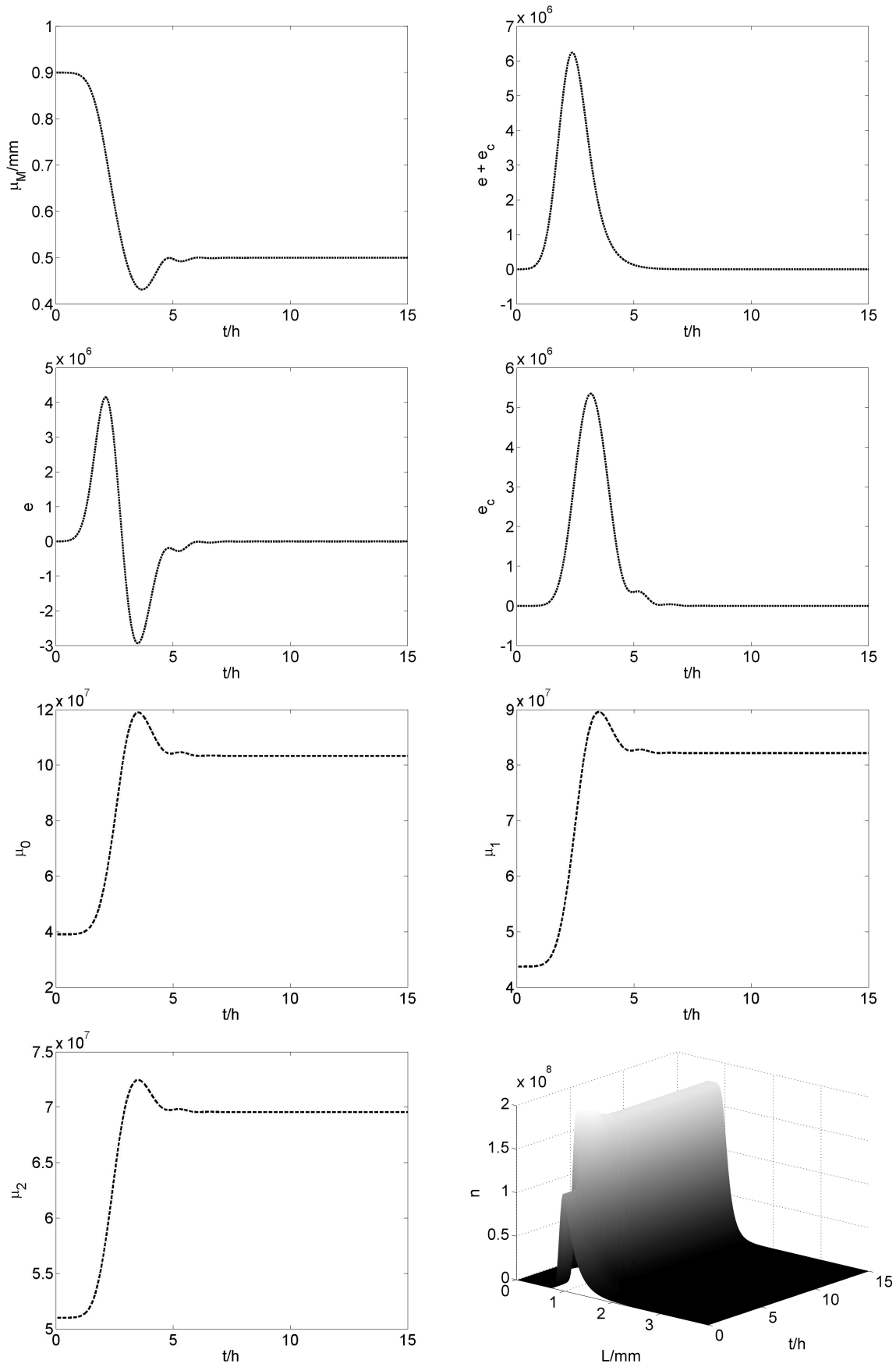
Figure 4.24: Start up discrepancy based control with parallel compensator
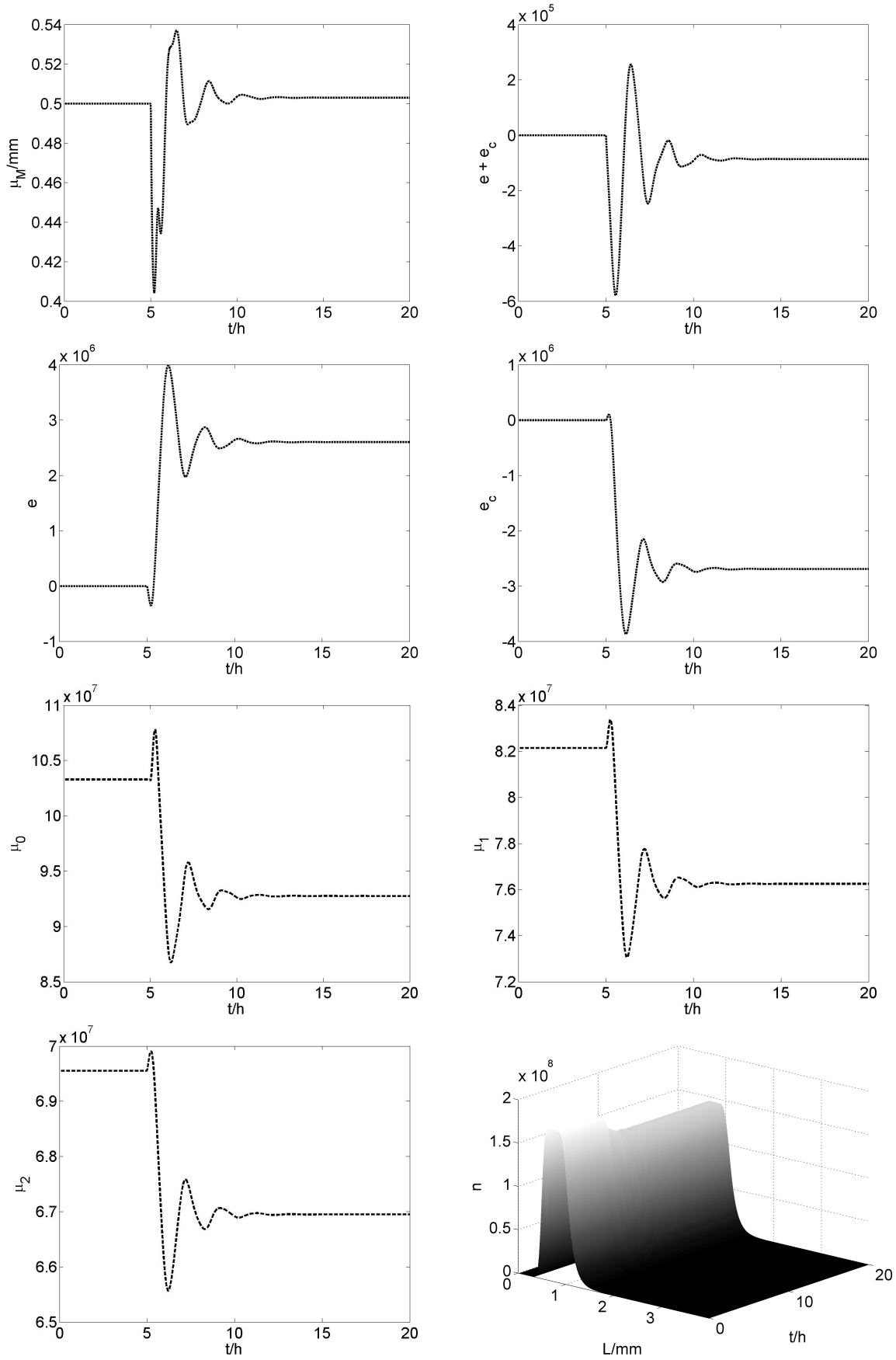
Figure 4.25: Disturbance resposense - increase of L_1 and L_2 by 5%

Chapter 5

Summary

5.1 Conclusion and future perspectives

Fluidized bed spray granulation is an important particulate process. For a continuous operation two typical configurations are fluidized bed spray granulation with internal and external product classification. Both operation schemes possess interesting dynamical behavior strongly depending on process parameters, e.g. changes in suspension injection rate or mill grade may render the desired steady state particle size distribution unstable and lead to the occurrence of limit cycles. In order to operate the process on a wide range of process parameters, which is desirable from a particle production point of view, feedback stabilization is the main issue. In addition, feedback control greatly improves transient behavior.

Although research in control of particulate processes has recently gained increasing attention control of continuous fluidized bed spray granulation has not been studied, yet. In this Thesis two control approaches have been proposed. The first control approach applies linear infinite dimensional systems theory in order to design a robust finite dimensional control law by H_∞-loopshaping methods. Here, controller robust stability margin in the sense of the gap metric is used to cope with discretization errors and errors due to linearization at different set points. Combining this controller with an appropriate start-up strategy results in a linear control law guaranteeing stability in a certain neighborhood of the steady state trajectory with reasonable control performance. Although control design is straightforward, derivation of an appropriate design model and the associated error bounds is quite laborious.

The second control approach uses a generalized distance measure, called discrepancy, and the associated stability theory in order to design a stabilizing control law for the nonlinear infinite dimensional plant. The choice of the appropriate discrepancy is motivated by the preceding linear control approach and physical insight. As the proposed design guarantees only stability in the sense of Lyapunov with respect to the two chosen discrepancies, i.e. norms of the second and third moment of the particle size error distribution, conditions for pointwise convergences of the particle size distribution, i.e. convergence in a L_∞-norm, have to be studied. It has been shown, that pointwise convergence can be achieved if and only if the zero dynamics associated with the chosen discrepancies are stable. This is again a very difficult problem for this class of distributed parameter systems. However, it has been shown that studying the zero dynamics of the discrete and linearized approximations of the population balance equations for the particle size distribution gives at least a result
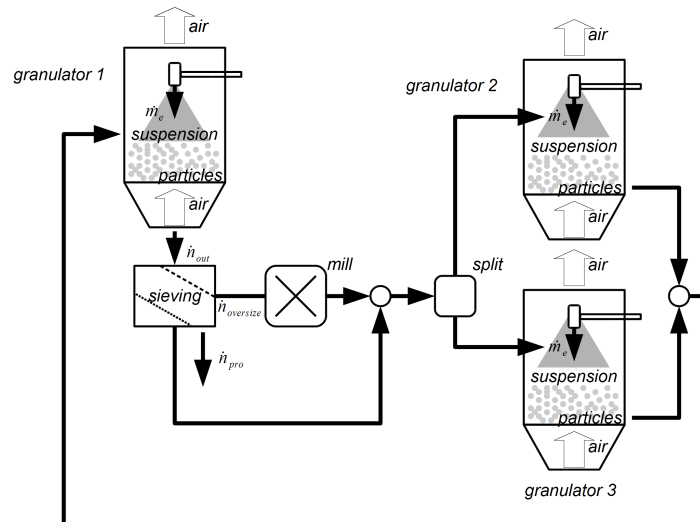
Figure 5.1: Production process with coupled fluidized bed spray granulators

being valid in a neighborhood of the steady state particle size distribution. In order to overcome the problem of unstable zero dynamics for the continuous fluidized bed spray granulation with external product classification an appropriate parallel compensator has been designed, being able to shift the open loop zeros into the left half plane.

From a practical and industrial point of view future work should concern the experimental validation of the proposed control laws. Here, the online measurement of the particle size distribution will be a main issue. A short overview on measurement methods is given in Appendix E.

In addition, application to more complex configurations, e.g. schemes involving several fluidized bed spray granulators [1] as shown in Fig. 5.1, and different processes described by population balance models, e.g. crystallization, drum granulation [13, 14] and bioreactors [41], should be an issue. Especially, the proposed discrepancy based control approach is a promising alternative to other control approaches. From a theoretical point of view the proposed control approaches should be augmented by adaptation algorithms and robustified in order to cope for model uncertainties and parameter variations. In addition, combined models, e.g. including several population balance equations, or particulate systems in flow fields provide an interesting field for future research.

Appendix A

Numerical solution of population balance equations

For simulation, analysis and discretization based control design numerical discretization methods have to be applied to the presented models of continuous fluidized bed spray granulation with internal and external product classification. As will be shown the population balance equations can be represented as conservation laws. Thus, application of finite volume discretization is preferable. Typically, convergence results are stated for the full-discrete case, i.e. discretization in space and time, for simulation and control design the semi-discrete case, i.e. applying the method of lines first discretizing in space and then using a possibly different method for time discretization, is more appropriate. The reasons are twofold:

1. applying a discretization in two steps allows the use of high-order accurate time integration methods, e.g. Runge-Kutta methods, and variable time step methods.

2. a discretization in space results in a high-order continuous-time state-space model, which can be investigated by finite dimensional continuous-time analysis and control methods, whereas a discretization in space and time results in a high-order discrete-time state-space model.

In the following, important convergence results for the full-discrete case are stated (see [44, 45, 46] for a more detailed presentation) and then extended to the semi-discrete case demanding for specialized time integration algorithms called strong stability preserving or total variation diminishing methods (for further details see [47, 48, 49, 50, 51, 52, 53].

A.1   Conservation laws

The presented population balance models can be represented as scalar hyperbolic systems

$$\frac{\partial n}{\partial t} + \frac{\partial}{\partial L}\left[Gn + \int_0^L \left(\dot{n}_{prod} + B\right) dL'\right] \;=\; 0 \qquad\qquad \text{(A.1)}$$

$$\frac{\partial n}{\partial t} + \frac{\partial}{\partial L}\left[Gn + \int_0^L \left(\dot{n}_{prod} + \dot{n}_{oversize} - \dot{n}_{mill}\right) dL'\right] \;=\; 0 \qquad\qquad \text{(A.2)}$$

or more general

$$\frac{\partial u}{\partial t} + \frac{\partial f(u)}{\partial x} = 0. \tag{A.3}$$

Here, u is the solution of the conservation law. Integrating this equation over a time interval $[t_1, t_2]$ and a space interval $[x_1, x_2]$ gives rise to the integral form of the conservation law.

$$\int_{x_1}^{x_2} u(t_2)dx = \int_{x_1}^{x_2} u(t_1)dx + \int_{t_1}^{t_2} f(u(x_1, t))dt - \int_{t_1}^{t_2} f(u(x_2, t))dt \tag{A.4}$$

A solution u of the integral form (A.4) of the conservation law is called a weak solution of (A.3).

A.2 Convergence - full-discrete case

In order to derive a numerical approximation scheme for (A.3) or (A.4) the inner grid points $x_{j-1/2}$ and $x_{j+1/2}$ are introduced at the time points t_k and t_{k+1}.

$$\int_{x_{j-1/2}}^{x_{j+1/2}} u(t_{k+1})dx = \int_{x_{j-1/2}}^{x_{j+1/2}} u(t_k)dx + \int_{t_k}^{t_{k+1}} f(u(x_{j-1/2}, t))dt - \int_{t_k}^{t_{k+1}} f(u(x_{j+1/2}, t))dt. \tag{A.5}$$

Using the following approximation for the cell average

$$\bar{u}_j^k = \frac{1}{\Delta x} \int_{x_{j-1/2}}^{x_{j+1/2}} u(x, t_k)dx \tag{A.6}$$

one gets

$$\bar{u}_j^{k+1} = \bar{u}_j^k + \frac{1}{\Delta x} \left[\int_{t_k}^{t_{k+1}} f(u(x_{j-1/2}, t))dt - \int_{t_k}^{t_{k+1}} f(u(x_{j+1/2}, t))dt \right]. \tag{A.7}$$

The approximation of the average flux through $x_{j+1/2}$ can be interpreted as a numerical flux F_j leading to a discretized version of the conservation law.

$$F_j \approx \frac{1}{\Delta t} \int_{t_k}^{t_{k+1}} f(u(x_{j+1/2}, t))dt \tag{A.8}$$

A discrete conservation law is said to be in conservation form if it has the following form

$$U_j^{k+1} = U_j^k - \frac{\Delta t}{\Delta x} \left[F_j - F_{j-1} \right]. \tag{A.9}$$

Here F_j is the numerical flux function, which may depend on the numerical solution U_p^k at time step k at different grid points p. In the following, only a dependence of two arguments, i.e. $F(U_{j-1}, U_j)$, will be used. Generalizations to more arguments are straight forward.

Courant, Friedrichs and Lewy showed that a numerical method for a conservation law can only be convergent if its numerical domain of dependence contains the true domain of dependence at least in the limit for Δx and Δt going to zero [42]. This is due to the fact,

that for conservation laws the information propagation speed is finite and therefore the solution $u(x,t)$ at a point (x,t) depends only on the initial solution u_0 at the point $x - f't$, where f' is the characteristic propagation speed. Therefore, the time step Δt can not be chosen independently from the spatial grid Δx. For an unidirectional flow, e.g. $f' > 0$, information propagates at each time step $\Delta t f'$. For an one-side method with a domain of dependence as $[Q_j, Q_{j-1}]$ with $Q_j - Q_{j-1} = \Delta x$ no information should propagate further than Δx per time step Δt. In this case the CFL (Courant, Friedrichs, Lewy) condition reads

$$\Delta t f' \leq \Delta x \qquad (A.10)$$

or

$$\frac{\Delta t f'}{\Delta x} \leq 1. \qquad (A.11)$$

In order to show convergence of the numerical solution U of (A.9) to a weak solution u, i.e. u is a solution of (A.4), the following preliminary definitions are needed.

Definition 12 (Consistency). *The numerical method is called consistent with the original conservation law if the numerical flux F is equal to the flux f for u being constant ($u = \bar{u}$), i.e.*

$$F(\bar{u}, \bar{u}) = f(\bar{u}). \qquad (A.12)$$

Definition 13 (Lipschitz continuity). *F is Lipschitz continuous in its arguments if there exists a constant $K \geq 0$ such that*

$$\left| F(U_{j-p}^k, \ldots, U_{j+q}^k) - F(U_{j-1-p}^k, \ldots, U_{j-1+q}^k) \right| \leq K \max_{-p \leq i \leq q} \left(|U_{j+i}^k - U_{j-1+i}^k| \right). \qquad (A.13)$$

Definition 14 (Total variation). *The total variation TV is defined as*

$$TV(v) = \limsup_{\varepsilon \to 0} \frac{1}{\varepsilon} \int_{-\infty}^{\infty} |v(x) - v(x - \varepsilon)| dx. \qquad (A.14)$$

A conservative method with a Lipschitz continuous numerical flux F is total variation stable (TV-stable) if there exists $\Delta t_0, R > 0$ such that the total variation $TV(U^k)$ is bounded by R, i.e.

$$TV(U^k) \leq R, \qquad (A.15)$$

for all $\Delta t < \Delta t_0$.

The fact that the numerical approximation scheme, i.e. the discrete conservation law (A.9), has been derived directly from the integral conservation law (A.4) suggests that the discrete solution U gives a feasible approximation of a weak solution u of (A.4). This has been proven by Lax and Wendroff [43].

Theorem 5. *[43] Let U_l be a sequence of numerical approximations for a sequence of grids $\Delta t_l, \Delta x_l$, with $\Delta t_l, \Delta x_l \to \infty$ for $l \to \infty$, generated by a conservative and consistent method. If U_l converges to a function u, i.e. $\|U_l - u\|_1 \to 0$ for $l \to \infty$ and there is an $R > 0$ for each time T such that the total variation $TV(U_l)$ is smaller than R for all t with $0 \leq t \leq T$, then u is a weak solution of the conservation law.*

Here, convergence of the numerical approximations U_l is assumed. In order to guarantee convergence of a sequence of numerical approximations the method should be total variation stable.

Theorem 6. *[44, p. 164] A numerical method in conservation form is convergent, i.e. U_l converges to a weak solution for $l \to \infty$ in the L_1-norm, if it is consistent with the conservation law, the numerical flux F is Lipschitz continuous and if the method is TV-stable.*

For a given numerical scheme TV-stability is probably the most difficult part to show. Therefore, the notions of total variation diminishing and l_1-contracting have been introduced. In the following, it will be shown that a l_1-contracting numerical method is total variation diminishing and thus TV-stable.

Definition 15 (Total variation diminishing). *A numerical method is called total variation diminishing if*

$$TV(U^{k+1}) \leq TV(U^k) \tag{A.16}$$

for an arbitrary grid function U^k.

Obviously, for a total variation diminishing method the total variation of the initial solution $TV(U^0)$ can be used as a bound for the total variations at arbitrary time steps $TV(U^k)$.

$$TV(U^k) \leq TV(U^0) \tag{A.17}$$

Therefore, total variation diminishing methods are total variation stable for a finite total variation of the initial solution.

Definition 16 (l_1-contracting). *Suppose U^k and V^k are two solutions generated by a numerical method on different grids with $U^k - V^k$ having compact support, i.e. $U^k - V^k$ vanishes for sufficiently small or large indexes. Then the numerical method is called l_1-contracting if*

$$\|U^{k+1} - V^{k+1}\|_1 \leq \|U^k - V^k\|_1. \tag{A.18}$$

Thus, a l_1-contracting numerical method is total variation diminishing. This is important as for a given numerical approximation scheme the property of l_1-contraction can be easier verified than total variation stability.

A.3   Convergence of the upwind scheme

As has been shown in the previous chapter, the main ingredients to prove convergence of a numerical method in conservation form to a weak solution are total variation stability, which guarantees convergence, and consistency together with Lipschitz continuity, which gives that the limit is a weak solution.

As the main task is design of stabilizing control, we limit ourselves to a simple upwind scheme, which gives only first order accurate results. The upwind scheme can be derived from the general discrete conservation law in conservation form (A.9)

$$U_j^{k+1} = U_j^k - \frac{\Delta t}{\Delta x} \left[F(U_{j-p}^k, \ldots, U_{j+q}^k) - F(U_{j-1-p}^k, \ldots, U_{j-1+q}^k) \right] \tag{A.19}$$

for a reduced stencil, i.e. setting $p = 0$ and $q = 1$,

$$U_j^{k+1} = U_j^k - \frac{\Delta t}{\Delta x} \left[F(U_j^k, U_{j+1}^k) - F(U_{j-1}^k, U_j^k) \right] \tag{A.20}$$

and using the following discrete flux

$$F(v, w) = f(v). \tag{A.21}$$

The upwind scheme therefore reads

$$U_j^{k+1} = U_j^k - \frac{\Delta t}{\Delta x} \left[f(U_j^k) - f(U_{j-1}^k) \right]. \tag{A.22}$$

The upwind scheme is consistent as the numerical flux (A.21) satisfies the consistency condition (A.12). In addition, Lipschitz continuity of the numerical flux F directly follows from Lipschitz continuity of the continuous flux f.

In order to prove convergence of the upwind scheme it is sufficient to show that the method is l_1-contracting, which gives that it is total variation diminishing and therefore total variation stable for initial conditions with bounded total variation.

Theorem 7. *[44, p. 168] For a positive characteristic propagation speed, i.e. $f' > 0$, a fulfilled CFL condition, i.e.*

$$0 \leq \frac{\Delta t}{\Delta x} f' \leq 1. \tag{A.23}$$

and two grid functions U^k and V^k with $U^k - V^k$ having compact support, the upwind scheme is l_1-contracting.

A.4 Convergence - semi-discrete case

So far, fully-discrete methods have been discussed, i.e. numerical methods discrete in time and space. From a practical point of view it is sometimes preferable if the discretization is done in two stages, first discretizing in space. This approach is called the method of lines. It reduces the distributed parameter system to a high dimensional system of ordinary differential equations.

$$\frac{du}{dt} = L(u) \tag{A.24}$$

Here, u is the space discretized approximation of the solution and $L(u)$ represents the discrete flux approximation of the true flux. Obviously, the semi-discrete representation (A.24) is equivalent to the fully-discrete method (A.9), when applying the forward Euler method for time discretization.

$$u^{k+1} = u^k + \Delta t L(u^k) \tag{A.25}$$

The main advantage using the method of lines approach is, that applying standard high order ODE solvers (e.g. Runge-Kutta methods) high temporal accuracy is achievable. The open question here is, whether applying a high order ODE method still guarantees

convergence, i.e. total variation stability. In the following, a general Runge-Kutta scheme is studied.

$$u^{(0)} = u^k \tag{A.26}$$

$$u^{(i)} = \sum_{j=0}^{i-1} \left(\alpha_{i,j} u^{(j)} + \Delta t \beta_{i,j} L(u^{(j)}) \right) \quad i = 1, \ldots, m \tag{A.27}$$

$$u^{k+1} = u^{(m)} \tag{A.28}$$

Here, the coefficients $\alpha_{i,j}$ and $\beta_{i,j}$ are assumed to be nonnegative, i.e. $\alpha_{i,j} \geq 0$ and $\beta_{i,j} \geq 0$. In addition by consistency the coefficients $\alpha_{i,j}$ fulfill the following equality

$$\sum_{j=0}^{i-1} \alpha_{i,j} = 1 \quad i = 1, \ldots, m. \tag{A.29}$$

The main advantage using this representation is that for $\alpha_{i,j} \geq 0$ and $\beta_{i,j} \geq 0$ the Runge-Kutta schemes are just a combination of Euler forward steps. The following theorem shows that if the semi-discrete scheme is TV-stable for the Euler forward step, i.e. if the equivalent fully-discrete scheme is TV-stable, then the semi-discrete scheme is TV-stable applying an appropriate high order Runge-Kutta scheme.

Theorem 8. *[53, p. 12] If the forward Euler method is total variation stable and fulfills the CFL condition with a time step Δt, then the Runge-Kutta method with $\alpha_{i,j} \geq 0$ and $\beta_{i,j} \geq 0$ is total variation stable if it fulfills the following CFL condition*

$$\frac{\Delta t}{\Delta x} \max_{i,j} \left(\frac{\beta_{i,j}}{\alpha_{i,j}} \right) f' \leq 1. \tag{A.30}$$

Due to the fact that the presented Runge-Kutta schemes guarantee TV-stability they are called total variation dimishing (TVD) or strong stability preserving (SSP) Runge-Kutta schemes. For numerical time integration the following third order Runge-Kutta scheme (Table A.4) can be used

$$u^{(0)} = u^k \tag{A.31}$$

$$u^{(1)} = u^{(0)} + \Delta t L \left(u^{(0)} \right) \tag{A.32}$$

$$u^{(2)} = \frac{3}{4} u^{(0)} + \frac{1}{4} u^{(1)} + \frac{1}{4} \Delta t L \left(u^{(1)} \right) \tag{A.33}$$

$$u^{(3)} = \frac{1}{3} u^{(0)} + \frac{2}{3} u^{(2)} + \frac{2}{3} \Delta t L \left(u^{(2)} \right) \tag{A.34}$$

$$u^{k+1} = u^{(3)}. \tag{A.35}$$

The coefficients $\alpha_{i,j}$ and $\beta_{i,j}$ clearly satisfy the aforementioned assumptions.

$\alpha_{1,0} = 1$			$\beta_{1,0} = 1$		
$\alpha_{2,0} = 3/4$	$\alpha_{2,1} = 1/4$		$\beta_{2,0} = 0$	$\beta_{2,1} = 1/4$	
$\alpha_{3,0} = 1/3$	$\alpha_{3,1} = 0$	$\alpha_{3,2} = 2/3$	$\beta_{3,0} = 0$	$\beta_{3,1} = 0$	$\beta_{3,2} = 2/3$

Table A.1: Coefficients $\alpha_{i,j}$ and $\beta_{i,j}$ for a strong stability preserving Runge-Kutta scheme

Appendix B

Steady state calculation - internal product classification

The steady state particle size distribution $n_s(L)$ is the solution of the following integro-differential equation

$$\frac{dn_s}{dL} = \frac{1}{G}\left(\frac{b\dot{V}_e}{\frac{1}{6}\pi L_0^3}\delta(L - L_0) - K\sigma(L - L_1)n_s\right).$$ \hfill (B.1)

As the right hand side consists of piecewise constant functions integration is done piecewise.

$\boxed{L \in [0, L_0)}$

$$\frac{dn_s}{dL} = 0$$ \hfill (B.2)

$$n_s(L) = n_s(0) = 0.$$ \hfill (B.3)

$\boxed{L \in [L_0, L_1)}$

$$\frac{dn_s}{dL} = \frac{1}{G}\frac{b\dot{V}_e}{\frac{1}{6}\pi L_0^3}\delta(L - L_0)$$ \hfill (B.4)

$$n_s(L) = \frac{1}{G}\int_{L_0}^{L}\frac{b\dot{V}_e}{\frac{1}{6}\pi L_0^3}\delta(L' - L_0)dL'$$ \hfill (B.5)

$$= \frac{b\dot{V}_e}{\frac{1}{6}\pi G L_0^3}$$ \hfill (B.6)

$\boxed{L \in [L_1, \infty)}$

$$\frac{dn_s}{dL} = -\frac{1}{G}Kn_s \tag{B.7}$$

$$n_s(L) = n_s(L_1) - \frac{1}{G}\int_{L_1}^{L} Kn_s dL' \tag{B.8}$$

$$\int_{n_s(L_1)}^{n_s(L)} \frac{1}{n_s}dn_s = -\frac{K}{G}\int_{L_1}^{L} 1 dL' \tag{B.9}$$

$$\ln(n_s(L)) - \ln(n_s(L_1)) = -\frac{K}{G}(L - L_1) \tag{B.10}$$

$$n_s(L) = n_s(L_1)\exp\left(-\frac{K}{G}(L - L_1)\right) \tag{B.11}$$

$$n_s(L) = \frac{b\dot{V}_e}{\frac{1}{6}\pi G L_0^3}\exp\left(-\frac{K}{G}(L - L_1)\right) \tag{B.12}$$

The steady state solution $n_s(L)$ (eq. B.13) can hence be written as follows

$$n_s(L) = \frac{b\dot{V}_e}{\frac{1}{6}\pi G L_0^3}\left[(\sigma(L - L_0) - \sigma(L - L_1)) + \sigma(L - L_1)\exp\left(-\frac{K}{G}(L - L_1)\right)\right]. \tag{B.13}$$

It has to be mentioned that the solution n_s still depends on G. In order to resolve this dependence the steady state solution n_s is inserted into the equation for G.

$$G = \frac{2(1 - b)\dot{V}_e}{\pi \int_0^\infty L^2 n_s dL} \tag{B.14}$$

$$= \frac{2(1 - b)\dot{V}_e}{\pi \int_0^\infty L^2 \frac{b\dot{V}_e}{\frac{1}{6}\pi G L_0^3}\left[(\sigma(L - L_0) - \sigma(L - L_1)) + \sigma(L - L_1)e^{\left(-\frac{K}{G}(L - L_1)\right)}\right] dL} \tag{B.15}$$

$$= \frac{2(1 - b)}{\frac{b}{\frac{1}{6}G L_0^3}\left[\int_{L_0}^{L_1} L^2 dL + \int_{L_1}^\infty L^2 e^{\left(-\frac{K}{G}(L - L_1)\right)} dL\right]} \tag{B.16}$$

Solving the integrals

$$\int_{L_0}^{L_1} L^2 dL \;=\; \frac{1}{3}\left(L_1^3 - L_0^3\right) \tag{B.17}$$

$$\int_{L_1}^{\infty} L^2 e^{-\frac{K}{G}(L-L_1)} dL \;\overset{P.I.}{=}\; -\frac{L^2 G}{K} e^{-\frac{K}{G}(L-L_1)}\Big|_{L_1}^{\infty} + 2\int_{L_1}^{\infty} \frac{LG}{K} e^{-\frac{K}{G}(L-L_1)} dL \tag{B.18}$$

$$=\; \frac{L_1^2 G}{K} + 2\int_{L_1}^{\infty} \frac{LG}{K} e^{-\frac{K}{G}(L-L_1)} dL \tag{B.19}$$

$$\overset{P.I.}{=}\; \frac{L_1^2 G}{K} - 2\frac{LG^2}{K^2} e^{-\frac{K}{G}(L-L_1)}\Big|_{L_1}^{\infty} + 2\int_{L_1}^{\infty} \frac{G^2}{K^2} e^{-\frac{K}{G}(L-L_1)} dL \tag{B.20}$$

$$=\; 2\frac{L_1^2 G}{K} + 2\frac{L^1 G^2}{K^2} + 2\frac{G^2}{K^2} e^{\frac{L_1 K}{G}}\left[-\frac{G}{K} e^{-\frac{KL}{G}}\right]_{L_1}^{\infty} \tag{B.21}$$

$$=\; \frac{L_1^2 G}{K} + 2\frac{L_1 G^2}{K^2} + 2\frac{G^3}{K^3} \tag{B.22}$$

yields

$$G \;=\; \frac{2(1-b)}{\frac{6b}{GL_0^3}\left[\frac{1}{3}\left(L_1^3 - L_0^3\right) + \frac{L_1^2 G}{K} + 2\frac{L_1 G^2}{K^2} + 2\frac{G^3}{K^3}\right]}. \tag{B.23}$$

After some rearrangement this gives a nonlinear equation for the growth rate G.

$$\frac{6b}{L_0^3}\left(\frac{1}{3}\left(L_1^3 - L_0^3\right) + \frac{L_1^2 G}{K} + 2\frac{L_1 G^2}{K^2} + 2\frac{G^3}{K^3}\right) = 2(1-b) \tag{B.24}$$

Appendix C

Steady state calculation - external product classification

The steady state particle size distribution $n_s(L)$ is the solution of the following integro-differential equation

$$\frac{dn_s}{dL} = \frac{K_s}{G(\mu_{2,s})}\left(-T_2 n_s + n_M(\mu_{M,s})\int_0^\infty L^3 T_1 n_s dL\right), \tag{C.1}$$

$$= a\left(-T_2 n_s + n_M(\mu_{M,s})b\right), \tag{C.2}$$

where $a = \frac{K_s}{G(\mu_{2,s})}$ and $b = \int_0^\infty L^3 T_1 n_s dL$. As the right hand side consists of piecewise defined functions integration is done piecewise. Here, we assume that milled particles are smaller than product particles, i.e. $\mu_M + \sigma_M < L_2$.

$\boxed{L \in [0, \mu_M - \sigma_M)}$

$$\frac{dn_s}{dL} = 0 \tag{C.3}$$

$$n_s(L) = n_s(0) = 0 \tag{C.4}$$

$\boxed{L \in [\mu_M - \sigma_M, \mu_M + \sigma_M)}$

$$\frac{dn_s}{dL} = abn_M(\mu_{M,s}) \tag{C.5}$$

$$n_s(L) - n_s(\mu_M - \sigma_M) = ab\int_{\mu_M - \sigma_M}^L n_M(\mu_{M,s})dL' \tag{C.6}$$

$$n_s(L) = abk_M\int_{\mu_M - \sigma_M}^L 1 dL' \tag{C.7}$$

$$n_s(L) = abk_M(L - (\mu_M - \sigma_M)) \tag{C.8}$$

$\boxed{L \in [\mu_M + \sigma_M, L_2)}$

$$\frac{dn_s}{dL} = 0 \tag{C.9}$$

$$n_s(L) = n_s(\mu_M + \sigma_M) = 2abk_M\sigma_M \tag{C.10}$$

$L \in [L_2, \infty)$

$$\frac{dn_s}{dL} = -aT_2 n_s \tag{C.11}$$

$$\int_{n(L_2)}^{n(L)} \frac{1}{n} dn = -a \int_{L_2}^{L} 1 dL \tag{C.12}$$

$$n(L) = n(L_2) exp(-a(L - L_2)) \tag{C.13}$$

$$n(L) = 2abk_M \sigma_M exp(-a(L - L_2)) \tag{C.14}$$

Using equations (C.4),(C.8),(C.10) and (C.14) the steady state particle size distribution n_s can be represented as follows

$$
\begin{aligned}
n_s(L) &= abk_M \left[(L - (\mu_M - \sigma_M))(\sigma(L - (\mu_M - \sigma_M)) - \sigma(L - (\mu_M + \sigma_M))) \right. \\
&\quad + 2\sigma_M (\sigma(L - (\mu_M + \sigma_M)) - \sigma(L - L_2)) \\
&\quad \left. + 2\sigma_M \exp(-a(L - L_2))\sigma(L - L_2) \right] \tag{C.15} \\
&= abk_M \left[(L - \mu_M + \sigma_M)\sigma(L - \mu_M + \sigma_M) - (L - \mu_M - \sigma_M)\sigma(L - \mu_M - \sigma_M) \right. \\
&\quad \left. + 2\sigma_M (1 - \exp(-a(L - L_2)))\sigma(L - L_2) \right] \tag{C.16} \\
n_s(L) &= b\bar{n}_s(L) \tag{C.17}
\end{aligned}
$$

It has to be mentioned that the solution n_s still depends on a and b, i.e. K, G and the third moment of the oversize fraction $b = \int_{L_1}^{\infty} L^3 n_s dL$. At first, the dependence on $a = \frac{K_s}{G(\mu_{2,s})}$ is removed.

$$
\begin{aligned}
b &= \int_{L_1}^{\infty} L^3 n_s dL \tag{C.18} \\
&= \int_{L_1}^{\infty} L^3 \exp(-a(L - L_2)) dL \tag{C.19} \\
&= 2abk_M \sigma_M \int_{L_1}^{\infty} L^3 \exp(-a(L - L_2)) dL \tag{C.20} \\
1 &= 2ak_M \sigma_M \exp(aL_2) \int_{L_1}^{\infty} L^3 \exp(-aL) dL \tag{C.21}
\end{aligned}
$$

The integral $\int_{L_1}^{\infty} L^3 \exp(-aL) dL$ can be solved by successive partial integration.

$$
\begin{aligned}
\int_{L_1}^{\infty} L^3 e^{aL} dL &\overset{P.I.}{=} \left. \frac{L^2 e^{aL}}{a} \right|_{L_1}^{\infty} - \frac{3}{a} \int_{L_1}^{\infty} L^2 e^{aL} dL \tag{C.22} \\
&\overset{P.I.}{=} \left. \frac{L^3 e^{aL}}{a} \right|_{L_1}^{\infty} - \left. \frac{3L^2 e^{aL}}{a^2} \right|_{L_1}^{\infty} + \frac{6}{a^2} \int_{L_1}^{\infty} L e^{aL} dL \tag{C.23} \\
&\overset{P.I.}{=} \left[\left(\frac{L^3}{a} - \frac{3L^2}{a^2} + \frac{6L}{a^3} \right) e^{aL} \right]_{L_1}^{\infty} - \frac{6}{a^3} \int_{L_1}^{\infty} e^{aL} dL \tag{C.24} \\
&= \left[\left(\frac{L^3}{a} - \frac{3L^2}{a^2} + \frac{6L}{a^3} - \frac{6}{a^4} \right) e^{aL} \right]_{L_1}^{\infty} \tag{C.25} \\
&= \left(-\frac{L_1^3}{a} + \frac{3L_1^2}{a^2} - \frac{6L_1}{a^3} + \frac{6}{a^4} \right) e^{aL_1} \tag{C.26}
\end{aligned}
$$

This gives with eq. (C.21) a nonlinear equation for a.

$$\frac{1}{2k_M \sigma_M} = \left(L_1^3 + \frac{3L_1^2}{a} + \frac{6L_1}{a^2} + \frac{6}{a^3} \right) e^{a(L_2 - L_1)} \tag{C.27}$$

For a given initial mass, i.e. $m_0 = \frac{\rho\pi}{6}\mu_{3,0}$, the third moment of the steady state solution $n_s(L) = b\bar{n}_s(L)$ gives an additional equation for b.

$$m_0 = \frac{\rho\pi}{6} \int_0^\infty L^3 n_s(L) dL \tag{C.28}$$

$$= b\frac{\rho\pi}{6} \int_0^\infty L^3 \bar{n}_s(L) dL \tag{C.29}$$

$$b = \frac{m_0}{\frac{\rho\pi}{6} \int_0^\infty L^3 \bar{n}_s(L) dL} \tag{C.30}$$

Appendix D

Important inequalities

- Cauchy-Schwarz inequality

$$\int_0^1 uwdx \leq \left(\int_0^1 u^2dx\right)^{1/2}\left(\int_0^1 w^2dx\right)^{1/2} \tag{D.1}$$

- Young's inequality

$$ab \leq \frac{\gamma}{2}a^2 + \frac{1}{2\gamma}b^2 \tag{D.2}$$

- Poincare's inequality

$$\int_0^1 w^2dx \leq 2w^2(1) + 4\int_0^1\left(\frac{\partial w}{\partial x}\right)^2 dx \tag{D.3}$$

$$\int_0^1 w^2dx \leq 2w^2(0) + 4\int_0^1\left(\frac{\partial w}{\partial x}\right)^2 dx \tag{D.4}$$

- Agmon's inequality

$$\max_{x\in[0,1]}|w(x,t)|^2 \leq w(0)^2 + 2\|w(t)\|_2\left\|\frac{\partial w}{\partial x}\right\|_2 \tag{D.5}$$

$$\max_{x\in[0,1]}|w(x,t)|^2 \leq w(1)^2 + 2\|w(t)\|_2\left\|\frac{\partial w}{\partial x}\right\|_2 \tag{D.6}$$

Appendix E

Measurement of particle size distribution and its moments

The proposed models involve the particle size distribution as the system state, therefore any control law involving state feedback will require a state measurement or at least a state estimation (e.g. [15]). Here, we will focus only on a direct measurement of the particle size distribution. It is well known that this may cause problems when dealing with non-spherical particles and chord-length based measurement methods. However, in pure granulation processes, i.e. no agglomeration, breakage and attrition, the particles are typically spherically shaped.

Typical measurement principles being applied for particle size distribution measurement are

- Laser diffraction methods. Here, the diffraction pattern of a particle ensemble is analyzed applying Fraunhofer or Mie diffraction theory, depending on the size range.

- Single particle optical sizing. Here, a single particle passes an optical sensor with a known velocity. The measured signal may be either the shadow on the sensor element or the reflected laser beam. In both cases the pulse length gives with the known velocity the length of the respective particle chord. Reconstruction of the particle size distribution from the chord-length distribution is still an area of active research [16, 17, 18, 20, 23, 24].

- Video imaging. Here, particles are captured while passing through a detection zone. Applying image processing algorithms, the 2D and 3D particle size distribution can be calculated from the acquired images [19, 20, 22, 21, 25].

Bibliography

[1] M. Dosta & S. Heinrich & J. Werther, Fluidized bed spray granulation: Analysis of the system behaviour by means of dynamic flowsheet simulation, Powder Technoloy 204, 2010, pp. 71-82.

[2] R. Fan & D.L. Marchisio & R.O. Fox, Application of the direct quadrature method of moments to polydisperse gas-solid fluidized beds, Powder Technoloy 139, 2004, pp. 7-20.

[3] R. Grosch & H. Briesen & W. Marquardt & M. Wulkow, Generalization and numerical investigation of QMOM, AIChE Journal 53, 2007, pp. 207-227.

[4] S. Heinrich & M. Peglow & M. Ihlow & M. Henneberg & L. Mörl, Analysis of the start-up process in continuous fluidized bed spray granulation by population balance modeling, Chem. Eng. Sci. 57, 2002, pp. 4369-4390.

[5] R. McGraw, Description of aerosol dynamics by the quadrature method of moments, Aerosol Sci. and Tech. 27, 1997, pp. 255-265.

[6] L. Mörl & M. Mittelstrass & J. Sachse, Zum Kugelwachstum bei der Wirbelschichttrocknung von Lösungen oder Suspensionen, Chem. Techn. 29, 1977, Heft 10, pp. 540-542.

[7] L. Mörl & S. Heinrich & M. Peglow, Fluidized bed spray granulation, in Granulation (handbook of powder technology), Elsevier, 2006, pp. 21-188.

[8] M. Peglow, Beitrag zur Modellierung von eigenschaftsverteilten dispersen Systemen am Beispiel der Wirbelschicht-Sprühgranulation, PhD thesis, 2005.

[9] R. Radichkov & T. Müller & A. Kienle & S. Heinrich & M. Peglow & L. Mörl, A numerical bifurcation analysis of continuous fluidized bed spray granulation with external product classification, Chem. Eng. and Proc. 45, 2006, pp. 826-837.

[10] D. Ramkrishna, Population balances: theory and applications to particulate systems in engineering, Academic Press Inc., 2000.

[11] R. Schütte & A. Ruhs & I. Pelgrim & C.-J. Klasen & L. Kaiser, Fluidised bed spray granulation process producing two or more different size distributions, German patent DE000019639579C1, 1998.

[12] A.W. Vreman & C.E. van Lare & M.J. Hounslow, A basic population balance model for fluid bed spray granulation, Chem. Eng. Sci. 64, 2009, pp. 4389-4398.

[13] I. T. Cameron & F. Y. Wang & C. D. Immanuel & F. Stepanek, Process systems modelling and applications in granulation: A review, Chem. Eng. Sci. 60, 2005, pp. 3723-3750.

[14] T. Glaser & C. F. W. Sanders & F. Y. Wang & I. T. Cameron & J. D. Litster & J. M. H. Poon & R. Ramachandran & C. D. Immanuel & F. J. Doyle III, Model predictive control of continuous drum granulation, Journal of Process Control, 2009, pp. 615-622.

[15] A. Bück & M. Peglow & E. Tsotsas & M. Mangold & A. Kienle, Model-based measurement of particle size distributions in layering granulation processes, AIChe Journal 57, 2010, pp. 929-941.

[16] J. Worlitschek, Monitoring, modeling and optimization of batch cooling crystallization, PhD thesis, ETH Zürich, 2003.

[17] M. Li & D. Wilkinson, Determination of non-spherical particle size distribution from chord length measurements. Part 1: Theoretical analysis, Chem. Eng. Sci. 60, 2005, pp. 3251-3265.

[18] M. Li & D. Wilkinson, Determination of non-spherical particle size distribution from chord length measurements. Part 2: Experimental validation, Chem. Eng. Sci. 60, 2005, pp. 4992-5003.

[19] J. Eggers & M. Kempkes & M. Mazzotti, Measurement of size and shape distributions of particles through image analysis, Chem. Eng. Sci. 63, 2008, pp. 5513-5521.

[20] M. Kempkes & J. Eggers & M. Mazzotti, Measurement of particle size and shape by FBRM and in situ microscopy, Chem. Eng. Sci. 63, 2008, pp. 4656-4675.

[21] M. Kempkes & T. Vetter & M. Mazzotti, Measurement of 3D particle size distributions by stereoscopic imaging, Chem. Eng. Sci. 65, 2010, pp. 1362-1373.

[22] B. Bujak & M. Bottlinger, Three-Dimensional Measurement of Particle Shape, Part. Part. Syst. Charact. 25, 2008, pp. 293-297.

[23] C. Fischer & M. Peglow & E. Tsotsas, Restoration of particle size distributions from fiber-optical in-line measurements in fluidized bed processes, Chem. Eng. Sci. 66, 2011, pp. 2842-2852.

[24] M. Mangold, Use of a Kalman Filter to reconstruct particle size distributions from FBRM measurements, Chem. Eng. Sci. 70, 2011, pp. 99-108.

[25] L. Cao, Entwicklung einer kameragestützten Inline Partikelgrößenanalyse, diploma thesis, University Magdeburg, 2011.

[26] P. K. Pathath & A. Kienle, A numerical bifurcation analysis of nonlinear oscillations in crystallization processes, Chem. Eng. Sci. 57, 2002, pp. 4391-4399.

[27] T. Chiu & P. Christofides, Robust Nonlinear Control of a Continuous Crystallizer, Computers and Chemical Engineering Supplement, 1999, pp. 257-260.

[28] T. Chiu, Nonlinear model-based control of particulate processes, PhD thesis, 2000.

[29] P. Christofides, Model-based control of particulate processes, Kluwer Academic Publ., 2002.

[30] P. Christofides & N. El-Farra & M. Li & P. Mhaskar, Model-based control of particulate processes, Chem. Eng. Sci. 63, 2008, pp. 1156-1172.

[31] R. Eek, Control and dynamic modeling of industrial suspension crystallizers, PhD thesis, TU Delft, 1995.

[32] S. Palis & A. Kienle, Stabilization of continuous fluidized bed spray granulation - a Lyapunov approach, NOLCOS 2010.

[33] S. Palis & A. Kienle, Stabilization of continuous fluidized bed spray granulation, PBM 2010.

[34] S. Palis & A. Kienle, Stabilization of continuous fluidized bed spray granulation with external product classification, Chem. Eng. Sci. 70, 2012, pp. 200-209.

[35] S. Palis & A. Kienle, Diskrepanzbasierte Regelung der kontinuierlichen Flüssigkristallisation, at - Automatisierungstechnik 60, 2012.

[36] U. Vollmer & J. Raisch, H_∞-Control of a continuous crystallizer, Control Eng. Practice 9, 2001, pp. 837-845.

[37] U. Vollmer & J. Raisch, Population balance modeling and H_∞-controller design for a crystallization process, Chem. Eng. Sci. 57, 2002, pp. 4401-4414.

[38] U. Vollmer & J. Raisch, Modeling, simulation and stabilizing H_∞-control of an oscillating continuous crystallizer with fines dissolution, Chem. Eng. Sci. 58, 2003, pp. 3473-3488.

[39] A. D. Randolph, CSD dynamics, stability and control, AIChE Symposium Series 76, 1980, pp. 1-5.

[40] A. D. Randolph & M. A. Larson, Theory of particulate processes, Academic Press Inc., 1988.

[41] G.-Y. Zhu & A. Zamamiri & M. Henson & M. A. Hjortso, Model predictive control of continuous yeast bioreactors using cell population balance models, Chem. Eng. Sci. 55, 2000, pp. 6155-6167.

[42] R. Courant & K. Friedrichs & H. Lewy, Über die partiellen Differenzengleichungen der mathematischen Physik, Mathematische Annalen, 100, 1928, pp. 32-74.

[43] P. Lax & B. Wendroff, Systems of conservation laws, Comm. on pure and applied mathematics 13, 1960, pp. 217-237.

[44] R. J. LeVeque, Numerical methods for conservation laws, Birkhäuser, 1992.

[45] R. J. LeVeque, Nonlinear conservation laws and finite volume methods for astrophysical fluid flow, Springer, 1998.

[46] R. J. LeVeque, Finite-volume methods for hyperbolic problems, Cambridge University Press, 2004.

[47] C.-W. Shu & S. Osher, Efficient implementation of essentially non-oscillatory shock-capturing schemes, Journal of Computational Physics, 77, 1988, pp. 439-471.

[48] C.-W. Shu, Essentially non-oscillatory annd weighted essentially non-oscillatory schemes for hyperbolic conservation laws, ICASE Report No. 97-65, 1997.

[49] C.-W. Shu, A survey of strong stability-preserving high-order time discretization methods, In Collected Lectures on the Preservation of Stability under Discretization, SIAM, 2002.

[50] S. Gottlieb & C.-W. Shu, Total variation diminishing Runge-Kutta schemes, Mathematics of Computation, 67, 1998, pp. 73-85.

[51] S. Gottlieb & C.-W. Shu & E. Tadmor, Strong Stability-Preserving High-Order Time Discretization Methods, SIAM Review 43, 2001, pp. 89-112.

[52] S. Gottlieb & D. I. Ketcheson & C.-W. Shu, High order strong stability preserving time discretizations, Journal of scientific computing 38, 2009, pp. 251-289.

[53] S. Gottlieb & D. I. Ketcheson & C.-W. Shu, Strong stability preserving Runge-Kutta and multistep time discretizations, World Scientific, 2010.

[54] F. M. Callier & J. Winkin, Infinite dimensional system transfer functions, In Analysis and optimization of systems: state and frequency domain approaches for infinite-dimensional systems, Springer, 1992.

[55] R. Curtain & H. Zwart, An introduction to infinite-dimensional linear systems theory, Springer, 1995.

[56] R. Curtain, Model reduction for control design for distributed parameter systems, In Research directions in distributed parameter systems, SIAM, 2003.

[57] R. Curtain & K. Morris, Transfer functions of distributed parameter systems: A tutorial, Automatica 45, 2009, pp. 1101-1116.

[58] C. Foias & H. Özbay & A. Tannenbaum, Robust control of infinite dimensional systems : frequency domain methods, Springer, 1996.

[59] T. T. Georgiou & M. Smith, Robust stabilization in the gap metric: controller design for distributed plants, Trans. on Automatic Control 37, 1992, pp. 1133-1143.

[60] J. R. Grad & K. A. Morris, Solving the linear quadratic optimal control problem for infinite-dimensional systems, Computers & Mathematics with Applications 32, 1996, pp. 99-119.

[61] K. A. Morris, Convergence of controllers designed using state space methods, NASA Contractor Report 189575, ICASE Report No. 91-85, 1991.

[62] K. A. Morris, Design of finite-dimensional controller for infinite-dimensional systems by approximation, Journal of Mathematical Systems, Estimation and Control 4, 1994, pp. 1-30.

[63] K. A. Morris, H_∞-output feedback of infinite-dimensional systems via approximation, Systems & Control Letters 44, 2001, pp. 211-217.

[64] J. Reinschke & M. C. Smith, Designing robustly stabilising controllers for LTI spatially distributed systems using coprime factor synthesis, Automatica 39, 2003, pp. 193-203.

[65] G. Obinata & B. Anderson, Model Reduction for Control System Design, Springer, 2001.

[66] B. L. Jones & E. C. Kerrigan, When is the discretization of a spatially distributed system good enough for control?, Automatica 46, 2010, pp.1462-1468.

[67] D. C. McFarlane & K. Glover, Robust Controller Design using Normalised Coprime Factor Plant Descriptions, Springer Verlag, Lecture Notes in Control and Information Sciences 138, 1989.

[68] D.C. McFarlane & K. Glover, A Loop Shaping Design Procedure using H_∞ Synthesis, IEEE Transactions on Automatic Control 37, 1992, pp. 759-769.

[69] G. Vinnicombe, Measuring Robustness of Feedback Systems, PhD thesis, Department of Engineering, University of Cambridge, 1993.

[70] G. E. Dullerud & F. Paganini, A course in robust control theory: a convex approach, Springer, 1999.

[71] M. Green & D. J. N. Limebeer, Linear robust control, Pearson, 1994.

[72] S. Skogestad & I. Postlethwaite, Multivariable feedback control, Wiley, 2007.

[73] K. Zhou & J. C. Doyle & K. Glover, Robust and optimal control, Prentice-Hall, 1996.

[74] K. Zhou & J. C. Doyle, Essentials of robust control, Prentice-Hall, 1998.

[75] W. Subov, Methods of A. M. Lyapunov and their application [in Russian], Leningrad, 1957.

[76] A. Movtschan, Stability of processes with respect to two metrics [in Russian], Journal of Applied Mathematics and Mechanics 24, 1960, pp. 988-1001.

[77] T. Sirasetdinov, On the theory of stability of processes with distributed parameters [in Russian], Journal of Applied Mathematics and Mechanics, 1967, pp. 37-48.

[78] T. Sirasetdinov, Stability of systems with distributed parameters [in Russian], 1987.

[79] A. Martynjuk & R. Gutovski, Integral inequalities and stability of motion [in Russian], Naukowa Dumka, 1979.

[80] A. Balogh & M. Krstic, Infinite-dimensional backstepping-style feedback transformations for a heat equation with an arbitrary level of instability, European Journal of Control 8, 2002, pp. 165-177.

[81] S. P. Banks, State-space and frequency-domain methods in the control of distributed parameter systems, Peter Peregrinus Ltd., 1983.

[82] A. G. Butkovskiy, Distributed control systems, Nauka Press Moskva, 1965.

[83] P. D. Christofides, Nonlinear and robust control of PDE systems: methods and applications to transport-reaction processes, Birkhäuser, 2000.

[84] J-M. Coron & B. d'Andrea-Novel & G. Bastin, A strict Lyapunov function for boundary control of hyperbolic systems of conservation laws, IEEE Transactions on Automatic Control 52, 2007, pp. 2 - 11.

[85] D. Franke, Systeme mit örtlich verteilten Parametern, Springer, 1987.

[86] E.-D. Gilles, Systeme mit verteilten Parametern, Oldenbourg, 1973.

[87] J. de Halleux & C. Prieur & J-M. Coron & B. d'Andrea-Novel & G. Bastin, Boundary feedback control in networks of open channels, Automatica 39, 2003, pp. 1365-1376.

[88] J. de Halleux, Boundary control of quasi-linear hyperbolic initial boundary-value problems, PhD thesis, 2004.

[89] M. Kishida & R. D. Braatz, Internal model control of infinite dimensional systems, Proc. Conference on Decision and Control, 2008.

[90] M. Krstic & A. Smyshlyaev, Boundary control of PDEs, SIAM, 2008.

[91] M. Krstic & A. Smyshlyaev, Adaptive boundary control for unstable parabolic PDEs - Part I: Lyapunov design, IEEE Transactions on Automatic Control 53, 2008, pp. 1575-1591.

[92] M. Krstic, Delay compensation for nonlinear, adaptive and PDE systems, Birkhäuser, 2009.

[93] J. L. Lions, Optimal control of systems governed by partial differential equations [in Russian], MIR Moskva, 1972.

[94] Z.-H. Luo & B.-Z. Guo & O. Morgul, Stability and stabilization of infinite dimensional systems with applications, Springer, 1999.

[95] E. Monifi, Root-locus theory for infinite-dimensional systems, PhD thesis, 2007.

[96] J. Oostveen, Strongly stabilizable distributed parameter systems, SIAM, 2000.

[97] C. Prieur & J. Winkin & G. Bastin, Robust boundary control of systems of conservation laws, Mathematics of Control, Signals and Systems 20, 2008, pp. 173 - 197.

[98] M. S. de Queiroz & D. M. Dawson & S. P. Nagarkatti & F. Zhang, Lyapunov-based control of mechanical systems, Birkhäuser, 2000.

[99] C. D. Rahn, Mechatronic control of distributed noise and vibration: a Lyapunov approach, Springer, 2001.

[100] A. Smyshlyaev & E. Cerpa & M. Krstic, Boundary stabilization of a 1-D wave equation with in-domain anti-damping, SIAM Journal of Control and Optimization, vol. 48, pp. 4014-4031, 2010.

[101] V. Y. Tertychny-Dauri, Adaptive mechanics [in Russian], Faktorial Press Moskva, 2003.

[102] R. Seydel, Practical bifurcation and stability analysis, Springer, 2009.

[103] A. Isidori, Nonlinear Control Systems: An Introduction, Springer, 1995.

[104] A. Isidori, Nonlinear Control Systems II, Springer, 1995.

[105] A. L. Fradkov & I. V. Miroshnik & V. O. Nikiforov, Nonlinear and adaptive control of complex systems, Kluwer Academic Publishers, 1999.

[106] M. Krstic & I. Kanellakopoulos & P. Kokotovic, Nonlinear and adaptive control design, Wiley-Interscience, 1995.

[107] M. Krstic & H. Deng, Stabilization of nonlinear uncertain systems, Springer, 1998.

[108] H. Nijmeijer, A. J. van der Schaft, Nonlinear dynamical control systems, Springer, 1996.

[109] R. Marino & P. Tomei, Nonlinear control design, Prentice-Hall, 1995.

[110] Q. Lu & Y. Sun, Nonlinear control systems and power system dynamics, Kluwer Academic Publishers, 2001.

[111] Z. Qu, Robust control of nonlinear uncertain systems, Wiley, 1998.

[112] A. van der Schaft, L_2-Gain and passivity techniques in nonlinear control design, Springer, 2000.

[113] R. Sepulchre & M. Jankovic & P. Kokotovic, Constructive nonlinear control, Springer, 1997.

[114] J.-J. E. Slotine & W. Li, Applied nonlinear control, Prentice-Hall, 1991.

[115] E.D. Sontag, A universal construction of Artstein's theorem on nonlinear stabilization, Systems and Control Letters 13, 1989, pp. 117-123.

[116] M. Sackmann, Modifizierte Optimale Regelung - Stabilitätsorientierter nichtlinearer Reglerentwurf, at - Automatisierungstechnik 53, 2005, pp. 367-377.

[117] M. Sackmann & V. Krebs, Modified optimal control: robust stabilization of nonlinear uncertain systems, Proc. of the IFAC Conf. on Cont. Syst. Design, 2000, pp. 197-202.

[118] V. Hahn & H. Unbehauen, Direct adaptive control schemes for non-minimum phase systems, Conf. on Applications of Adaptive and Multivariable Control, 1982, pp. 170-175.

[119] R. Rothfuß, Anwendung der flachheitsbasierten Analyse und Regelung nichtlinearer Mehrgrößensysteme, VDI Fortschritt-Berichte Reihe 8, 1997.

[120] H. Schwarz, Changing the unstable zero dynamics of nonlinear systems via parallel compensation, Int. Conf. on Control, 1996.

[121] H. Schwarz, Systems theory of nonlinear control: an introduction, Shaker, 2000.

[122] F. Svaricek, Nulldynamik linearer und nichtlinearer Systeme: Definitionen, Eigenschaften und Anwendungen, at - Automatisierungstechnik 54, 2006.

[123] S. Waldherr & M. Zeitz, Flat inputs in the MIMO case, Symp. on Nonlinear Control Systems, 2010.

[124] M. Zeitz, Flachheitsbasierter Entwurf linearer zeitvarianter SISO-System, at - Automatisierungstechnik 58, 2010.

[125] M. Zeitz, Differenzielle Flachheit: Eine nützliche Methodik auch für lineare SISO-Systeme, at - Automatisierungstechnik 58, 2010.

[126] K.-J. Engel & R. Nagel, A short course on operator semigroups, Springer, 2005.

[127] A. Jüngel, Eine Einführung in die Halbgruppentheorie, Vorlesungsskript, 2001.

[128] A.-M. Wazwaz, A first course in integral equations, World Scientific, 1997.